

MINISTRY OF EDUCATION AND SCIENCE OF UKRAINE
NATIONAL TECHNICAL UNIVERSITY OF UKRAINE
"IGOR SIKORSKY KYIV POLYTECHNIC INSTITUTE"

MINISTRY OF EDUCATION AND SCIENCE OF UKRAINE
NATIONAL TECHNICAL UNIVERSITY OF UKRAINE
"IGOR SIKORSKY KYIV POLYTECHNIC INSTITUTE"

Qualifying scientific work
on the manuscript rights

YU JUNJIE

UDC [661.183:666.363-048.77]:502.17(043.3)

THESIS

**MATERIALS BASED ON SILICA AND ALUMINOSILICATES FOR
ENVIRONMENTAL PROTECTION**

161 Chemical Technology and Engineering
16 Chemical and bioengineering

Applying for the Doctor of Philosophy degree

The dissertation contains the results of own research. The use of ideas, results and texts of other authors are linked to the corresponding source

_____ Yu Junjie

Supervisor: Tobilko Viktoriia, Candidate of Technical Sciences, Associate Professor

Kyiv - 2025

ABSTRACT

Yu Junjie. Materials based on silica and aluminosilicate for environmental protection. – Qualification research work presented as a manuscript.

Dissertation for the degree of Doctor of Philosophy in specialty 161 Chemical Technologies and Engineering. – National Technical University of Ukraine “Igor Sikorsky Kyiv Polytechnic Institute,” Kyiv, 2025.

This dissertation is devoted to the development of silicate materials based on natural and artificial raw materials for protecting water from pollution by various toxic substances. The development of water purification technologies for removing heavy metal ions and organic dyes using effective adsorption materials based on accessible and low-cost raw materials is economically justified. Promising materials in this regard include natural (layered aluminosilicates), artificial (synthesized silicas), and even technogenic silicates (fly ash). By applying various surface modification methods to inorganic materials using modern synthesis techniques, it is possible to obtain new chemically and thermally stable sorbents with improved structural-adsorption characteristics and physicochemical properties. The production of so-called “low-cost” materials based on natural aluminosilicate raw materials in granulated form enables quick separation of solid and liquid phases after adsorption purification, without the need for special equipment. A key and topical issue is the study of specific features of obtaining materials based on modified synthetic silicas and aluminosilicates, as well as the investigation of physicochemical patterns involved in the removal of heavy metals and cationic dyes from water using such materials.

The first chapter of the dissertation presents an analytical review of scientific literature on adsorption materials used for the protection of aquatic environments. It examines the sources of heavy metal ions and organic dyes entering water, as well as existing methods for purifying natural and wastewater from such pollutants. Special attention is given to adsorption processes, the factors influencing them, and the practical application of sorption materials in water treatment technologies. The chapter also analyzes methods for obtaining mesoporous adsorbents based on synthetic

silicates (silica) and natural or artificial aluminosilicate materials. Various approaches to chemical modification of these materials and their fields of application are studied.

The second chapter describes the methodologies for obtaining adsorption materials, including synthetic silica with a zero-valent iron layer, amino-functionalized silica, commercial silica gel modified with nickel oxide, granulated samples based on saponite and sodium alginate, and mesoporous adsorbents synthesized using fly ash. A list of reagents, materials, and equipment used to prepare the adsorbents is provided. The reliability of the obtained results is ensured by the use of modern instrumental research methods. Surface morphology of the materials was studied using scanning electron microscopy with energy-dispersive X-ray spectroscopy and transmission electron microscopy. Phase composition and surface chemistry were analyzed using X-ray diffraction, X-ray photoelectron spectroscopy, and infrared spectroscopy. Porous structure parameters were determined using low-temperature nitrogen adsorption-desorption methods. Thermal stability was assessed using differential thermal analysis and thermogravimetric analysis. In addition, the rheological properties of clay suspensions were measured, along with functional group content on the surface of the adsorbents and granule stability in aqueous media. Sorption techniques were used to study the physicochemical characteristics of heavy metal ion and dye removal from water. Inductively coupled plasma atomic emission spectrometry was applied to determine initial and equilibrium concentrations of copper ions, while the spectrophotometric method was used for determining dye concentrations in solution.

The third chapter is devoted to the synthesis and characterization of dendritic mesoporous silica nanoparticles (DMSNs) modified with zero-valent iron and 3-aminopropyltriethoxysilane, as well as to the study of their efficiency in removing copper ions from aqueous solutions. The optimal synthesis parameters were determined, particularly the influence of synthesis time on the formation of monodisperse silica microspheres with controlled structural and physicochemical characteristics. X-ray diffraction analysis revealed a broad diffraction peak at $2\theta = 22^\circ$, indicating the formation of amorphous silica in all samples, regardless of synthesis duration (1.5, 3, and 5 hours – labeled as DMSN-1.5, DMSN-3, and DMSN-5). Infrared

spectroscopy confirmed the presence of characteristic vibrational bands for Si – OH, O – Si – O, and Si – O – Si bonds, typical for amorphous SiO₂. Surface morphology studies using scanning electron microscopy revealed that the silica microspheres synthesized under different stirring durations are monodisperse spheres with a diameter of approximately 200 nm and contain visible pores. The DMSN-1.5 sample exhibited a nanoscopic rim structure around 7 nm in thickness and well-defined mesopores. Extending the synthesis time to 3 hours caused the thin nanosheet-like edges to transform into thicker ribbon-like rims, increasing their size to 16 nm, while maintaining the overall 200 nm particle diameter. Further extending the reaction time to 5 hours resulted in edge thickening up to 22 nm, but also led to partial loss of monodispersity, suggesting that prolonging the synthesis beyond this point is not advisable. Low-temperature nitrogen adsorption–desorption analysis showed that all SiO₂ microsphere samples exhibit type IV isotherms with H3-type hysteresis loops according to IUPAC classification, indicating mesoporous structures formed by uniform spherical particles. The pore sizes ranged from approximately 5 to 50 nm. The specific surface areas were 504 m²/g, 452 m²/g, and 308 m²/g for DMSN-1.5, DMSN-3, and DMSN-5, respectively. It was concluded that a synthesis time of 1.5 hours is optimal for achieving a high specific surface area and favorable morphology without significant pore coalescence or excessive rim thickening.

A adsorbent material (Fe⁰@DMSN) was obtained by depositing zero-valent iron particles onto the surface of DMSN-1.5. Successful modification was confirmed by scanning and transmission electron microscopy, X-ray phase analysis, and infrared spectroscopy. The low-temperature nitrogen adsorption–desorption isotherms of the studied samples correspond to type IV isotherms according to IUPAC classification, featuring H3-type hysteresis loops typical for mesoporous materials. The specific surface area of the modified sample was found to be nearly half that of the synthesized DMSN, which may be attributed to Fe⁰ occupying or partially blocking the DMSN pore channels. Pore size distribution revealed a broad range of pore diameters between 3 and 50 nm. It was established that under pH = 5.7, the maximum adsorption capacity of Fe⁰@DMSN toward copper ions reached 39.8 mg·g⁻¹, which is approximately 57

times higher than that of the unmodified DMSN-1.5 ($0.7 \text{ mg} \cdot \text{g}^{-1}$). The kinetics of Cu^{2+} removal were described by a pseudo-first-order model.

An amino-functionalized adsorbent (DMSN- NH_2) was obtained by chemically modifying dendritic mesoporous silica nanoparticles with 3-aminopropyltriethoxysilane. It was determined that the content of $-\text{NH}_2$ groups in the modified sample is significantly higher than the content of $-\text{OH}$ groups in the unmodified material: 2.03 meq/g versus 0.16 meq/g , respectively. Successful attachment of amino groups to the surface of the silica particles was confirmed by infrared spectroscopy and thermal analysis methods. The low-temperature nitrogen adsorption–desorption isotherms of both samples correspond to type IV isotherms with H3-type hysteresis loops according to the IUPAC classification. This is characteristic of mesoporous materials, as confirmed by the obtained pore size distribution. It was found that the unmodified DMSN exhibits almost no adsorption capacity toward copper ions at pH 6, with a removal efficiency of only 15%. In contrast, DMSN- NH_2 demonstrates highly efficient Cu(II) removal across the entire tested pH range, with only a slight decrease in removal efficiency from 99% to 87% as the pH increases from 3 to 6. The adsorption equilibrium was reached relatively quickly. Structural-sorption, morphological, and adsorption studies showed that amino functionalization of the DMSN surface significantly enhances its efficiency in removing copper ions from aqueous solutions. X-ray photoelectron spectroscopy results indicate the formation of coordination bonds between Cu^{2+} ions and amino groups, suggesting a combination of physical adsorption and chemisorption processes. Regeneration studies of the used adsorbent indicate its potential for repeated use.

The forth chapter presents the results of adsorption removal of copper ions and methylene blue using materials based on commercial silica gel modified with nickel oxide at different mass ratios ($\text{SiO}_2@0.5\text{NiO}$ and $\text{SiO}_2@\text{NiO}$). X-ray diffraction analysis confirmed the successful deposition of nickel oxide on the silica surface. The obtained low-temperature nitrogen adsorption–desorption isotherms correspond to type IV according to IUPAC classification, indicating a mesoporous structure. The hysteresis loop shape suggests that the porous structure of all samples is formed by

spherical particles of uniform size, arranged in a homogeneous packing with cylindrical pore channels. These materials also exhibit a narrow mesopore size distribution in the range of approximately 2.5–3 nm, as confirmed by pore size distribution data. It was shown that in the series $\text{SiO}_2 > \text{SiO}_2@0.5\text{NiO} > \text{SiO}_2@\text{NiO}$, the specific surface area of the adsorbents decreased from 411 m²/g to 186 m²/g. The commercial SiO_2 exhibited practically no copper ion adsorption, with a maximum capacity of 0.2 mg/g at pH 5.5. For the modified samples, the degree of Cu^{2+} removal increased with increasing pH. The maximum adsorption capacities at pH 5.5 were 0.9 mg/g for $\text{SiO}_2@0.5\text{NiO}$ and 1.7 mg/g for $\text{SiO}_2@\text{NiO}$. Copper ion removal was found to be relatively fast. Adsorption equilibrium was established within 1 hour, with 51% removal achieved within the first 15 minutes for $\text{SiO}_2@\text{NiO}$ - significantly higher than for unmodified SiO_2 . These results indicate that the sorption capacity of silica gel is significantly enhanced after surface modification with nickel oxide. Specifically, the maximum adsorption capacity increased by approximately 5 times for $\text{SiO}_2@0.5\text{NiO}$ and by nearly 10 times for $\text{SiO}_2@\text{NiO}$. The study also showed that methylene blue removal from solution by the synthesized materials occurred rapidly. The highest adsorption capacity (19.3 mg/g) was observed for the sample with a SiO_2 to NiO mass ratio of 1:0.5.

The fifth chapter presents experimental data on the removal of copper ions using sorbent materials based on natural and technogenic aluminosilicates. Granules were obtained using saponite modified with ferrihydrite and sodium alginate, as well as a mesoporous adsorbent derived from fly ash coated with a zeolite layer. To obtain granules that are stable in aqueous media, the rheological behavior of clay suspensions based on saponite and biopolymer with varying component mass ratios was investigated. It was established that these systems are thixotropic, and their viscosity—when the same amount of sodium alginate is added—depends on the solid phase content. Based on these results, the appropriate conditions for granulation were selected. It was found that the amount of sodium alginate added significantly affects the stability of the granules in water. The structural-sorption characteristics and thermal properties of the resulting granulated adsorbents were studied, and their potential application for the

removal of heavy metal ions from water was demonstrated. The morphology, phase composition, and chemical structure of sorbents based on aluminosilicate microspheres with a zeolite coating were examined. It was shown that during synthesis, fly ash serves as the source of silicon, while the aluminate solution provides sodium and aluminum. The deposition of a zeolite phase on the surface of fly ash increased the sorption capacity for copper ions from 4.94 mg/g to 6.53 mg/g. However, to further improve efficiency, longer synthesis durations at higher temperatures are required.

This study presents, for the first time, an in-depth investigation into the synthesis of adsorption materials based on dendritic mesoporous silica and commercial silica gel with enhanced structural and sorption characteristics. These improvements were achieved through surface modification with zero-valent iron nanoparticles, 3-aminopropyltriethoxysilane, and nickel oxide. The rheological behavior of suspensions based on natural and modified saponite with sodium alginate was examined, and the optimal conditions were determined for producing granulated, water-stable, low-cost adsorbents. Additionally, a mesoporous material coated with a zeolite layer was synthesized using technogenic aluminosilicate waste (fly ash) under relatively simple synthesis conditions and with accessible laboratory equipment. The physicochemical mechanisms of copper ion and methylene blue dye removal using the synthesized adsorbents were studied. The results confirm the promising potential of these materials for efficient purification of water contaminated with such pollutants.

From a practical standpoint, the functional materials obtained in this work may be applied in the development of new effective sorbents based on silicates and natural or artificial aluminosilicates for protecting aquatic environments from inorganic and organic toxicants. These sorbents are especially relevant for use in the chemical, food, and mining industries.

Key words: silicon dioxide, tetraethoxysilane, silica, aluminosilicates, modification, morphology, water purification, adsorption, sorption capacity, heavy metals, organic dyes

List of the PhD candidate's publications:

Articles published in Ukrainian peer-reviewed scientific journals (Category "B"):

1. **Yu, J.**, Bondarieva, A., Tobilko, V., & Pavlenko, V. (2023). Adsorption removal of Cu (II) using Ni-modified silica gel. *Water and Water Purification Technologies*, 3(37), 3-12. <https://doi.org/10.20535/2218-930032023302423>
2. **Yu, J.**, & Tobilko, V. (2024). Absorption removal of copper (II) from water by zero valent iron loaded dendritic mesoporous silica. *Technology audit and production reserves*, 5(3 (79)), 6-12. <https://doi.org/10.15587/2706-5448.2024.314231>
3. **Yu, J.**, & Tobilko, V. (2024). Removal of methylene blue from water by NiO-modified silica gel. *Technology audit and production reserves*, 6(3 (80)), 47-52. <https://doi.org/10.15587/2706-5448.2024.319822>
4. Fomenko, O., Makovetskyi, O., Bondarieva, A., Tobilko, V., & **Yu, J.** (2024). Obtaining granular adsorbents based on biopolymers and clay minerals. Bulletin of NTUU «Igor Sikorsky Kyiv Polytechnic Institute», Series «Chemical Engineering, Ecology and Resource Saving», (3), 93–103. <https://doi.org/10.20535/2617-9741.3.2024.312425> (in Ukraine)

Articles published in periodical scientific journals indexed in international databases:

5. Tobilko, V. Y., **Yu, J.**, & Bondarieva, A. I. (2024). Effect of synthesis time on the morphology of monodisperse silica microspheres. *Journal of Chemistry and Technologies*, 32(4), 932-938. <https://doi.org/10.15421/jchemtech.v32i4.315165>. The journal indexed in international databases Scopus (ISSN: 2663-2942). According to SCImago Journal and Country Rank at the time of publication, it belongs to the quartile Q4 (2024).
6. **Yu Junjie**, Bondarieva Antonina, Pylypenko Ihor, Tobilko Viktoriia, Sabov Tomash, Gumenna Mariana, Tomila Tamara, Inshyna Olena (2025). Amino-functionalized dendritic mesoporous silica nanoparticles for removal of copper from

aqueous solutions. *J. Ecol. Eng.*, 26(6), 365-377. <https://doi.org/10.12911/22998993/202979>. The journal indexed in international databases Scopus (ISSN: 2299-8993). According to SCImago Journal and Country Rank at the time of publication, it belongs to the quartile Q2 (2025).

Conference proceedings abstracts:

7. Bondarieva, A., **Yu, J.**, Tobilko, V. (2022). Saponite based composite materials for removal of inorganic toxicants. Abstract Book of participants of the International research and practice conference «Nanotechnology and nanomaterials» (NANO-2022). Lviv, Ukraine, August 25-27, 2022, P. 276.

8. **J. Yu**, V.Yu. Tobilko, A.I. Bondarieva. Synthesis of mesoporous silica nanospheres. Book of abstracts of Ukrainian Conference with International Participation “Chemistry, Physics and Technology of Surface” (11-12 October 2023 p., Kyiv). P. 179

9. **Yu Junjie**, Bondareva A.I., Tobilko V.Yu. Study of synthesis conditions on the structural properties of mesoporous silica nanospheres. Abstract Book of the III All-Ukrainian Internet Conference of Young Scientists “Prospects of Chemistry in the Modern World” (November 22, 2023, Zhytomyr). P. 31-32 (in Ukraine).

АНОТАЦІЯ

Юй Цзюньцзе. Матеріали на основі кремнезему та алюмосилікатів для захисту навколишнього середовища. – Кваліфікаційна наукова праця на правах рукопису.

Дисертація на здобуття наукового ступеня доктора філософії за спеціальністю 161 Хімічні технології та інженерія. – Національний технічний університет України «Київський політехнічний інститут імені Ігоря Сікорського», Київ, 2025.

Дисертація присвячена одержанню силікатних матеріалів на основі природної та штучної сировини для захисту водного басейну від забруднення токсикантами різної природи. Економічно доцільним є розробка технологій очищення вод від іонів важких металів та органічних барвників із використанням ефективних сорбційних матеріалів на основі доступної і дешевої сировини. Перспективними в цьому плані є природні (шаруваті алюмосилікати), штучні (синтезовані кремнеземи), в тому числі, техногенні (зола-винос) силікати. Застосовуючи різні способи модифікування поверхні неорганічних матеріалів із використанням сучасних методів синтезу, можна отримати новітні хімічно- та термостійкі сорбенти з покращеними структурно-сорбційними характеристиками та фізико-хімічними властивостями. Одержання так званих «low-cost» матеріалів на основі природної алюмосилікатної сировини у гранульованій формі дозволить швидко розділяти тверду та рідкі фази після сорбційного очищення без застосування спеціального обладнання. Важливим та актуальним питанням є дослідження особливостей одержання матеріалів на основі модифікованих синтетичних кремнеземів і алюмосилікатів та вивчення фізико-хімічних закономірностей видалення важких металів та катіонних барвників із вод з їх використанням.

У першому розділі дисертаційної роботи викладено аналітичний огляд наукової літератури щодо адсорбційних матеріалів, які використовуються для захисту водного середовища. Розглянуто джерела потрапляння іонів важких

металів та органічних барвників у водні об'єкти та існуючі методи очищення природних та стічних вод від такого роду забруднення. Особливу увагу приділено адсорбційним процесам, факторам, які впливають на їх перебіг та практичному використанню сорбційних матеріалів у технології водоочищення. Проаналізовано методи одержання мезопоруватих адсорбентів на основі синтетичних силікатів (кремнеземів) і природної та штучної алюмосилікатної сировини. Вивчено різні способи їх хімічного модифікування та сфери застосування.

Другий розділ містить опис методик одержання адсорбційних матеріалів (синтетичного кремнезему з нанесеним шаром нуль валентного заліза, амінофункціоналізованого кремнезему, комерційного силікагелю, модифікованого оксидом нікелю, гранульованих зразків на основі сапоніту і альгінату натрію та мезопоруватих адсорбентів, одержаних з використанням золи-виносу). Приведено список реагентів, матеріалів та перелік обладнання, яке було використано для отримання адсорбентів. Достовірність отриманих результатів у дисертаційній роботі була забезпечена використанням сучасних інструментальних методів досліджень. Для вивчення морфології поверхні одержаних матеріалів була застосована скануюча електронна мікроскопія з енергодисперсійною рентгенівською спектроскопією та трансмісійна електронна мікроскопія, для визначення фазового складу композитів та хімії поверхні - рентгенографічний метод аналізу, рентгенівська фотоелектронна та інфрачервона спектроскопії, для визначення параметрів поруватої структури зразків - метод низько температурної адсорбції-десорбції азоту, для визначення термічної стабільності матеріалів - диференціально-термічний та гравіметричний аналізи. Крім того, було використано метод визначення реологічних характеристик глинистих суспензій, методи для визначення вмісту функціональних груп на поверхні адсорбентів, метод визначення стійкості гранул у водному середовищі, сорбційні методи для визначення фізико-хімічних особливостей видалення іонів важких металів та органічних барвників із вод, метод атомно-емісійної спектроскопії з індуктивно зв'язаною плазмою для визначення вихідних та

рівноважних концентрацій іонів міді та спектрофотометричний метод визначення вмісту барвників у розчині.

Третій розділ присвячено синтезу та характеристиці дендритних мезопоруватих наночасточок кремнезему (DMSN), модифікованих нульвалетним залізом і 3-амінопропілтриетоксисиланом та дослідженню їх ефективності щодо видалення іонів міді з водних розчинів. Встановлено оптимальні параметри, а саме, вплив часу синтезу, на одержання монодисперсних кремнеземних мікросфер з контрольованими структурними та фізико-хімічними характеристиками. Аналіз дифрактограм отриманих зразків виявив наявність одного широкого дифракційного піку при $2\theta = 22^\circ$, що свідчить про одержання аморфного кремнезему незалежно від часу синтезу, який складав від 1,5, 3 та 5 годин (DMSN-1.5; DMSN-3; DMSN-5). З використанням методу інфрачервоної спектроскопії підтверджено, що зразки містять коливальні смуги, а саме, Si-OH, O-Si-O та Si-O-Si, які характерні для аморфного SiO₂. Дослідження морфології поверхні методом скануючої мікроскопії встановило, що мікросфери кремнезему, отримані в результаті синтезу, проведеному при різній тривалості перемішування, являють собою монодисперсні сфери діаметром приблизно 200 нм та містять пори. Так, сферичний кремнеземний матеріал DMSN-1.5 має нанорозмірний край близько 7 нм та чіткі мезопори. Проведення синтезу впродовж 3 годин призводить до перетворення країв кремнеземних сфер з тонких нанолістів на товстіші стрічкоподібні краї. Зокрема, розміри цих крайових нанолістів збільшуються з 7 нм до 16 нм. При цьому відбувається виключно збільшення товщини країв, тоді як загальна морфологія з діаметром часточок 200 нм зберігається. При проведенні синтезу впродовж 5 годин ширина країв продовжує потовщуватися, досягаючи 22 нм. При цьому частина матеріалу втрачає свою монодисперсну природу, що вказує на те, що подальше збільшення часу реакції є недоцільним. Встановлено, що для всіх зразків мікросфер SiO₂, досліджених методом низькотемпературної адсорбції-десорбції азоту, характерні ізотерми, що належать до ізотерм IV типу з петлями гістерезису типу H3 згідно за класифікацією IUPAC. Характер петель гістерезису вказує на те, що

мезопорувата структура всіх зразків складається зі сферичних частинок одного розміру. Для DMSN-1.5; DMSN-3; DMSN-5 розміри пор усіх мікросфер коливаються в діапазоні від 5 нм до 50 нм, а питома поверхня складає 504, 452 та 308 м²/г відповідно. Встановлено, що час синтезу 1,5 години є оптимальним для досягнення високої питомої площі поверхні та морфології без значної коалесценції пор або потовщення країв.

Одержано сорбуючий матеріал (Fe⁰@DMSN) шляхом нанесення часточок нульвалентного заліза на поверхню DMSN-1.5. Успішне модифікування підтверджено методами скануючої та просвічуючої мікроскопії, рентгенофазовим аналізом та інфрачервоною спектроскопією. Отримані ізотерми низькотемпературної адсорбції/десорбції азоту досліджуваних зразків належать до ізотерм IV типу згідно з класифікацією IUPAC з петлею гістерезису типу H3, що характерно для мезопористих матеріалів. Значення питомої площі поверхні для модифікованого зразка майже вдвічі менше, ніж для синтезованого DMSN, що може бути пов'язано з тим, що часточки Fe⁰ займають або частково блокують канали пор DMSN. Розподіл пор за розміром показує широкий діапазон від 3 нм до 50 нм. Встановлено, що при pH = 5,7 максимальна адсорбційна здатність Fe⁰@DMSN по відношенню до іонів міді становить 39,8 мг·г⁻¹, що приблизно в 57 разів вище, ніж у вихідного матеріалу DMSN-1,5 (0,7 мг·г⁻¹), а кінетичний процес видалення Cu²⁺ описується моделлю псевдо-першого порядку.

Отримано амінофункціоналізований адсорбент шляхом хімічної модифікації дендритних мезопоруватих наночасточок кремнезему 3-амінопропілтриетоксисиланом (DMSN-NH₂). Визначено, що вміст груп -NH₂ у модифікованому зразку значно вищий, ніж вміст груп -OH у вихідному матеріалі – 2,03 мекв/г та 0,16 мекв/г відповідно. Підтверджено успішне проходження прикріплення аміногруп на поверхні часточок кремнезему інфрачервоною спектроскопією та термічними методами аналізу. Низькотемпературні ізотерми адсорбції/десорбції азоту обох досліджуваних зразків, згідно з класифікацією IUPAC, відносяться до IV типу з петлями гістерезису H3. Такий тип ізотерми характерний для матеріалів з мезопористою структурою, що

підтверджується отриманим розподілом пор. Встановлено, що вихідний DMSN практично не проявляє адсорбційної здатності до іонів міді при $\text{pH} = 6$. Ступінь очищення складає лише 15%. На противагу цьому, DMSN-NH₂ демонструє високоефективне видалення Cu(II) у всьому досліджуваному діапазоні, з незначним зниженням ступеня очищення з 99% до 87% при збільшенні pH від 3 до 6. Показано, що встановлення адсорбційної рівноваги відбувається досить швидко. Структурно-сорбційні, морфологічні та адсорбційні дослідження показали, що модифікування поверхні DMSN аміногрупами значно підвищує ефективність видалення іонів міді з водних розчинів. Результати рентгенівської фотоелектронної спектроскопії вказують на утворення координаційних зв'язків між іонами Cu²⁺ та аміногрупами, що свідчить про поєднання процесів фізичної адсорбції та хемосорбції. Дослідження регенерації відпрацьованого матеріалу свідчать про те, що можливе його повторне використання.

У четвертому розділі приведені результати адсорбційного видалення іонів міді та метиленового блакитного матеріалами на основі комерційного силікагелю та оксиду нікелю з різним масовим співвідношенням компонентів (SiO₂@0,5NiO та SiO₂@NiO). За допомогою рентгенофазового аналізу підтверджено успішне нанесення оксиду нікелю на поверхню діоксиду кремнію. Отримані ізотерми низькотемпературної адсорбції/десорбції азоту належать до ізотерм IV типу згідно з класифікацією IUPAC, що вказує на мезопорувату структуру матеріалів. Характер петель гістерезису вказує, що пориста структура всіх зразків утворена сферичними частинками однакового розміру з однорідною упаковкою, яку утворюють циліндричні канали пор. Також ці матеріали мають вузький діапазон мезопор, близько 2,5 – 3 нм, що підтверджується розподілом пор за радіусами. Показано, що в ряду SiO₂ > SiO₂@0,5NiO > SiO₂@NiO питома площа поверхні адсорбентів зменшилася з 411 м²/г до 186 м²/г. Встановлено, що комерційний SiO₂ практично не сорбує іони міді, а максимальне значення сорбції становить 0,2 мг/г при $\text{pH} = 5,5$. Для модифікованих зразків ступінь видалення Cu²⁺ зростає одночасно зі збільшенням pH . Таким чином, максимальні значення сорбції спостерігаються при $\text{pH} = 5,5$ і дорівнюють 0,9 мг/г та 1,7 мг/г для зразків

$\text{SiO}_2@0,5\text{NiO}$ та $\text{SiO}_2@\text{NiO}$ відповідно. Показано, що видалення міді відбувається досить швидко. Час встановлення сорбційної рівноваги в системі становить 1 годину. При цьому протягом перших 15 хвилин ступінь видалення для зразка $\text{SiO}_2@\text{NiO}$ становить 51%, що значно вище, ніж у немодифікованого SiO_2 . Отримані результати свідчать про те, що сорбційна ємність силікагелю після модифікації його поверхні оксидом нікелю значно підвищується. Так, для зразка $\text{SiO}_2@0,5\text{NiO}$ збільшення максимального значення сорбції становить майже 5 разів, а для $\text{SiO}_2@\text{NiO}$ – майже 10 разів. Показано, що видалення метиленового блакитного з розчину синтезованими матеріалами відбувається досить швидко, а максимальну адсорбційну здатність (19.3 мг/г) має зразок з масовим співвідношенням SiO_2 до NiO (1:0,5).

У п'ятому розділі представлені експериментальні дані по видаленню іонів міді матеріалами на основі алюмосилікатів природного та техногенного походження. Одержано гранули з використанням модифікованого феригідритом сапоніту та альгінату натрію і мезопоруватий адсорбент на основі золи-виносу з нанесеним шаром цеоліту. Для отримання стійких у водному середовищі гранул було досліджено реологічну поведінку глинистих суспензій на основі сапоніту та біополімеру з різними масовими співвідношеннями компонентів. Встановлено, що ці системи є тиксотропними, а їх в'язкість при введенні однакової кількості альгінату натрію залежить від вмісту твердої фази. На основі цих даних підібрано необхідні умови для гранулювання. Встановлено, що на стабільність гранул у водному середовищі суттєво впливає кількість альгінату натрію, доданого до суспензії. Досліджено структурно-сорбційні характеристики та термічні властивості отриманих гранульованих адсорбентів та показано перспективи їх застосування в очищенні води від забруднення іонами важких металів. Досліджено морфологію, фазовий та хімічний склад сорбентів на основі алюмосилікатних мікросфер з нанесеним шаром цеоліту. Показано, що у процесі синтезу зола-винос виступає джерелом силіцію, а алюмінатний розчин – натрію та алюмінію. Встановлено, що осадження цеолітної фази на поверхню золи-виносу збільшує сорбційну здатність міді з 4,94 мг/г до 6,53 мг/г, але для

підвищення ефективності необхідно проводити більш тривалий синтез при вищій температурі.

У роботі вперше досліджено особливості одержання адсорбційних матеріалів на основі дендритного кремнезему та комерційного силікагелю із покращеними структурно-сорбційними характеристиками за рахунок модифікування їх поверхні часточками нульвалентного заліза, 3-амінопропілтриетоксисиланом та оксидом нікелю. Вивчено реологічну поведінку суспензій природного та модифікованого сапоніту із альгінатом натрію та підібрано необхідні умови для отримання гранульованих і стабільних у водному середовищі «low-cost» адсорбентів. Одержано мезопоруваний матеріал із нанесеним цеолітним шаром, на основі техногенних алюмосилікатних відходів (золи-виносу), використовуючи відносно прості умови синтезу та доступне апаратурне забезпечення. Вивчено фізико-хімічні особливості видалення сполук міді та метиленового блакитного отриманими адсорбентами і встановлено перспективність їх використання для ефективного очищення вод від таких забруднювачів.

Практична значимість роботи полягає в тому, що отримані функціональні матеріали можуть бути використані при розробці нових ефективних сорбентів на основі силікатів, природних та штучних алюмосилікатів для захисту водного середовища від токсикантів неорганічної та органічної природи на підприємствах хімічної, харчової та гірничо-видобувної промисловостей.

Ключові слова: діоксид кремнію, тетраетоксисилан, кремнезем, алюмосилікати, модифікація, морфологія, очищення води, адсорбція, сорбційна ємність, важкі метали, органічні барвники

Список публікацій здобувача:

Статті у наукових фахових виданнях України категорії «Б»:

1. Yu, J., Bondarieva, A., Tobilko, V., & Pavlenko, V. (2023). Adsorption removal of Cu (II) using Ni-modified silica gel. *Water and Water Purification Technologies*, 3(37), 3-12. <https://doi.org/10.20535/2218-930032023302423>

2. **Yu, J., & Tobilko, V.** (2024). Absorption removal of copper (II) from water by zero valent iron loaded dendritic mesoporous silica. *Technology audit and production reserves*, 5(3 (79)), 6-12. <https://doi.org/10.15587/2706-5448.2024.314231>
3. **Yu, J., & Tobilko, V.** (2024). Removal of methylene blue from water by NiO-modified silica gel. *Technology audit and production reserves*, 6(3 (80)), 47-52. <https://doi.org/10.15587/2706-5448.2024.319822>
4. **Фоменко, О. В., Маковецький, О. Л., Бондарєва, А. І., Тобілко, В. Ю., & Юй, Ц.** (2024). Одержання гранульованих адсорбентів на основі біополімерів та глинистих мінералів. *Вісник НТУУ “КПІ імені Ігоря Сікорського”. Серія: Хімічна інженерія, екологія та ресурсозбереження*, (3), 93-103. <https://doi.org/10.20535/2617-9741.3.2024.312425>

Статті у періодичних наукових виданнях, проіндексованих у міжнародних базах даних:

5. **Tobilko, V. Y., Yu, J., & Bondarieva, A. I.** (2024). Effect of synthesis time on the morphology of monodisperse silica microspheres. *Journal of Chemistry and Technologies*, 32(4), 932-938. <https://doi.org/10.15421/jchemtech.v32i4.315165>
Журнал цитується у наукометричних базах даних Scopus (ISSN: 2663-2942). За даними SCImago Journal and Country Rank на момент публікації належить до квартиля Q4 (2024).
6. **Yu Junjie, Bondarieva Antonina, Pylypenko Ihor, Tobilko Viktoriia, Sabov Tomash, Gumenna Mariana, Tomila Tamara, Inshyna Olena** (2025). Amino-functionalized dendritic mesoporous silica nanoparticles for removal of copper from aqueous solutions. *J. Ecol. Eng.*, 26(6), 365-377. <https://doi.org/10.12911/22998993/202979>.
Журнал цитується у наукометричних базах даних Scopus і Web of Science (ISSN: 2299-8993). За даними SCImago Journal and Country Rank на момент публікації належить до квартиля Q2 (2025).

Тези доповідей:

7. Bondarieva, A., **Yu, J.**, Tobilko, V. (2022). Saponite based composite materials for removal of inorganic toxicants. Abstract Book of participants of the International research and practice conference «Nanotechnology and nanomaterials» (NANO-2022). Lviv, Ukraine, August 25-27, 2022, P. 276.
8. **J. Yu**, V.Yu. Tobilko, A.I. Bondarieva. Synthesis of mesoporous silica nanospheres. Book of abstracts of Ukrainian Conference with International Participation “Chemistry, Physics and Technology of Surface” (11-12 October 2023 p., Kyiv). P. 179.
9. **Юй Цзюньцзе**, Бондарєва А.І., Тобілко В.Ю. Дослідження умов синтезу на структурні властивості мезопористих кремнеземних наносфер. Збірник матеріалів III Всеукраїнської інтернет-конференції молодих вчених «Перспективи хімії в сучасному світі» (22 листопада 2023 р., м. Житомир). С. 31-32.

CONTENT

INTRODUCTION.....	22
CHAPTER 1. ADSORPTION MATERIALS FOR ENVIRONMENTAL PROTECTION.....	26
1.1 Features of water purification from pollution by inorganic and organic substances.....	26
1.1.1 Sources of heavy metal ions and organic dyes in the aquatic environment.....	26
1.1.2 Methods of water purification from pollution by inorganic and organic substances.....	30
1.2 Application of adsorption process for water purification.....	34
1.2.1 Principles of adsorption and influence of external factors on the adsorption process.....	34
1.2.2 Practical application of adsorbents for water purification.....	39
1.3 Materials based on silica and aluminosilicates for water treatment	
1.3.1 Mesoporous silicas: methods of their production, surface modification and practical applications.....	44
1.3.2 Adsorbents based on aluminosilicates raw materials.....	57
Conclusions to Chapter 1.....	59
CHAPTER 2. RESEARCH OBJECTS AND METHODS.....	61
2.1 Research objects.....	61
2.1.1 Reagents, materials, experimental instruments and equipment	61
2.1.2 Method for preparation of dendritic mesoporous silica nanoparticles.....	63
2.1.3 Method for preparation of zero-valent iron supported by dendritic mesoporous silica nanoparticles.....	64
2.1.4 Method for preparation of amino-functionalized dendritic mesoporous silica nanoparticles.....	64

2.1.5 Method for preparation of silica gel modified with nickel oxide.....	65
2.1.6 Method for preparation of granular adsorption materials based on clay minerals and biopolymers.....	66
2.1.7 Method for preparation mesoporous adsorbents from coal fly ash.....	67
2.2 Research methods.....	67
2.2.1 Methods for studying the surface morphology of the obtained materials.....	68
2.2.2 Methods for determining the phase composition of samples and surface chemistry.....	69
2.2.3 Methods for determining the parameters of the porous structure of samples.....	71
2.2.4 Methods for determining the thermal stability of the materials	72
2.2.5 Methods for determining the rheological characteristics of the suspensions.....	72
2.2.6 Methods for determining of the content of functional groups on the surface of samples.....	73
2.2.7 Methods for determining of the stability of the granules in the aqueous medium.....	74
2.2.8 Methods for determining sorption characteristics.....	74
Conclusions to Chapter 2	76
CHAPTER 3. SILICA-BASED MESOPOROUS MATERIALS FOR AQUEOUS POLLUTANTS REMOVAL.....	77
3.1 Synthesis and characterization of dendritic mesoporous silica nanoparticles.....	77
3.2 Adsorption removal of copper (II) from water by zero-valent iron loaded dendritic mesoporous silica nanoparticles.....	84
3.3 Adsorption removal of copper (II) from water by amino-functionalized dendritic mesoporous silica nanoparticles.....	93

Conclusions to Chapter 3.....	107
CHAPTER 4 MODIFIED COMMERCIAL SILICA GEL USED FOR HEAVY METAL IONS AND ORGANIC DYES REMOVAL FROM AQUEOUS SOLUTIONS.....	110
4.1 Adsorption removal of copper (II) from water by NiO-modified silica gel.....	110
4.2 Adsorption removal of methylene blue from water by NiO- modified silica gel.....	118
Conclusions to Chapter 4.....	126
CHAPTER 5 MATERIALS BASED ON ALUMINOSILICATES FOR ADSORPTION REMOVAL HEAVY METAL IONS FROM AQUEOUS SOLUTIONS.....	128
5.1 Preparation of granular materials based on biopolymers and clay minerals for adsorption removal heavy metal ions from water.....	128
5.2 Adsorption removal of copper (II) from water by mesoporous adsorbents from coal fly ash.....	140
Conclusions to Chapter 5.....	147
CONCLUSIONS.....	149
REFERENCES.....	152

INTRODUCTION

Sorption materials based on synthetic mesoporous silicas and natural or artificial mineral raw materials (aluminosilicates) have found wide application in the removal of inorganic and organic toxicants from water. Considerable attention to such adsorbents is due to the possibility of widely varying the structural and sorption characteristics of composite materials based on them. Other advantages of silicate carriers include their availability, as well as mechanical, thermal, chemical, radiation, and biological stability.

By chemically modifying the surface of synthetic dendritic mesoporous silicas and natural aluminosilicates (saponite) and technogenic (fly ash) origin, it is possible to purposefully change the physicochemical properties of silicate sorbents, thereby obtaining composite materials with unique surface structure and morphology. Effective modifiers in this context may include zero-valent iron particles, metal oxides and oxyhydroxides (such as nickel oxide and ferrihydrite), as well as organosilicon compounds (e.g., 3-aminopropyltriethoxysilane). However, the widespread application of powdered sorbents is limited by their high dispersity, which complicates the implementation of continuous technological processes. To solve this issue, the granulation of dispersed materials can be performed. The production of low-cost granulated adsorbents based on saponite and sodium alginate significantly improves the technological efficiency of adsorption-based water purification by facilitating the separation of the solid and liquid phases after the sorption process.

In this regard, the study of the specific features of obtaining dendritic mesoporous silicas and powdered and granulated aluminosilicates with modified surfaces, as well as their use for the sorptive removal of hazardous inorganic and organic toxicants from contaminated water, is of current relevance.

Relevance to scientific programs, plans, and themes. This dissertation was carried out in accordance with the research plans of the Department of Chemical Technology of Ceramics and Glass, Faculty of Chemical Technology, National Technical University of Ukraine “Igor Sikorsky Kyiv Polytechnic Institute,” under the

research topic: “Functional silicate materials with modified surfaces” (0124U001967, 2024–2026 pp.).

Purpose and Objectives of the Research. The aim of this research is to develop powdered and granulated multifunctional adsorption materials based on dendritic silica, commercial silica gel, saponite, and fly ash for the protection of water from pollution by inorganic and organic toxicants.

To achieve this aim, the following objectives were pursued:

- ✓ Synthesis of sorption materials based on synthetic silicates:
 - Dendritic silica modified with zero-valent iron particles and 3-aminopropyltriethoxysilane;
 - Commercial silica gel modified with nickel oxide;
- ✓ Synthesis of sorption materials based on aluminosilicates:
 - Granules based on saponite modified with ferrihydrite and sodium alginate;
 - Fly ash with a deposited zeolite layer;
- ✓ Investigation of the morphology, surface chemistry, phase composition, and structural-sorption characteristics of the obtained composites;
- ✓ Determination of the physicochemical features of the removal of heavy metals (copper) and organic dyes (methylene blue) from aqueous solutions using the synthesized sorption materials.

Object of the Study – Structural-sorption characteristics and physicochemical properties of modified silicates and aluminosilicates.

Subject of the Study – Specific features of the synthesis of mesoporous adsorption materials based on synthetic silicas and natural or technogenic aluminosilicates; physicochemical aspects of purifying model water systems contaminated with heavy metals and organic dyes using the obtained adsorbents.

Research Methods. The following instrumental methods were used in this study: to examine the surface morphology of the obtained materials – scanning electron microscopy combined with energy-dispersive X-ray spectroscopy and transmission electron microscopy; to determine the phase composition of the initial materials, composites, and surface chemistry of the samples – X-ray diffraction analysis, X-ray

photoelectron spectroscopy, and infrared spectroscopy; to assess the parameters of the porous structure of the sorbents – the low-temperature nitrogen adsorption-desorption method; to evaluate the thermal stability of the materials – differential thermal and thermogravimetric analyses; inductively coupled plasma atomic emission spectrometry and spectrophotometric methods were applied to determine the initial and equilibrium concentrations of copper ions and dye in the solutions, respectively.

Scientific Novelty of the Obtained Results. The following scientific results were obtained for the first time in this dissertation:

- ✓ the specific features of synthesizing adsorption materials based on dendritic silica and commercial silica gel with enhanced structural and sorption characteristics were studied through surface modification with zero-valent iron particles, 3-aminopropyltriethoxysilane, and nickel oxide;
- ✓ based on the study of the rheological behavior of suspensions of natural and modified saponite with sodium alginate, optimal conditions were determined for obtaining granulated and water-stable low-cost adsorbents;
- ✓ a mesoporous material with a deposited zeolite layer was obtained using technogenic aluminosilicate waste (fly ash) under relatively simple synthesis conditions and accessible equipment;
- ✓ the physicochemical features of copper compound and methylene blue removal by the obtained adsorbents were investigated, and their potential for effective water purification from such pollutants was established.

Practical Significance of the Obtained Results. The obtained functional materials can be used in the development of new efficient sorbents based on silicates and natural or synthetic aluminosilicates for the protection of water environments from inorganic and organic toxicants.

The scientific principles and experimental approaches formulated during the course of the study can be integrated into the educational process as laboratory exercises for the academic components “New Ceramic Materials and Methods of their Synthesis” within the educational and professional master's program “Chemical Technologies of Inorganic Binders, Ceramics, Glass, and Polymeric and Composite

Materials” and “Chemical Technologies for Environmental Protection” within the educational and scientific master's program “Chemical Technologies and Engineering” (specialty G1 Chemical Technologies and Engineering) at the Department of Chemical Technology of Ceramics and Glass, Faculty of Chemical Technology, Igor Sikorsky Kyiv Polytechnic Institute.

Personal Contribution of the Author. The main results of the dissertation were obtained and published independently by the author. The author’s personal contribution includes the analysis of literature sources relevant to the research topic, the synthesis of sorption materials, the execution of sorption experiments, the processing and documentation of experimental results, and the writing of scientific articles. The discussion and planning of experiments, formulation of research tasks, and drawing of conclusions were carried out in collaboration with the scientific supervisor, PhD in Technical Sciences, Associate Professor, and Head of the Department of Chemical Technology of Ceramics and Glass, Viktoriia Tobilko.

Approbation of the Dissertation Results. The main provisions and scientific results of the dissertation research were presented and discussed at the International Research and Practice Conference “Nanotechnology and Nanomaterials” (NANO-2022) (Lviv, Ukraine, 2022); the Ukrainian Conference with International Participation “Chemistry, Physics and Technology of Surface” (Kyiv, Ukraine, 2023); and the III All-Ukrainian Internet Conference of Young Scientists “Prospects of Chemistry in the Modern World” (Zhytomyr, Ukraine, 2023).

Publications. A total of 9 scientific papers have been published on the topic of the dissertation, including: 4 articles in professional scientific journals of Ukraine in the specialty 161 Chemical Technologies and Engineering, among which 2 articles have more than two co-authors (including the applicant); 2 articles in peer-reviewed scientific journals indexed in the Scopus database, one of which belongs to the second quartile (Q2) and the other to the fourth quartile (Q4) according to the SCImago Journal and Country Rank classification; and 3 conference abstracts published in the proceedings of international and national conferences.

Structure and Scope of the Dissertation. The total volume of the dissertation is presented on 194 pages of printed text and includes an introduction, five chapters, general conclusions, and a list of references. The work is illustrated with 24 tables and 51 figures. The list of references includes 259 sources.

CHAPTER 1. ADSORPTION MATERIALS FOR ENVIRONMENTAL PROTECTION

1.1 Features of water purification from pollution by inorganic and organic substances

1.1.1 Sources of heavy metal ions and organic dyes in the aquatic environment

Water is essential to life and seems to be everywhere and inexhaustible, covering 140 million square miles of the Earth's surface, or about 72% of the planet's surface. However, most water resources are not directly usable, and more than 1.1 billion people worldwide are suffering from a shortage of clean water [1]. The adequacy or otherwise of a country's water resources has a bearing on its long-term development. The four major civilizations of history were all born in areas rich in water resources, so it can be seen that the availability of sufficient freshwater resources is crucial to the development of a civilization. However, with the development of civilization, a large number of heavy industries and human activities produce a variety of wastewater through various ways to produce serious pollution of the water environment. For example, heavy metal pollution of water bodies, dye pollution, agricultural residual pesticides, various organic pollutants and so on [2 - 5]. If wastewater containing various pollutants is discharged directly without control, it will not only cause a devastating disaster to the already insufficient freshwater resources, but also jeopardize the health of the people who depend on these water sources. Recent studies have shown that water pollution is becoming a major cause of death and disease in the world, with about 14,000 people worldwide losing their lives directly or indirectly every day [6]. However, civilization needs to progress, science and technology need to develop. How to safeguard the progress of civilization at the same time with maintaining good human survival of water resources in due course has become the mainstream of research in today's era. In order to find a way to control water pollution, we need to fully understand the causes

of pollution and the characteristics and structure of various types of pollutants to find a way to control pollutants.

Usually, people collectively refer to metal elements with a density greater than 5g/cm^3 as heavy metals, for example, the common heavy metals in life are copper (Cu), lead (Pb), cadmium (Cd), mercury (Hg), chromium (Cr), and arsenic (As) and so on. Some trace heavy metal elements are even essential components needed by the human body, such as iron (for oxygen exchange and transportation), zinc (related to human development), chromium (to enhance the role of insulin on sugar and lipids), and so on. However, if the human body ingests water containing heavy metals or consumes contaminated aquatic products for a long time, the heavy metal ions in the human body will slowly accumulate, and when exceeding a certain concentration it will pose a serious threat to human health, leading to a series of chronic diseases, including nerve damage, renal failure, immune system disorders, and the risk of causing cancer [7]. For example, in the sixties and seventies of the last century, Japan's Bucheon Plain near the people due to long-term reference mine emissions of cadmium-containing wastewater, caused by cadmium poisoning, excessive heavy metal cadmium ions in the human body to gather, resulting in bone deformities, even coughing may cause bone fractures, a large number of patients with pain unbearable, and even some people cannot stand the pain and suicide [8]. Excess heavy metal ions are not only harmful to the human body but also cause irreversible damage to the natural environment. Excessive heavy metals in water will disrupt the balanced environment in natural bodies of water, and in severe cases will lead to the widespread death of organisms in the water. Due to the high mobility of water bodies, water bodies contaminated by heavy metals will spread from point to point, further spread to a wider area, and even flow into the urban groundwater system or farmland irrigation system, thus either directly or indirectly into the human body.

Heavy metal ions enter water bodies and ecosystems in various ways, mainly from mining, domestic wastewater, agricultural irrigation and manufacturing waste.

Mining and smelting: With the development of industry, a large number of ores have been discovered and mined by human beings, which involves the technology of

ore refining. Often, a large amount of water is used for cleaning and processing when refining metals, which results in a large amount of wastewater or sludge containing heavy metal ions being discharged directly into nearby bodies of water. For example, lead, mercury and arsenic are common pollutants in mining areas, and these heavy metal ions will spread to all nearby water bodies with the water flow [9].

Domestic Wastewater: In modern life, a large number of industrially prepared products such as batteries, paints and automobiles contain heavy metals. When the wastewater is discharged into water bodies without treatment or through improper treatment methods, heavy metal ions also enter the water bodies around the city, enter the groundwater, and return to the urban water supply cycle [10].

Agricultural irrigation: While modern agriculture is advancing by leaps and bounds, human beings are no longer satisfied with the use of natural fertilizers. In modern farming activities, people have begun to use large quantities of fertilizers and pesticides containing heavy metals such as copper, zinc and arsenic in order to reap greater benefits. However, with the extensive use of these substances, it leads to the retention of heavy metals in the usual farming activities and their accumulation in the soil and eventually seeping into the surface water systems such as groundwater and rivers with rainwater. When these heavy metals are absorbed by plants and animals in the water, they return to the food chain, causing harm to human health and the ecosystem [11].

Manufacturing: Industry is the cornerstone of human progress and development, and a multitude of industrial products facilitate modern human life. However, in the process of manufacturing them, factories at all levels of the process inevitably produce a large amount of wastewater containing heavy metal ions. Usually, factories have their own set of wastewater treatment processes to control the wastewater discharged within the safety standards required by the region where they are located. However, in some underdeveloped areas, factories often discharge untreated or inadequately treated wastewater directly into rivers, lakes and oceans in order to save costs, resulting in widespread pollution [12].

Dye pollution is another common environmental pollution problem, mostly

found in countries and regions with a large number of light industries such as paper, textile, leather, and cosmetics [13, 14]. It is especially common in countries with emerging economies, such as China, India and Vietnam in Asia. In these developing countries, the rapid advancement of industrial processes has resulted in the slow improvement of domestic environmental policies and measures. Factories engaged in related industries discharge a large amount of poorly treated dye-containing wastewater into rivers and lakes, causing serious water pollution problems. In addition, since the current wastewater treatment design covers a large area and is expensive in terms of construction and operation costs, small and medium-sized factories ignore wastewater treatment in order to save operation costs, which further aggravates the water pollution problem [15, 16].

Industrial dyes are designed with chemical stability in mind to give better durability to industrial products containing the dye [17]. However, this characteristic also makes it more difficult for degradation to occur under natural conditions after entering a body of water. Some dyes can withstand natural means of water purification such as washing, light and microbial decomposition, thus causing persistent pollution [18]. After the entry of various dye compounds into natural water bodies, the water will be caused by a wide range of discoloration, thus seriously affecting the degree of light transmission of water. As we all know, a large number of primary producers in the water obtain the energy needed for survival through photosynthesis [19]. When the water is polluted by dyes and reduces the rate of passage of its light source, it will seriously interfere with the photosynthesis of aquatic organisms, so that they are unable to obtain the energy needed for growth, resulting in the death of a great number of aquatic plants [20]. In compliance with the biosphere in the water, when a large number of primary producers are dead, the other organisms in the water will also die out due to the actual loss of the source of food. According to the aquatic biosphere, when the primary producers die off in large numbers, other aquatic organisms will also die out because they have no food source. In addition, dyes, as the crystallization of modern industry, have a complex and varied organic structure, including many dye molecules containing aromatic rings and azo bonds, and if organisms are exposed to such

carcinogenic molecules for a long period of time, they will increase the risk of cancer and poisoning [21].

1.1.2 Methods of water purification from pollution by inorganic and organic substances

The self-purification function of the water is slow and limited, when the pollutants in the water reach a certain amount, the water will lose its self-purification ability [22]. And these non-naturally degradable substances after reaching a certain concentration not only pose a serious threat to human health, but also destroy the balanced environment in the water, which will lead to the death of water organisms on a large scale in serious cases [23]. Therefore, timely management of water pollutants is not only to protect human health, but also an important measure to protect the natural ecological environment. Therefore, for the long-term development of human society, finding a suitable method to address pollutants (such as heavy metal ions and dye molecules) in water bodies has become a contemporary research theme. At present, the commonly used methods for treating pollution in water bodies are in the following directions:

Adsorption: Adsorption is the use of adsorbents to adsorb harmful substances in water to the surface by physical or chemical methods, and then by removing the adsorbent's to achieve the purification of water bodies [24]. Adsorbent usually has a large specific surface area and rich pore structure, after it is put into the wastewater, the harmful substances through physical adsorption or chemical bonding attached to the surface of the adsorbent or within the pore space, forming a stable structure [25]. In addition, depending on the functional groups and structures on the surface of the designed adsorbent, it is possible to achieve targeted removal of specific ions, which allows it to be used in certain specific fields [26]. Common adsorbent materials include activated carbon, zeolites, natural minerals, as well as nanomaterials and biomass materials (e.g., chitosan, microbial mycobacteria, etc.) that have been widely used in recent years. However, some of the limitations of adsorption methods are that

adsorbents are usually prone to adsorption saturation and failure after prolonged and intensive use, and therefore, as with membrane filtration methods, the adsorbents in the wastewater need to be replaced frequently to maintain optimal adsorption results [27]. In recent decades of research, in order to improve the adsorption efficiency of adsorbents and reduce economic costs, researchers have developed a large number of adsorbents with different characteristics. For example, they use waste materials in life to prepare adsorbents, thereby turning waste into treasure, or modify the surface of adsorbents to greatly enhance the adsorption performance, or develop adsorbents with automatic solid-liquid separation functions, which can be separated from water by physical means after adsorption is completed, etc.

Membrane Filtration: Membrane filtration is a highly efficient wastewater treatment technology that filters and separates pollutants in the water column through a semi-permeable membrane [28]. Membrane filtration is commonly used in factory wastewater outfalls, especially in industries with high concentrations of pollutant residues from production processes such as metalworking, electronics manufacturing, and chemicals. The method utilizes filter membranes of different pore sizes to retain harmful molecules in the water to prevent wastewater containing large amounts of pollutants from being discharged directly into natural bodies of water, blocking pollution at its source. The membrane filtration method is simple to operate, has a high removal efficiency, and is suitable for the removal of a wide range of pollutants. However, its supporting equipment and later maintenance costs are high, and the membrane is easily blocked by pollutants, requiring regular inspection, cleaning and replacement [29].

Ion exchange method: In the ion exchange method, wastewater containing metal ions and dye molecules flows through the exchange bed containing ion exchange resin or mineral, using ion exchange to selectively replace toxic ions (copper, lead, cadmium, etc.) with less harmful ions (such as sodium, potassium ions) [30]. In this process, the more harmful ions are adsorbed and retained by the resin, while the exchanged less toxic substances are released into the wastewater, thus reducing the level of pollutants in the water. The advantage of this method is that specific toxic

molecules can be treated by designing the ion exchange bed to have a high removal rate and work well at lower concentrations. However, it is not effective enough in treating higher concentrations of wastewater and is prone to secondary pollution [31].

Phytoremediation: Phytoremediation is a low-cost, aesthetically pleasing and environmentally friendly remediation technique. This technique can remediate water bodies that have been contaminated over a large area. In practice, people plant these plants with restorative functions and make them grow in polluted waters, using the roots of the plants to absorb harmful substances in the water. In the process of plant growth, harmful molecules will be gradually accumulated in the plant body. After reaching a certain level, the accumulated pollutants are removed at once by harvesting, thus achieving the purpose of purifying the water [32]. Generally speaking, phytoremediation is a relatively simple and low-cost restoration technology, which does not require professional personnel to operate, and is suitable for receiving large areas of polluted waters. However, the disadvantages are obvious. Since pollutants are slowly collected through the roots of plants, the time required is much longer than other treatment methods. And most of the plants are not suitable for growing in the water environment is very harsh areas, so it can only be applied in less seriously polluted waters.

Chemical precipitation: Chemical precipitation is the use of target ions and precipitant chemical reaction, the formation of insoluble precipitates, so as to remove harmful substances in water [33]. Commonly used precipitants include hydroxides, sulfides, and carbonates. Chemical precipitation has the advantages of easy operation and high removal efficiency, and is particularly suitable for industrial wastewater containing high concentrations. However, the treatment of wastewater pollutants using chemical precipitation produces a large amount of sludge, which often contains high concentrations of heavy metals and other hazardous substances, and must be properly treated to avoid secondary contamination. In addition, the precipitation effect may be affected by the pH value of the water. If the pH value is out of control, the precipitated hazardous substances will be re-dissolved and return to the wastewater, so the operating conditions need to be precisely controlled in practice to ensure the best

removal effect.

In conclusion, in order to completely solve the problem of heavy metals and dyes pollution in water bodies and obtain a clean and hygienic water environment researchers have made a lot of efforts. Nowadays, among the known methods, the adsorption method is considered to be one of the most effective methods for water pollution treatment, which impresses people with its low cost and high efficiency of water purification [34, 35]. Of course, the current adsorption method also has corresponding shortcomings, such as the adsorption efficiency is still to be improved as well as the desorption problem of the adsorbent after adsorption. Therefore, in order to better design and manufacture a perfect adsorbent and make the adsorption method a perfect solution to the problem of water pollution, the exploration and understanding of the adsorption process is essential.

1.2 Application of adsorption process for water purification

1.2.1 Principles of adsorption and influence of external factors on the adsorption process

Adsorption is a widely used method in modern water treatment, which is characterized by low operating costs, high purification efficiency as well as flexibility in design and operation. The emergence of the term adsorption can be traced as far back as 1881 when it was introduced by the German scientist Heinrich Kayser [36]. Adsorption is the process by which an adsorbent obtains a specific component from an adsorbed object, both by attracting ions or molecules out of a liquid (or gas) through van der Waals' forces or chemical bonding, and by binding them to the surface of the adsorbent. In wastewater treatment, adsorption is the process by which an adsorbent transfers polluting molecules or ions (such as harmful heavy metal ions and dye molecules) from the water to the surface of the adsorbent by adsorption [37].

Adsorption can be categorized into physical adsorption and chemical adsorption according to the type of adsorption force (van der Waals force vs. chemical bonding), in addition, ion exchange is usually considered as a special type of chemical adsorption.

However, in practice, adsorption is a complex process and from time to time, both types of adsorption occur simultaneously [38]. Schematic representation of several of the most common adsorption mechanisms are presented in Fig. 1.1.

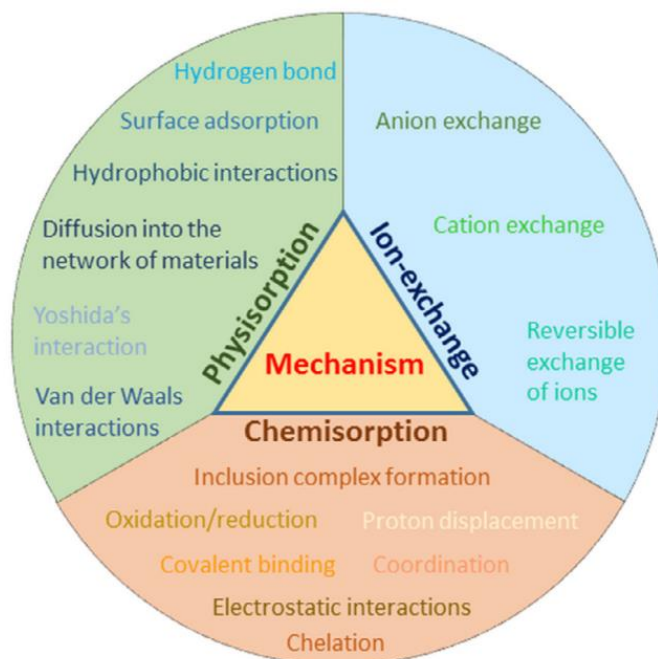


Fig. 1.1. Schematic representation of several of the most common adsorption mechanisms [38]

Physical adsorption: Physical adsorption is the adsorption of adsorbate onto the surface of an adsorbent through the van der Waals forces between objects. Physical adsorption is usually less selective and is suitable for the removal of a wide range of molecules or ions. In practice, because the adsorption energy required for physical adsorption is very low (usually less than 8 kJ/mol), it can be realized at low temperatures without the addition of external energy [39]. In addition, the resolution process of the adsorbent is also a criterion for an excellent adsorbent because it is related to the reusability of the adsorbent, whereas physical adsorption requires only a small amount of energy to resolve the adsorbed substance after adsorption due to the low bonding energy, which makes reuse much easier, which is a great economic advantage. However, because van der Waals forces are weakly electrostatic, physical sorption is usually susceptible to the reaction environment. When the reaction changes significantly (e.g., temperature increases), physical sorbed adsorbates are susceptible

to desorption, whereby ions or molecules originally adsorbed by the adsorbent are disconnected from the adsorbent and returned to the environment [40]. In addition, physical adsorption is also characterized by multilayer adsorption and faster adsorption rate. Multilayer adsorption is due to the fact that there is no strong chemical bonding between adsorbate and adsorbent, so that adsorbed substances can be attached layer by layer on the surface of the adsorbent, such as the adsorption of rust by magnets to form a multilayer structure. The adsorption process does not need to overcome high energy barriers, so the rate of adsorption is faster and usually reaches equilibrium shortly after the adsorption begins [41].

Chemisorption: Chemisorption is the process of adsorption of an adsorbate onto the surface of an adsorbent through strong covalent or ionic bonds. Chemisorption has a high adsorption energy, usually greater than 16 KJ/mol, which usually makes chemisorption require a high temperature to occur, but the higher adsorption energy also means that the adsorbate is more difficult to detach, so chemisorption is often irreversible [42]. In contrast to the low selectivity of physical adsorption, chemisorption has higher selectivity, and the functional groups on the surface of the adsorbent can be engineered to the desired structure for specific ions, hence its superior performance in removing some single or specific pollutant wastewaters [43]. Adsorption efficiency is also greatly influenced by the surface area of the adsorbent, and in chemisorption, the rate of adsorption is usually slower because adsorbate binding to the adsorbent needs to occur at specific active sites. Therefore, the adsorbent usually requires materials with a larger surface area, such as nano-materials or materials with a mesoporous structure, which provide more active sites for pollutants to bind to for the same amount of mass. Comparison of physical adsorption and chemical adsorption are presented in Table 1.1 [39 - 43].

Table 1.1 - Comparison of physical adsorption and chemical adsorption

Adsorption method	Physisorption	Chemisorption
Adsorption type	Van der Waals force	Chemical bonding (covalent or ionic)
Reversibility	Reversible	Usually irreversible
Adsorption energy	Low (<8 kJ/mol)	High (>16 kJ/mol)
Number of adsorption layers	Multilayer	Monolayer
Adsorption temperature	Suitable for low temperature conditions	Better at high temperatures
Selectivity	Low	High

The adsorption process is a complex process, various environmental parameters or the structure of the adsorbent itself will affect the efficiency of adsorption in different degrees. For example, the type of adsorbent, temperature, solution pH, stirring speed, reaction time and so on [44, 45]. In order to remove pollutants from water more efficiently and to improve the adsorption effect of adsorbents, it is crucial to have an in-depth understanding of the influence mechanisms of these factors. The following is a summary of the effects of major external factors on the adsorption process.

Temperature: The mechanism by which temperature affects the adsorption process is more complex and depends mainly on the type of adsorption. Generally, if the adsorption is chemisorption, since during chemisorption, a certain amount of energy is required to overcome the activation energy, which creates a chemical bond link with the adsorbent. Therefore, at higher temperatures, it tends to help overcome the activation energy for chemisorption and increase the rate of adsorption, but higher temperatures also mean that there is a greater possibility of destroying the physical structure of the adsorbent, resulting in the inactivity of the adsorbent [46]. On the other hand, in the case of physical adsorption, higher temperatures generally have a negative effect. This is because physical adsorption relies on intermolecular van der Waals forces, a weak interaction that is more stable at low temperatures, however, when the temperature rises, the adsorbate will be more likely to detach from the surface of the adsorbent, leading to a decrease in adsorption [47]. In addition, the change of temperature also has a certain effect on the adsorbate, in the high temperature

environment will accelerate the kinetic energy of the adsorbate molecules, making them more active in the medium, thus increasing the probability of their capture by the adsorbent, however, too high a temperature also affects the stability of the adsorbate, such as some organic molecules will be molecularly dissociated at high temperatures or other side reactions [48]. Therefore, in the practical application of the adsorbent, the temperature should be adjusted according to the characteristics of the adsorbent and the type of pollutant, and the comparison group and pre-experiment should be set up to achieve the best adsorption effect.

Effect of pH of the solution on adsorption: pH is one of the most important parameters affecting the adsorption process. Almost all the experiments of new adsorbents for the treatment of hazardous wastewater will explore the pH value at the time of adsorption [49]. The pH value of the solution can seriously affect the adsorption process, such as: the ionization state of adsorbate, the surface charge of adsorbent, and triggering the competing ionic effect [50]. The pH of adsorbent solution is the most important parameter for the adsorption process. First of all, the change of pH affects the ionization state of adsorbates in wastewater, e.g., at alkaline pH ($\text{pH} > 7$), heavy metal ions in wastewater may exist in the form of hydroxide precipitates, which makes them easier to be removed by adsorption [51]. In addition, the change of pH also changes the surface charge of the adsorbent because in aqueous solution, the surface of most adsorbents carries different functional groups, such as carboxyl, amino or hydroxyl groups, which exhibit different ionic states at different pH values. For example, under acidic conditions, the amino group will be positively charged by protonation, which makes it easier to adsorb negatively charged pollutants in wastewater, while under alkaline conditions it may become uncharged or negatively charged, which gives it better adsorption of positively charged pollutants [52]. Finally, the change of pH can also cause competitive effects of other ions in the aqueous solution with the adsorbate. Since wastewater is a complex system containing a variety of different pollutants such as heavy metals, dyes and other small and large molecules. In practical adsorption operations such as the adsorption of heavy metal ions in water, a low pH value means a high concentration of hydrogen ions in the solution, which

compete with heavy metal ions for adsorption sites and thus reduce the adsorption efficiency of heavy metal ions; whereas at a high pH, due to the low concentration of hydrogen ions, the adsorption sites can be used for the binding of heavy metal ions, and thus the adsorption efficiency is higher. Therefore, in practical applications, it is necessary to select the pH that best suits the experimental conditions according to the nature of the adsorption object and the adsorbent itself [49 - 52].

Stirring speed and time: Stirring speed and time can affect the rate of adsorption by influencing the degree of diffusion of the adsorbate in solution. Proper agitation allows the adsorbate to move faster in solution, thereby increasing the chance of contact between the adsorbate and the adsorption sites on the surface of the adsorbent. However, excessive agitation may damage the physical structure of the adsorbent and affect its adsorption effect. The length of stirring time, on the other hand, affects the saturation of the adsorbent during the adsorption process. Adsorption is usually divided into a fast adsorption phase and a slow equilibrium phase, where the initial adsorption rate is faster because there are sufficient sites on the adsorbent surface for the adsorbate to bind rapidly. However, as time passes, the adsorption sites are gradually occupied, the adsorption rate slows down, and eventually reaches saturation equilibrium. Therefore, in practical applications, the control of stirring speed needs to balance the adsorption rate and the mechanical stability of the adsorbent to achieve the best adsorption efficiency. Connected to the actual application, the choice of contact time should be adsorption saturation as the goal, both to ensure adsorption efficiency and avoid unnecessary waste of energy and time [53].

Competition from other ions or molecules in the solution: In actual wastewater treatment, the wastewater to be treated often contains a variety of ions and organic molecules, which will compete with each other and the molecules to be adsorbed for the adsorption sites of the adsorbent, thereby affecting the adsorption of the target pollutants [54]. For example, Wang et al. tested the adsorption of three ions, Pb(II), Cu(II) and Zn(II) ions, from aqueous solution by hydroxyapatite-biochar nanocomposites, and found that other metal ions present in the water would compete with the heavy metals in the adsorption process. For example, the presence of Ca(II)

and Mg(II) reduced the removal of Cu(II) and Zn(II) by the adsorbent (Ca(II) had a greater effect than Mg(II)), whereas they had no effect on Pb(II) . Wang et al. noted that this was due to the fact that Mg(II) has a stronger covalent nature than Ca(II) , and thus Mg(II) ions displayed stronger hydration and thus less effect on the adsorbent [55].

Overall, external factors such as temperature, pH, stirring rate and contact time, and solution composition all play important roles in the adsorption process. In practice, finding out the optimal external experimental conditions for the adsorbent can significantly improve its removal efficiency of pollutants. Meanwhile, the design of the adsorbent needs to be selected and adjusted according to the actual pollution environment to ensure that the adsorbent can be adapted to the required application environment. The adsorbent and the adsorption environment constitute a complex system that often needs to be considered and optimized according to the actual situation in order to achieve the ideal adsorption effect.

1.2.2 Practical application of adsorbents for water purification

The selection of adsorbent is the top priority of the water adsorption process, and the performance of adsorbent directly affects the removal of water pollution. Excellent adsorbents often need to simultaneously meet high performance, high selectivity, excellent regeneration capability, environmental friendliness and controllable cost. In recent decades, in order to create a perfect adsorbent for water and to solve the water pollution problem completely by adsorption, researchers have tried various common and uncommon materials in life. The following are some of the common adsorbents available today:

Carbon-based adsorbent: Carbon, as one of the first adsorbent materials used by people, has been widely used in the field of water adsorption since its discovery. For example, in the ancient Egyptian era, people began to use burnt charcoal as a water purification material for removing odors and impurities in water [56]. With the progress of time, people are no longer satisfied with the use of natural charcoal, and various modern technologies such as activation, functionalization or nanocomposite

technology of carbon materials have been gradually discovered and applied. For example, Liu et al. prepared KOH-activated carbon (KAC) with different pore structures and used it for the adsorption and removal of perfluorooctanoic acid (PFOA) in the aqueous environment. Their study showed that the contribution of ultra-micropores (<1.2 nm) and small mesopores (2.0-3.0 nm) to the adsorption of PFOA was significant, and compared with the ordinary carbon material, the KAC material with the optimal pore structure increased the adsorption capacity by 2.61% for the PFOA. The adsorption capacity of the KAC material with optimal pore size structure for PFOA was increased by a factor of 2.61, and the adsorption rate was increased by a factor of 2.21 [57]. Liu et al. used the strategy of surface functionalization of activated carbon materials, and their group prepared a new Bamboo Activated Carbon (BAC) with the functionality of Ethylenediaminetetraacetic Acid (EDTA) by means of branch grafting BAC with EDTA functionality. The functionalized BAC@SiO₂-EDTA material increased the maximum adsorption capacity of Pb(II) and Cu(II) by a factor of 2.7 and 6.1, respectively, which was a significant enhancement in effect. Its subsequent study surfaces that the enhancement of the adsorption effect after branching is due to the presence of EDTA on the modified BAC which promotes the formation of chemical complexes. In addition, the negative charge on the surface of the modified material will also better attract and bind heavy metal ions [58]. Carbon-based materials have also led some scholars to utilize them for the development of composites due to their excellent stability and large specific surface area, e.g., Sarita et al. composited them with ZnO materials and applied them for the removal of Cd(II) from aqueous solution. The results confirmed that the maximum adsorption capacity of the composite ZnO@activated carbon nanocomposite for cadmium ions can reach 96.2 mg/g [59].

Metal-organic frameworks (MOFs): are a class of porous materials formed by metal ions or metal clusters (usually transition metals) connected with organic ligands through ligand bonds [60]. Since its birth in the 1990s, this kind of structure with adjustable pores and large specific surface area and diversity has attracted much attention in the field of adsorption [61]. This kind of MOFs material has excellent performance in both heavy metal adsorption and dye adsorption, for example, Jin et al.

prepared a Zr-based magnetic metal-organic skeleton composites (Zr-MFCs) modified with amino group and applied them to the adsorption and removal of heavy metals and dyes in the mixed solution at the same time. Their experimental results showed that the amino-modified Zr-based magnetic MFCs had good adsorption effects on heavy metals Pb^{2+} and methylene blue in water [62]. In addition, the structural flexibility of MOFs gives them higher designability, allowing them to selectively adsorb specific pollutants, which has good applicability in certain wastewater removals containing specific pollutants. Correspondingly, Lin et al. investigated the selectivity of the MOFs materials, which screened seven Zr-based metal-organic skeletons (Zr-MOFs) with different structures for the selective adsorption for the removal of organic arsenic acid (OAA) from aqueous media. The final results showed that among the seven different MOFs materials, MOF-808F exhibited the most excellent selectivity and reusability in the presence of competing ions, such as chloride ion, acetate ion and sulfate ion or after three consecutive adsorption runs, its adsorption efficiency for organic arsenic acid (OAA) did not decrease significantly [63]. Although MOFs materials have shown high adsorption efficiency in aqueous adsorption, problems such as their poor stability in aqueous environments and excessive cost have been limiting their industrial applications.

Nanomaterials: With the development of nanotechnology, nanomaterials are being used more and more widely in the field of adsorption. As nanomaterials have a larger specific surface area, which usually leads to insufficient coordination of atoms on their surfaces, resulting in a large number of unsaturated bonds on their surfaces, which makes the surface of the material extremely unstable and easy to combine with other atoms (such as heavy metal ions and dye molecules in water), which makes the nanomaterials show a strong effect in adsorption. Currently, common nanosorbents include nano-oxides, nanographene oxide and carbon nanotubes, and nano-zero-valent iron. Many researchers have conducted detailed studies in this field of research [64]. Zangiabadi M. and Yazdapanah N. in 2021 investigated the efficiency of nanosorbents and organic adsorbents for the removal of zinc ions (Zn^{2+}) and cadmium ions (Cd^{2+}) from industrial wastewater under the same experimental conditions. The results

showed that the nanoadsorbents could reach the adsorption equilibrium faster than the organic adsorbents (nanoadsorbents reached the adsorption equilibrium in 30 min, while the organic adsorbents took 120 min and longer) [65]. Hirpo et al. on the other hand, showed a keen interest in hybrid adsorption, and their group prepared a Fe_3O_4 - ZnO (FZRBC-DES) ternary adsorbent impregnated on DES-modified biochar and tested its adsorption capacity for anion ($\text{Cr}_2\text{O}_7^{2-}$), cation (Pb^{2+}), and organic molecule (diclofenac). The experimental results showed that this ternary composite nanosorbent fulfilled its adsorption task well, and its maximum adsorption capacity (Q_{max}) for Cr(VI), Pb(II) and DCF were 66.23, 384.62 and 24.33 mg/g, respectively [66]. Although the current study shows that nanomaterials have performance advantages for the treatment of water pollution, the high cost and difficulty of reuse limit their large-scale industrial application. However, the high cost and the difficulty of reuse limit the large-scale application of nanomaterials in industry.

Natural clay adsorbent: Natural adsorbents are considered to be a suitable industrial adsorbent due to their low cost, wide availability and environmental friendliness. Mineral materials such as saponite, zeolite and bentonite are usually negatively charged and can effectively adsorb cationic pollutants [67 - 69]. However, their adsorption efficiency, adsorption capacity, etc. are often inferior to other synthetic adsorbent materials. Therefore, in order to improve the defects of natural adsorbents, researchers have made a lot of attempts. Hai et al. used surface modification of industrial by-product fly ash (FA) and biochar (BC) with polyethyleneimine (PEI) to enhance the adsorption of natural organic matter (NOM). The results showed that under the optimal adsorption conditions, the adsorption capacity of the modified adsorbent for NOM was about three times higher than that of the original material, and it also had higher durability [70].

1.3 Materials based on silica and aluminosilicates for water treatment

1.3.1 Mesoporous silicas: methods of their production, surface modification and practical applications

Among the existing adsorbents, mesoporous silica materials have attracted additional attention for their unique internal pore structure. Its earliest discovery was in the 1970s, but it did not subsequently attract widespread attention [71]. This situation continued until 1992. In that year, researchers at Mobil Oil Corporation used micellar mesoporous framework templates to allow aluminosilicate gels to form the first silica material with mesopores in the templates. Since then, this new type of silica material with mesoporous structure has attracted a lot of attention and researchers [72]. Currently, according to the definition of the International Union of Pure and Applied Chemistry (IUPAC), ordered structures with pore sizes and pores of 2-50 nm are defined as mesoporous materials [73]. Before the discovery of mesoporous silica materials, the traditional silica has many shortcomings, such as irregular morphology, small specific surface area, etc. These shortcomings make it face many difficulties in practical applications. The emergence of mesoporous silica has changed this status quo, its controllable regular morphology and pore structure as well as adjustable pores make it possible to design different synthesis methods according to the different application areas, so that it can be adjusted microscopically. In addition, its large specific surface area makes it possible to have more surfaces involved in the actual reaction at the same mass. Therefore, the emergence of mesoporous silica materials has set off a research boom in various fields.

Among the mesoporous silica materials, two materials, MCM-41 and SBA-15, were the first to be discovered and the most widely studied. The former is a mesoporous solid synthesized by Mobil Oil in 1992 that has a high specific surface area and a tunable pore structure. The latter is a mesoporous silica material with pore sizes ranging from 4.6 to 30 nanometers, prepared by researchers at the University of California, Santa Barbara, who used amphiphilic triblock copolymers to direct the organization of polymerized silica species, in which the particles are also arranged in an ordered

hexagonal array [74]. Their structures laid the foundation for the synthesis of many other mesoporous materials, and since then, various mesoporous silica materials based on the MCM-41 and SBA-15 series have been successfully reported (spheres, rods, disks, powders, etc.). The schematic structural diagrams of SBA-15 and MCM-41 and the morphology of their derived silica materials are shown in Figure 1.2.

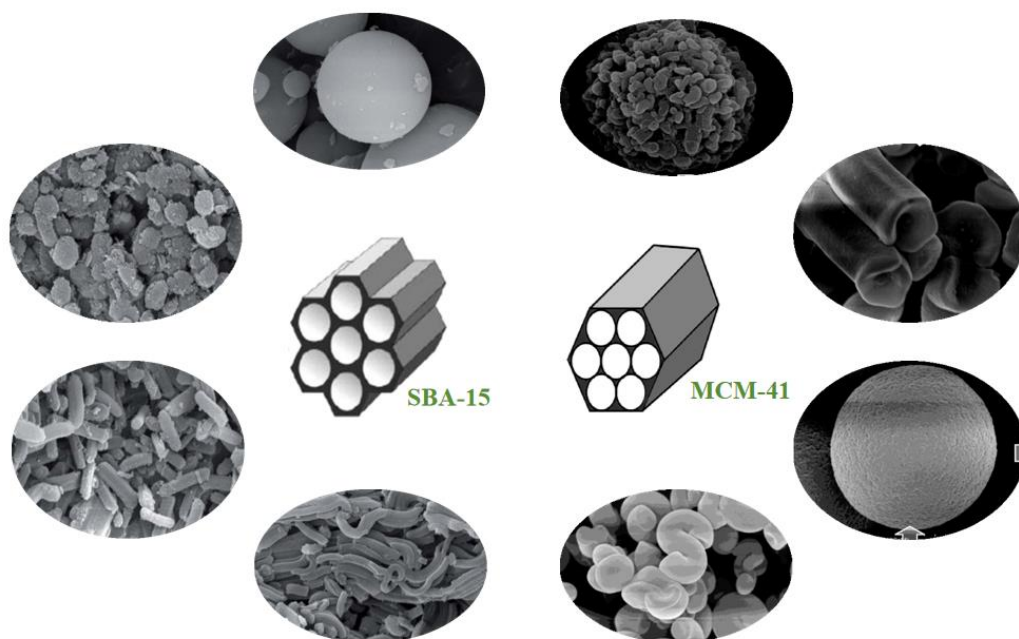


Fig. 1.2 - Schematic structure of SBA-15 and MCM-41 and morphology of their derived silica materials. SEM image source [75, 76]

MCM-41 is one of the earliest and most widely studied members of the mesoporous silica family. It is characterized by the construction of hexagonal porous mesoporous silica possessing a neat and orderly arrangement through templates. The diameter of these pores ranges from 2 to 10 nanometers [77]. Such a small pore size makes MCM-41 more suitable for the adsorption of smaller molecules such as heavy metals, dyes and pharmaceuticals [78, 79]. Additionally the highly uniform pore space allows the material to interact with reactive molecules in a consistent manner, thus building efficient and predictable adsorption behavior. Another distinctive feature of MCM-41 is the thin pore wall, which gives it a larger specific surface area [80].

However, the thinner pore walls also reduce their stability compared to other mesoporous materials, making them unsuitable for some extreme reaction conditions.

Synthesis route and method of MCM-41. MCM-41 is typically synthesized using a template method in which cetyltrimethylammonium bromide (CTAB) is used as a surfactant to form micelles in solution, which serve as a template for the condensation of silica precursors (e.g., tetraethyl orthosilicate, TEOS). After the silica is synthesized, the template is removed by calcination or solvent extraction, leaving a characteristic mesoporous structure [81]. The synthesis method and structural diagram of MCM-41 are shown in Figure 1.3. In addition, some scholars have also prepared MCM-41 by the sol-gel method, which can precisely control the pore size and surface properties by adjusting the pH, temperature, and surfactant concentration during the synthesis process, making it suitable for some applications with special requirements [82]. Besides the template method and gel method, high temperature hydrothermal method has also been applied to synthesize MCM-41, and the MCM synthesized by this method can provide thicker pore wall and more stable structure, which can be used to make up for the shortcomings of its poor stability, and is favorable for industrial applications [83].

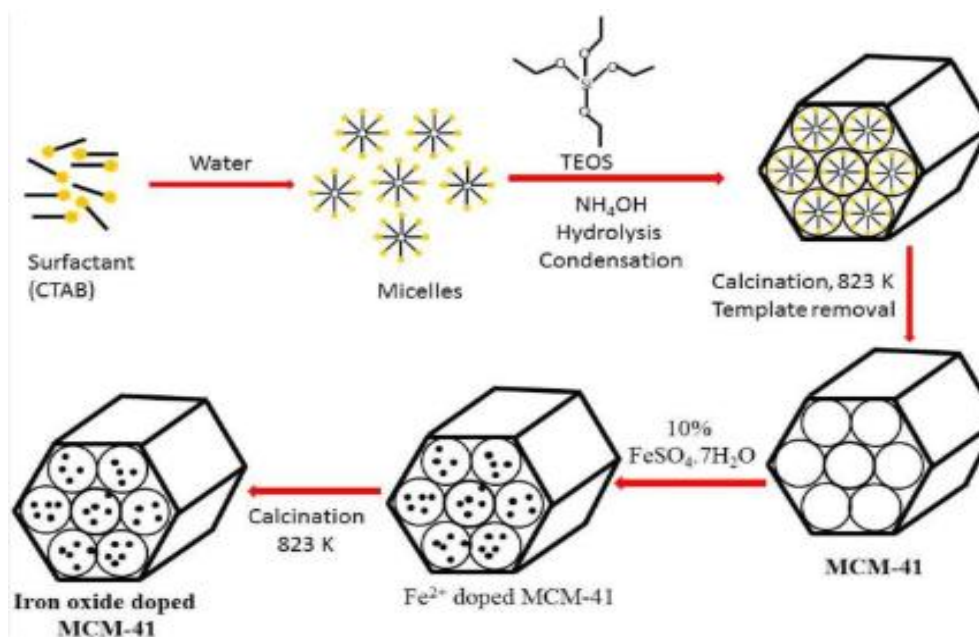


Fig. 1.3 - The synthesis method and structural diagram of MCM-41, and its method of compounding with iron ions [84]

SBA-15 (Santa Barbara Amorphous-15) was successfully prepared by researchers at the University of California in 1998 [73]. Similar to MCM-41, SBA-15 has a large specific surface area and hexagonally arranged mesopores. However, compared to the smaller pore size and thin pore wall structure of MCM-41, this mesoporous silica synthesized in acidic media has larger pore sizes (ranging from 5 nm to 30 nm) and thicker pore walls, resulting in greater structural stability and the ability to maintain its structural integrity in more complex environments. Studies have shown that the thicker pore walls of SBA-15 allow for greater structural stability and therefore less structural disruption after the reaction is complete, which allows for a certain degree of reusability, a property that greatly reduces the cost of use in industry [85]. In addition, its structural stability gives it the ability to be applied under harsh conditions, such as certain industrial wastewater and complex aqueous environments. Overall, the emergence of the SBA-15 series has greatly expanded the practical application range of mesoporous silica, enabling mesoporous silica to have the ability to work under harsh conditions.

Synthesis route and method of SBA-15. Synthesis of SBA-15 is typically done using a sol-gel method that uses triblock copolymers (e.g., Pluronic P123) as templates [86]. These copolymers first form micelles in solution, and then the silica precursor self-organizes around the micelles [87]. As with MCM-41, the silica precursor used in the synthesis of SBA-15 is usually TEOS, but other sodium silicate precursors can be used [88, 89]. After the silica precursor self-assembles around the micelles to form silica, the copolymer template is removed by calcination or solvent extraction to obtain the final mesoporous silica. The synthesis of SBA-15 can be tuned by adjusting certain conditions (e.g., temperature, pH, and type of solvent used) of the synthetic reaction species. Depending on the synthesis conditions, researchers can control the pore size, pore thickness, and appearance of the material. Fig. 1.4, shows a typical SBA-15 synthesis schematic.

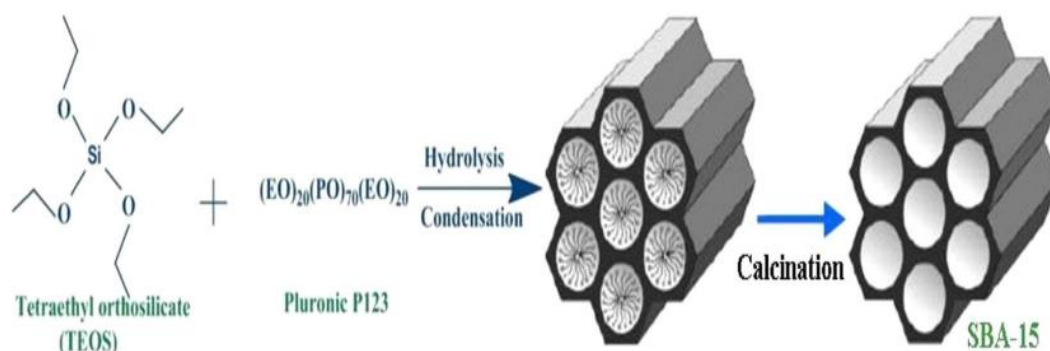


Fig. 1.4 - Schematic synthesis of a typical SBA-15 [90]

Monodisperse dendritic silica nanoparticles (DMSN). The appearance of MCM-41 and SBA-15 opened the door to mesoporous silica, and various improved syntheses based on them have been widely reported in recent decades. For example, Sreyashi et al. used tetrabutylammonium bromide salt as an accelerator to obtain an unprecedented monocrySTALLINE rod-shaped mesoporous silica MCM-41 by a simple one-step hydrothermal method, and this prepared rod-shaped mesoporous material exhibited a higher degree of hydrothermalization [91]. Valentina et al. on the other hand, developed a bottom-up synthesis method to prepare flat disc-like mesoporous silicananoparticles, known as nanodiscs (NDs), and applied them for bimodal delivery and improved cellular uptake [92], while Abdurrahman's team, on the other hand, utilized microspherical mesoporous silica to remove the cationic dye methylene blue from aqueous solution [93]. However, most of the prepared mesoporous silica is easy to agglomerate and not easy to maintain good dispersion. So people have made improvements in the traditional mesoporous silica preparation process to explore the greater possibilities of mesoporous silica materials. Among them, Cai's team first reported and discovered a kind of monodisperse mesoporous silica spheres synthesized by sol-gel soft template in 2001 [94], and then Brian et al. first used the name of mesoporous silica (MSN) to name all the spherical mesoporous silica materials with layered structure, and since then this nomenclature has been widely adopted by researchers [95]. However, it has been found that this MSN material usually has only narrow channels and pore openings, which, while enabling them to adsorb most small molecules, does not allow them to adsorb large molecules. This limits their wide

application in adsorption as well as in pharmaceuticals and other fields. Therefore, there is a need to expand the pore channels as well as the mesopore size of MSNs to extend their applications in different fields. Therefore, researchers have embarked on a new round of improvement in the preparation of MSNs to obtain novel spherical mesoporous silica that combines stability, wide pore space and pore channels for different applications. In this line of thought, dendritic silica materials with three-position hierarchical structures have been extensively studied in the last decade [94-98]. Compared with the conventional MCM-41 and SBA-15 in which the silica mesopores are arranged in a regular cylindrical or hexagonal shape, this new dendritic monodisperse mesoporous silica has a three-dimensional structure, in which the mesopores radiate outward in a radial pattern with the central core as the origin [99]. Its unique morphology is reminiscent of natural dendritic minerals and artificial dendritic molecules, and thus the nomenclature of dendritic silica (DMSN) has been gradually accepted (Fig. 1.5).

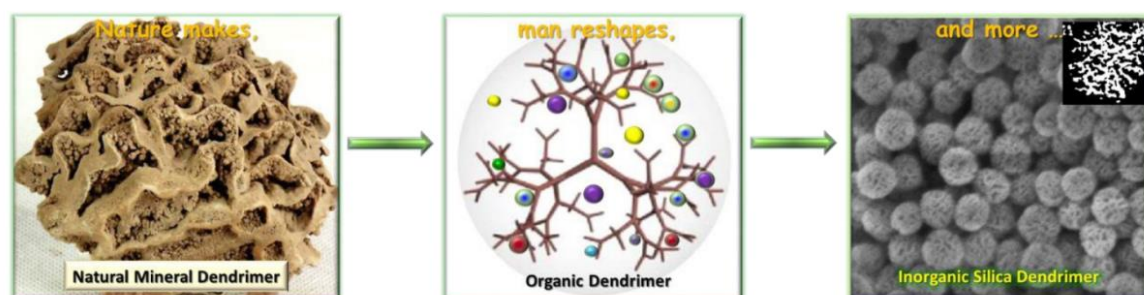


Fig. 1.5 - Schematic representation of natural dendritic mineral molecules as well as artificial organic dendrimer molecules and dendritic mesoporous silica nanospheres (DMSNs) with unique branching structures [99]

The dendritic structure emanates from the center and is formed by interconnected pores that expand uniformly in all directions. This dendritic structure not only increases the specific surface area, but also facilitates the rapid diffusion of molecules into the internal pores. This special structure makes DMSN highly efficient in the transportation and adsorption of macromolecules in applications such as the adsorption

of pollutants in water and drug delivery [100, 101]. The main morphological features of this DMSN with a central pore include the following:

Open pore structure: The unique inside-out dendritic pore structure facilitates the exposure of more reaction sites, and also allows for better diffusion and contact of guest molecules in the environment with the reaction sites, thus improving the efficiency of applications such as catalysis and adsorption.

Different pore size distribution: Thanks to its unique dendritic structure, DMSN typically has pores and internal pores of different sizes and capacities, thus providing hierarchical porosity. This stepped pore size enhances the transport and adsorption of different molecules.

Adjustable pore size: The pore size in DMSN can be adjusted by changing the synthesis conditions, e.g., by changing the reaction time or by changing the molar ratio of the surfactant. Typical pore sizes in DMSN range from 2 to 30 nm in a typical synthesis the tunability of the pores makes it more flexible for practical applications.

Biocompatibility and Stability: Similar to other silicone-based materials, DMSN is biocompatible and non-toxic, thus avoiding secondary contamination problems in practical applications. In addition, DMSN exhibits excellent stability under conditions such as high temperatures and harsh chemical environments, which is critical for applications in extreme environments.

Synthesis of monodisperse dendritic silica (DMSN). Unlike the synthesis of MCM-41 and SBA-15 with ordered structures, the preparation of DMSN is relatively complex and versatile. So far, the following synthetic methods including surfactant-assisted synthesis, microemulsification techniques and dual template methods have been widely used depending on the characteristics in the synthesis. They are summarized in Table. 1.2. The following are the main synthetic routes for DMSNs:

Table 1.2 - Characteristics of mesoporous silica under different preparation methods

Synthesis Methods	Formation Mechanism	Main Applications
Microemulsion-Template Method [102]	Microemulsion three-phase synergistic control of core-shell growth	Nanomedicine [103], catalysis[104]
Biphase Stratification Method [105]	The reaction occurs at the oil-water interface	Pollutant degradation [106], Adsorption [107].
Aqueous Solution Method [108]	No organic solvents, the silica-derived micelles grow orderly on the surface	Adsorption[109], medicine [110]

Microemulsion-Template Method

The microemulsion-template method is one of the most common methods for synthesizing DMSN. In the synthesis process, an oil-water mixture of water, surfactant and organic solvent is used to form microemulsion droplets, and this oil-water mixed phase will act as a template. Then silica precursors (e.g., tetraethyl orthosilicate (TEOS)) are added to the template, which hydrolyzes and condenses around the template, ultimately resulting in the formation of a dendritic mesoporous structure [111].

Biphase Stratification Method

The Biphase Stratification Method refers to a synthesis method in which the synthesis reaction occurs at the oil-water interface. This method dissolves the silicon source in the upper hydrophobic organic phase, and the surfactant is dispersed in the lower water phase. During the reaction, the silicon source diffuses from the oil phase to the water phase and undergoes hydrolysis and condensation reactions, forming an ordered co-assembly structure with the surfactant in the lower layer. Under the hydrophobic effect of the organic solvent, a radial dendritic mesoporous structure is formed, and finally, a silicon nanomaterial with hierarchical porous characteristics is generated [105].

Aqueous Solution Method

The Aqueous Phase Synthesis Method is a method for synthesizing dendritic mesoporous silica in a pure aqueous phase system without the need for organic solvents. Its main mechanism is to form composite micelles through anion-assisted templates (such as salicylate, heptafluorobutyrate, etc.) and cationic surfactant CTAB, and then guide the silicon source to assemble and grow in an orderly manner on the micelle surface through electrostatic action, eventually forming dendritic silica. This method avoids the use of organic solvents, so it has advantages in greenness and ease of operation, and is one of the most widely used synthesis strategies [112].

Surface modification of mesoporous silica and its complexes. Surface modification or complexation of mesoporous silica becomes essential when a single silica is not sufficient for a particular application. Typically, the modification of the surface of mesoporous silica consists of two aspects, one is the introduction of functional groups and organic molecules on its surface; the other approach is to use it as a substrate for complexing with other high-performance materials to enhance its performance in areas such as catalysis, drug delivery and adsorption of pollutants in water.

Introduction of Functional Groups and Organic Molecules: By introducing different functional groups on the surface of mesoporous silica, the chemical reactivity, selective adsorption ability and targeting ability in biomedical fields can be effectively enhanced. Common surface modification groups include amino, carboxyl, sulfhydryl and phosphate groups. These groups can interact with target molecules through covalent bonding or electrostatic attraction to enhance the functionality of the materials [101, 113].

Amino-functionalized: Amino-functionalized mesoporous silica can significantly improve its adsorption capacity for metal ions, especially for the removal of heavy metals (e.g. copper, lead, mercury, etc.) in water pollution [114, 115]. The amino group can be linked to the metal ions through complexation and can adsorb heavy metal ions in water more efficiently.

Sulfhydryl Modification: Sulfhydryl is a functional group that has an affinity

for heavy metals and can form strong bonds with heavy metal ions such as mercury, cadmium, and thallium to remove toxic metal contaminants. Roozbeh et al. demonstrated that sulfhydryl-modified mesoporous silica has a high affinity for the heavy metal thallium ion [116].

Polymer and biomolecule modification: Mesoporous silica can also be combined with polymers or biomolecules (e.g., DNA, antibodies) for drug delivery, gene therapy, and biosensors. Both selective recognition and treatment of specific cells or tissues can be achieved by modifying targeting molecules on the surface of the material [117].

Composite high-performance materials: Given the large number of pores and high specific surface area of mesoporous silica, as well as its excellent stability, in some applications, mesoporous silica with this characteristic is used as a substrate for loading high-performance materials (such as metal nanoparticles, oxides, or organic polymers) that can be easily agglomerated, and thus can provide a stable substrate for these reactive materials to greatly enhance their efficiency in specific reactions. The mesoporous silica stabilized substrate can give these reactive materials a stable base, thus greatly improving their reaction efficiency in specific reactions [118].

Metal nanoparticle composite: By introducing metal nanoparticles (e.g., gold, silver, palladium, platinum, etc.) into mesoporous silica, highly efficient catalysts can be formed for catalytic processes in organic chemical reactions. For example, palladium nanoparticles loaded on mesoporous silica can be used to exhibit efficient catalytic activity in hydrogenation reactions [119].

Magnetic nanomaterial composites: Magnetic adsorbents can be prepared by compositing mesoporous silica with magnetic nanomaterials (e.g., zero-valent iron), a system that is particularly suited for the rapid separation and regeneration of materials in pollutants, both by simply removing the reacting material from the reaction system through magnetic adsorption, thus eliminating the need for a post-reaction treatment step. For example, Roxana's group has applied this magnetically adsorbable silica mesoporous material to the adsorption of dyes in the water column, and after the

adsorption reaction is complete, the magnetic adsorbent can be removed from the water column under the influence of external magnetic forces [120].

Oxide composites: In fields such as photocatalysis, water adsorption and energy storage, mesoporous silica is also able to be composited with zinc oxide, titanium dioxide [121, 122]. Such composites are particularly promising for photocatalytic degradation of organic pollutants, selective adsorption and electrochemical sensors.

Practical applications of mesoporous materials. Given the unique properties of mesoporous silica, such as high specific surface area, tunable pore size and hole size on demand, and chemical stability, one can find it in a variety of fields. Their ability to encapsulate, adsorb and release molecules makes them multifunctional materials for applications such as environmental remediation, medicine and catalysis.

Mesoporous Silica in Medicine. Currently, one of the most widely used areas of mesoporous silica applications is in the biomedical direction. The tunable pore size, high specific surface area and biocompatibility of mesoporous silica materials make them ideal candidates for drug delivery, imaging and diagnostic applications. For example, in drug delivery systems, many researchers have been working on the application of mesoporous silica in drug delivery systems due to its ability to encapsulate various therapeutic agents, including small molecule drugs, proteins and nucleic acids. The porous structure of mesoporous silica gives it excellent loading capacity for drug molecules, while the large number of functional group sites on its surface can be specially functionalized with targeted ligands to achieve selective drug delivery to specific tissues or cells [123, 124]. In addition, they can be designed in synthesis to release drugs in response to specific stimuli such as pH, temperature or the presence of enzymes, which makes them particularly suitable for the controlled release of chemotherapeutic drugs in cancer therapy [125]. Mesoporous silica can also be used as an imaging agent for diagnostic purposes. By equipping the MSN surface with homing devices such as aptamers (Aps), this composite material functions as a cancer-targeting and imaging agent, as shown by Somayeh et al. both Ap-armed MSNs can actively deliver drugs to the target location, and at the same time, this structure can

effectively reduce the off-target effect, thus maximizing the therapeutic effect of drugs [126].

Application of mesoporous silica in the adsorption of water pollutants.

Mesoporous silica materials have great potential in the field of environmental remediation, especially in the adsorption of pollutants from water bodies. This is because they fulfill almost all the requirements of a good adsorbent, i.e., biocompatibility, environmental stability, high specific surface area, high loading capacity, and possession of a large number of functional groups that can be involved in the reaction [127]. Adsorption of pollutants on mesoporous silica is usually achieved by physical or chemical adsorption. Therefore, the addition of specific functional groups on the surface of mesoporous silica can significantly improve the adsorption capacity of mesoporous silica. For example, Lu et al. investigated MCM-41 and diaminylation MCM-41 as adsorbents for the removal of ciprofloxacin, and their results showed that the diaminylation MCM-41 had a more efficient ability to remove ciprofloxacin from the water column [128]. Ahmadsreza's team synthesized 3-mercaptopropyltrimethoxysilane-functionalized mesoporous fibrous silica nanospheres by a one-pot method and tested their adsorption properties for the toxic cationic dye crystal violet. The maximum adsorption capacity of 3-mercaptopropyltrimethoxysilane-functionalized mesoporous fibrous silica nanospheres reached 164.3 mg g⁻¹.

The rich surface and stable structure of mesoporous silica can also provide a stable carrier for other aqueous adsorbent materials. In order to increase the adsorption performance of mesoporous silica materials, researchers often try to composite them with other efficient adsorbents to increase the reactive charge strength or reactive sites. Deng et al. prepared a silicate-hydrochar composite in 2020, in which the hydrochar has abundant reactive functional groups but its small specific surface area and pore volume limit its role in adsorption. In this system, the silica has rich reactive functional groups but the small specific surface area and pore volume limit its role in adsorption, while the silica composite with hydrochar has rich mesopores on the surface and inside to make up for the lack of hydrochar material, this efficient hybrid silicate-

hydrothermal carbon composite shows excellent adsorption capacity for heavy metals Cu^{2+} and Zn^{2+} as well as tetracycline (TC) [129]. Li et al. on the other hand showed interest in magnetic materials, they synthesized a magnetic mesoporous silica (NZVI-SH-HMS) material by gel-sol and wet impregnation methods at room temperature, the surface of this material was co-modified by thiols and nano-zero-valent iron, and experiments showed that this material exhibited good ability to remove lead and cadmium ions from the water. In addition, the introduction of zero-valent iron brings about magnetic properties, so the adsorbent can be quickly separated from the solid-liquid using a magnet after adsorption [130].

Mesoporous silica in other applications. In addition to pharmaceuticals and adsorption, mesoporous silica materials play a role in catalysis, fuel cells and sensors [131 - 133]. In catalysis, the high surface area and well-defined pore structure of mesoporous silica materials provide an ideal environment for catalytic reactions to occur. Therefore, it is widely used as a catalyst or catalyst carrier for various chemical reactions, and one can significantly improve its catalytic activity by loading precious metals on its surface, such as modifying Au/Pd bimetallic alloy nanoparticles on mesoporous silica-modified gC₃N₄ nanosheets, which can significantly increase the ability of photocatalytic oxidation and reduction of hexavalent chromium [134]. Mesoporous silica materials can also be used as composite membranes in the field of fuel cells to improve the stability of the materials, for example, its composite with phosphotungstic acid to form a new proton exchange membrane for high-temperature fuel cells. The proton conductivity of the HPW/MCM-41 mesoporous silica inorganic PEM is 0.018 and 0.045 S cm⁻¹ at 25 and 150 °C, respectively [135]. In addition, mesoporous silica materials can be used in chemical sensors [136]. Due to their high surface area and adjustable pore size, mesoporous silica materials can be used for the detection of pollutants, biomolecules, or gases by adjusting their pore structure or functionalizing their surface to selectively adsorb target molecules. Functionalized mesoporous silica, for example, can interact specifically with the target analyte, thereby increasing the sensitivity and selectivity of the sensor [137].

In conclusion, mesoporous silica materials have a wide range of applications in different fields such as pharmaceuticals, water adsorption, catalysis, fuel cells and sensors due to their unique structural features, including extremely high specific surface area, adjustable pore size and chemical stability. Especially in the field of adsorption, the special morphology and adjustable pore size of mesoporous silica and rich surface functional groups endow it with excellent adsorption capacity for pollutants in water. In addition, its stable structure and large specific surface area allow it to be loaded or modified with other materials such as iron, nickel and other metals to obtain different functional groups and active sites, thus further expanding their use and performance. Therefore, the continuous development and functionalization of mesoporous silica (especially DMSNs) is very necessary, and we believe that the in-depth development and understanding of their adsorption mechanism and properties will bring perfect solutions in the fields of water pollutant treatment, biomedicine, and advanced energy systems someday in the future.

1.3.2 Adsorbents based on aluminosilicates raw materials

The production of sorption materials based on inexpensive natural raw materials for use in technologies for treating a wide range of contaminated wastewater, surface, and groundwater is based on the targeted regulation of the porous structure parameters and molecular structure of the surface layer of sorbents during their synthesis. The goal is to achieve optimal ion-exchange and adsorption properties with respect to inorganic and organic toxicants.

Natural layered silicates are widely used in the production of sorption materials for water purification from metal ions and organic substances [138 - 141]. On their basis, composites with unique physicochemical and structural-sorption properties are obtained [142, 143]. This is due to the adsorption and ion-exchange properties of clay minerals, their high dispersity, and their chemical and thermal stability [144].

The availability of various methods to regulate their structure and surface chemistry, the presence of industrial deposits, and the low cost of clays make them

suitable for many technological processes. Based on knowledge about the crystalline structure of clay minerals and with the use of modern physical and physicochemical research methods, mechanisms of interaction between layered silicates and various substances are studied. This allows researchers to find the most effective ways to control the adsorption, catalytic, and other properties of inorganic silicate sorbents, as well as to determine rational ways of their use.

Although natural aluminosilicates possess high dispersity and the ability to exchange and adsorb cations, various surface modification methods are applied to improve their structural and sorptive characteristics. These include mechanochemical, thermal, and chemical treatments using acid, alkali, and metal salt solutions, as well as organic and organosilicon compounds [145]. Significant attention is currently paid to sorbents based on natural clay minerals modified with polymers. This is due to the possibility of introducing functional groups of high-molecular compounds during synthesis, both into the interlayer space of clays and onto the surface of the mineral. The attached functional groups (hydroxyl, carboxyl, amino, etc.) significantly enhance the ability of clay sorbents to adsorb heavy metals from water due to their increased selectivity for such pollutants [146].

In [147], montmorillonite was synthesized and functionalized with 3-aminopropyltriethoxysilane (APTES). The resulting composite showed stronger adsorption capacity for Co^{2+} than the original clay mineral. In another study [148], a series of organomontmorillonites were synthesized and their efficiency towards Sr(II) ions was studied.

A key criterion for evaluating an adsorbent is its reusability. A sorption material was obtained by functionalizing vermiculite with hexylamine, which showed higher efficiency for As(III) than the original mineral. During five consecutive adsorption-desorption cycles, the modified vermiculite maintained high adsorption capacity, indicating strong regeneration potential [149]. In [150], vermiculite was modified with ethylamine to study its adsorption capacity for cesium. A material with high specific surface area and a branched porous structure was obtained, demonstrating much greater efficiency than the original mineral. The maximum cesium adsorption increased from

56.92 mg/g (original mineral) to 78.17 mg/g (modified sample).

Studies have shown that doping clay minerals with metal ions or their compounds significantly improves their adsorption properties. The incorporation of transition metal elements into the surface or interlayer space of aluminosilicates enhances their adsorption capacity for heavy metal ions and organic pollutants. For example, doping clay with iron ions can improve its adsorption characteristics for Cr(VI) and Cd(II) [151].

Using metal salts, urea, and palygorskite under hydrothermal crystallization conditions, a layered adsorbent was obtained that was highly effective in removing Pb^{2+} , Cu^{2+} , and Ni^{2+} ions from aqueous solutions [152]. Clay materials pillared with cerium compounds are promising adsorbents. They demonstrate high efficiency in purifying aqueous solutions contaminated with Cd^{2+} , Co^{2+} , and Cu^{2+} ions [153].

A composite geopolymer material based on bentonite clay with embedded Fe_3O_4 magnetic nanoparticles exhibited high affinity for copper, lead, nickel, and cadmium ions [154]. Nanocomposites based on kaolin and TiO_2 effectively remove Pb(II) and Cd(II) ions from aqueous solution, with maximum adsorption capacities reaching 333 mg/g for Pb(II) and 250 mg/g for Cd(II) [155].

Modification of clays with organic surfactants leads to the production of hybrid organic-inorganic composites capable of removing various organic and inorganic pollutants from water. For example, montmorillonite modified with octadecan-betaine can simultaneously adsorb bisphenol A and Cd^{2+} from aqueous solutions [156].

Natural and synthetic zeolites - hydrated aluminosilicates with a framework structure - are also of great scientific interest. They feature a system of regular channels and interconnected cavities that can hold ions, atoms, and molecules whose sizes match the free space. Because of their rigid crystalline structure with well-defined pore sizes, zeolites are effectively used for separating gas and liquid mixtures, purifying substances, and as catalysts. Synthetic zeolites are produced by hydrothermal crystallization in aqueous aluminosilicate systems (in the case of aluminosilicate zeolites) under atmospheric or elevated pressure [157].

Hydrothermal synthesis involves the effect of high temperatures on solutions

containing silicon and aluminum compounds. One promising source of Si and Al for zeolite synthesis is fly ash - a byproduct of coal combustion at power plants. Fly ash has low bulk density and thermal conductivity, and high stability in alkaline solutions and at high temperatures. The particle size of fly ash ranges from 5 to 500 μm . Chemically, these materials are multicomponent systems containing about 90 wt % of SiO_2 , Al_2O_3 , and Fe_2O_3 [158]. In [159], zeolite synthesized from fly ash using microwave-assisted thermonuclear and hydrothermal synthesis demonstrated high efficiency in removing Cu^{2+} , Zn^{2+} , Ni^{2+} , and Pb^{2+} ions from water.

New promising materials for removing heavy metals from aqueous environments include fly ash-based geopolymers [160]. Various nano-, micro-, and mesoporous composite materials for environmental protection have also been developed, with fly ash used as the main source of silicon and aluminum [161].

Thus, scientific interest in the development of sorption materials based on aluminosilicate raw materials is steadily growing. Researchers increasingly focus on surface functionalization of clay minerals, which improves the structural-sorption characteristics and physicochemical properties of the resulting materials. Sorbents derived from aluminosilicate raw materials hold great promise in the field of environmental protection due to their availability and low cost.

Conclusions to Chapter 1

The analytical review of the literature on methods for obtaining adsorption materials based on synthetic silicas, natural and artificial aluminosilicate raw materials was conducted. The sources of heavy metal ions and organic dyes entering water bodies were analyzed. Special attention was paid to adsorption processes that are economically feasible and effective for purifying water from inorganic and organic toxicants that are in low concentrations compared to other pollutants. It was shown that surface modification of synthesized silicas and aluminosilicates with zero-valent iron particles, organosilicon compounds, oxides and metal oxyhydroxides leads to a significant increase in their adsorption capacity.

CHAPTER 2

RESEARCH OBJECTS AND METHODS

2.1 Research objects

2.1.1 Reagents, materials, experimental instruments and equipment

The reagents required for the synthesis of the materials are shown in Table 2.1.

Table 2.1 - Main reagents required for the synthesis of the materials based on silica and aluminosilicates

Chemical reagents	Molecular formula	Manufacturer
Cetyltrimethylammonium bromide (CTAB)	$C_{19}H_{42}BrN$	MERCK, Germany
Triethanolamine (TEA)	$C_6H_{15}NO_3$	MERCK, Germany
Tetraethoxysilane (TEOS)	$SiC_8H_{20}O_4$	MERCK, Germany
Sodium Salicylate (NaSal)	$C_7H_5NaO_3$	MERCK, Germany
Sodium Borohydride	$NaBH_4$	MERCK, Germany
Iron(III) chloride hexahydrate	$FeCl_3 \cdot 6H_2O$	CHEMLABORREACTIV LLC (Ukraine)
Ethanol	C_2H_6O	CHEMLABORREACTIV LLC (Ukraine)
Nickel Nitrate	$Ni(NO_3)_2 \cdot 6H_2O$	Sigma-Aldrich (USA)
Nitric Acid	HNO_3	Sigma-Aldrich (USA)
Sucrose	$C_{12}H_{22}O_{11}$	Sigma-Aldrich (USA)
Sodium Hydroxide	$NaOH$	CHEMLABORREACTIV LLC (Ukraine)
Sodium Chloride	$NaCl$	CHEMLABORREACTIV LLC (Ukraine)
Sodium alginate	$(C_6H_7O_6Na)_n$	CHEMLABORREACTIV LLC (Ukraine)
Calcium chloride	$CaCl_2$	CHEMLABORREACTIV LLC (Ukraine)
Aluminum metal granulated	Al	CHEMLABORREACTIV LLC (Ukraine)

All chemicals used in this work were in analytic grade and used without further purification. The materials required for the synthesis of the materials based on commercial silica and aluminosilicates are shown in Table 2.2. The experimental instruments and equipment are shown in Table 2.3.

Table 2.2 - Materials required for the synthesis of the materials based on commercial silica and aluminosilicates

Materials	Description of the material	Manufacturer
Commercial High Purity Grade Silica Gel	Amorphous silica (SiO ₂)	Sigma-Aldrich (USA)
Saponite	Aluminosilicate from the Tashkivske deposit (Ukraine)	Limited Liability Company VELES (Ukraine)
Fly ash microsphere	Commercial aluminosilicate microspheres	Recycling Solutions Company (Poland)

Table 2.3 - Experimental instruments and equipment

Equipment	Model or specification	Manufacturer
Magnetic stirrer	JOANLAB	China
Top-drive mixer	JOANLAB	China
Analytical balance	RADWAG AS 220.R2	Poland
Technical balance	KERN EBM 1200-1	Germany
Heating drying oven	MEMMETR	Germany
Muffle furnace	SNOL	Ukraine
Centrifuge	MPW-340	Poland
Thermostat	TW-2.02 ELMI	Latvia
Shaker	OS-20	Latvia
Peristaltic pumps	G728-1-1	China
Conductometer	EZDO 4805	Taiwan
Mini laboratory pump	KNF LAB	Germany

2.1.2 Method for preparation of dendritic mesoporous silica nanoparticles

The dendritic mesoporous silica nanoparticles (DMSN) were synthesized by one-pot method according to a modified method described in [100, 162, 163]. In the first stage, 1.36 g of triethanolamine (TEA) were dissolved in a 500 ml of distilled water. The solution obtained should be placed in a water bath set at 80 °C with uniform stirring for a period of 30 minutes. Subsequently, 7.6 g of cetyltrimethylammonium bromide (CTAB) and 3.36 g of sodium salicylate (NaSal) should be added to the system, and stirring should continue for an additional hour. Concurrently, a solution comprising 80 ml of tetraethoxysilane (TEOS) and 10 ml of ethanol should be prepared and introduced to the mixture via peristaltic pump over a period of 30 minutes, with constant stirring. After that, the mixture was continuously stirred for a further 90 minutes at 80 °C. Then, the solid phase is separated from the liquid phase by centrifugation and washed three times with a mixture of water and ethanol. The resulting precipitate is then calcined at 550 °C for a period of 6 hours. The obtained sample is coded DMSN-1.5. The additional two samples were synthesised in a methodology analogous to that described above, with the stirring time increased from 90 minutes to 180 minutes and 300 minutes. Accordingly, these samples are coded DMSN-3 and DMSN-5, respectively. The general synthesis steps are shown in Fig. 2.1.

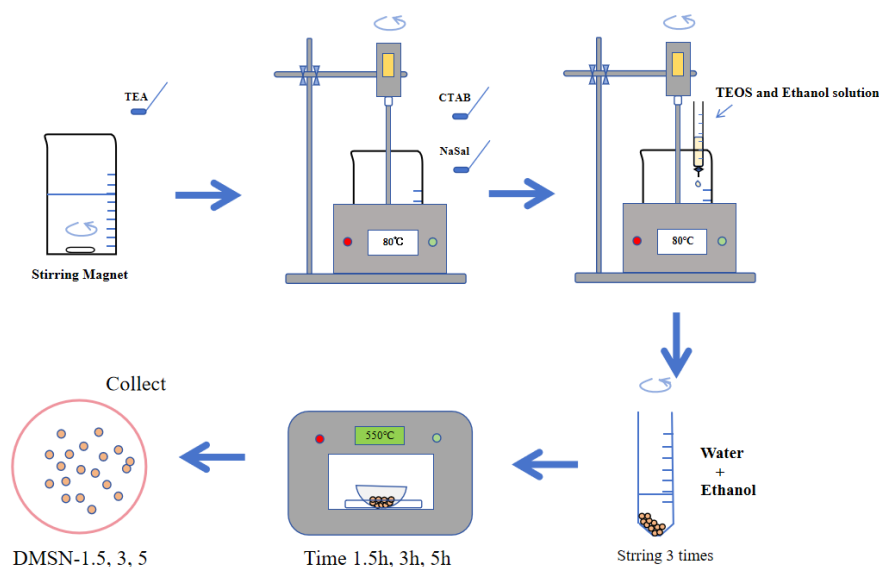


Fig. 2.1 - Preparation process of DMSN materials

2.1.3 Method for preparation of zero-valent iron supported by dendritic mesoporous silica nanoparticles

Zero-valent iron supported by dendritic mesoporous silica nanoparticles was synthesized according to a reported method with slight modifications [164]. The DMSN sample was mixed with a solution of $\text{FeCl}_3 \cdot 6\text{H}_2\text{O}$ of a certain concentration and stirred for 30 minutes on a magnetic stirrer. The mass ratio of Fe^0 to DMSN was 0.2:1. The resulting suspension ($\text{pH} = 2$) was quantitatively transferred to a three-neck flask and the process of reducing Fe^{3+} ions with 0.1N sodium borohydride solution under a nitrogen atmosphere was carried out. After that, the obtained composite ($\text{Fe}^0\text{@DMSN}$) was separated from the liquid phase by centrifugation and washed three times with alcohol. The resulting precipitate was dried under vacuum at 60°C and ground to a fraction of ≤ 0.1 mm.

2.1.4 Method for preparation of amino-functionalized dendritic mesoporous silica nanoparticles

The amino functionalization of the surface of the synthesized DMSN-1.5 was carried out by post-coupling using 3-Aminopropyltriethoxysilane (APTES) in an aqueous-alcoholic medium according to a modified procedure [165, 166]. For this purpose, a DMSN sample was placed in a water-alcohol solution (1:3) acidified with concentrated HCl. The mixture was transferred to a three-necked flask in a thermostat (temperature 80°C). With constant stirring, the APTES alcohol solution was added to the system, which was fed dropwise using a peristaltic pump for 1 hour. Fig. 2.2 shows a schematic of the setup illustrating this process.

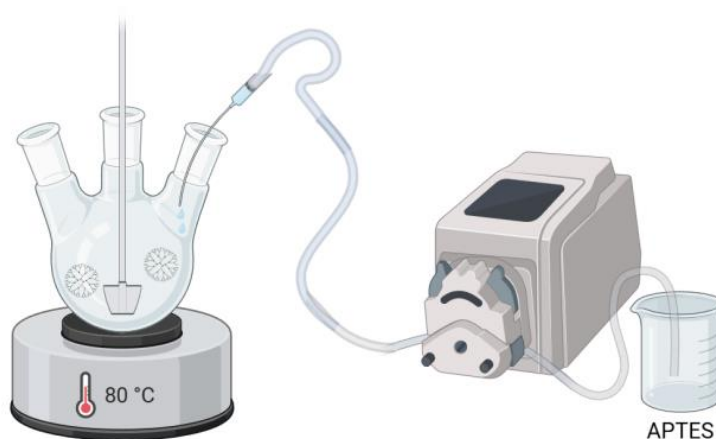


Fig. 2.2 - Schematic diagram of the installation for amino functionalization of DMSN surface

2.1.5 Method for preparation of silica gel modified with nickel oxide

Sorption materials were synthesized according to the modified method described in [167]. Fig. 2.3 schematically depicts the process of sorbent synthesis.

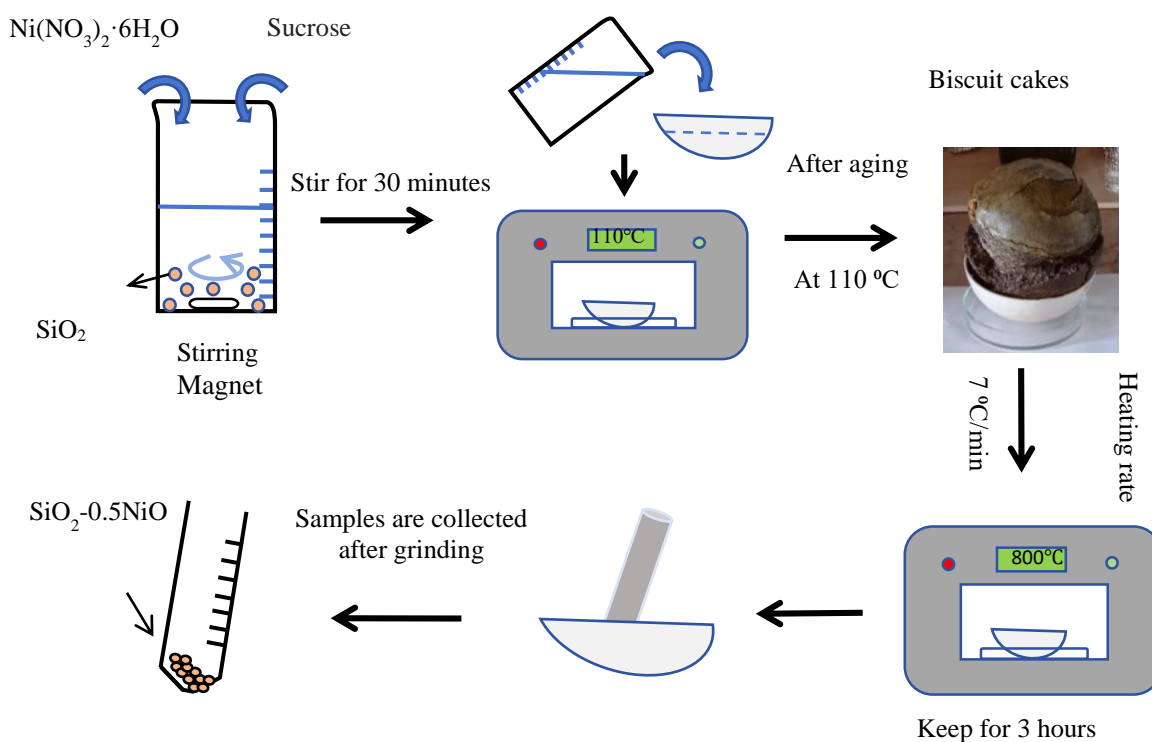


Figure 2.3 - Scheme of preparation of a sorbent based on silica gel modified with nickel oxide

First, 2 wt. % aqueous suspension of SiO_2 was prepared. Then, while continuing to stir with a magnetic stirrer, the calculated amount of $\text{Ni}(\text{NO}_3)_2 \cdot 6\text{H}_2\text{O}$ and sucrose was added sequentially. The mass ratio of NiO to SiO_2 was 1:1 and 0.5:1. After complete dissolution of the reagents, several cm^3 of HNO_3 were added and the mixture was stirred for 30 minutes at room temperature. The next stage of synthesis consisted of several successive stages of temperature treatment at 110 °C, 250 °C and 800 °C. After holding at 110 °C, the samples resembled biscuit cakes in appearance. The temperature of 800 °C corresponds to the thermolysis process in air, which was carried out at a heating rate of 7 °C/min and holding at the maximum temperature for 3 hours. For further studies, the fired samples were crushed and sieved to obtain a fraction ≤ 0.315 mm.

2.1.6 Method for preparation of granular adsorption materials based on clay minerals and biopolymers

To obtain adsorption materials, we used saponite from the Tashkivske deposit (Sap), which is a layered aluminosilicate of the smectite group with a 2:1 structure, and commercial sodium alginate (Alg), which is a natural polysaccharide, an anionic polymer derived from marine brown algae. The synthesis of ferrihydrite-modified saponite (Sap.Fh) with a mass ratio of clay mineral to Fe^{3+} equal to 1:1 was carried out according to the method [168]. The natural aluminosilicate (Sap-Alg) and iron-modified aluminosilicate (Sap.Fh-Alg) adsorbents were granulated according to the method described in the literature [169]. In this case, to ensure reproducible results, it is important to obtain a homogeneous suspension, which can be achieved by thoroughly mixing the experimental reagents for a defined period of time. Thus, the weight of the clay mineral or its modified form was added to a container with distilled water and continuously stirred with a paddle stirrer for 30 minutes. Then, a certain volume of 1.5% sodium alginate solution was gradually added to this mixture by drops and additionally stirred for another 30 minutes (as shown in Fig. 2.4, part A). To obtain granular adsorbents, the container with the prepared suspension was placed on the

platform of an orbital shaker, which stirred it at a given speed so that it could be fed dropwise into a vessel with a 0.2M CaCl_2 solution using a peristaltic pump. Ca^{2+} cations in this case act as a “cross-linking” agent (as shown in Fig. 2.4, part B) [170]. The formed spherical granules were left in this solution for a day and then washed with distilled water to remove excess salts. Washing was monitored using a conductometer. After that, the samples were dried in an oven in two stages: the first 2 hours at 80 °C and the second 2 hours at 105 °C.

Part A: Preparation of clay mineral suspension with sodium alginate

Part B: Granulation process

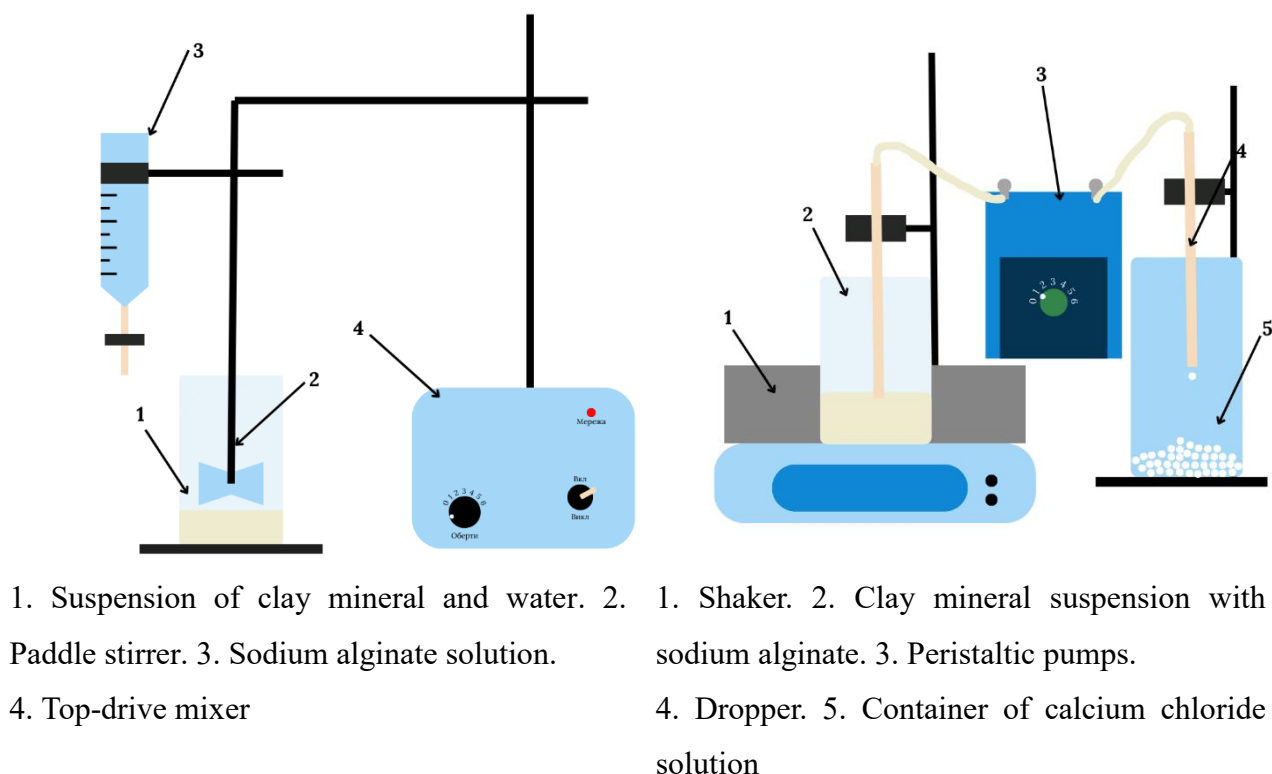


Fig. 2.4 - Scheme of preparation of granular adsorption materials based on clay minerals and biopolymers

2.1.7 Method for preparation of mesoporous adsorbents from coal fly ash

To obtain a mesoporous adsorbent based on fly ash, commercial aluminosilicate microspheres were used, which had a bulk density of 0.37 g/cm³ to 0.41 g/cm³, a

specific gravity of 0.65 g/cm³ to 0.75 g/cm³, and an average grain size of 140 µm to 155 µm. Additional sources of sodium and aluminum for obtaining zeolites were a solution of sodium aluminate (NaAlO₄), which contained 150 g/dm³ Na₂O and 50 g/dm³ Al₂O₃. To obtain it, granulated metallic aluminum was dissolved in a solution of sodium hydroxide. The synthesis of the zeolite phase on the surface of aluminosilicate microspheres was carried out at a temperature of 90 °C for 5 hours under thermostatic conditions with constant stirring. The ratio of solid and liquid phases was 1:50. The obtained material after the end of the synthesis was separated from the solution by decantation and repeatedly washed with distilled water from excess salts to a neutral pH value of the washing water. The washing was monitored using a conductometer. The resulting precipitate was dried at 90°C.

2.2 RESEARCH METHODS

The instrument and equipment information required for this experiment is shown in Table 2.4.

Table 2.4 - Experimental instruments and equipment

Equipment	Model or specification	Country of manufacture
Spectrophotometer	UNICO UV 2100	USA
Spectrophotometer	iCAP 7400 ICP-OES	USA
Rotational viscometer	Rheotest-2	Germany
Derivatograph	Q-1000, IOM	Hungary
X-ray photoelectron spectrometer	PHI 5600	USA
Surface Area and Pore Size Analyzer	Quantachrome NOVA-1200e	USA
Fourier transform infrared spectrometer	Bruker Vertex 70 model	Germany
X-ray diffractometer	XD-8	Germany
Scanning electron microscope	Nova Nano SEM450	USA
Transmission electron microscope	JEM-2010F	Japan

2.2.1 Methods for studying the surface morphology of the obtained materials

Scanning electron microscopy (SEM) with energy dispersive X-ray spectroscopy (EDS)

A Nova Nano SEM450 scanning electron microscope (Field Emission Scanning Electron Microscope) with energy dispersive X-ray spectroscopy (EDS) produced by FEI Company of the United States was used to scan and analyze the elements of the material to obtain the microscopic morphology and element distribution of the adsorbent. Before the study, a small amount of powder was applied to an adhesive conductive substrate (carbon tape SPI 05081-AB), which was covered with a thin (30 nm) layer of conductive material (Au/Pd mixture) using a Gatan 682 PECS device, in order to avoid local charge accumulation during the study by scanning electron microscopy. The analysis of the obtained images was performed using ImageJ software. Point elemental analysis was performed at different points on the surface to minimize the influence of possible surface inhomogeneities.

Transmission electron microscopy (TEM)

High-resolution TEM images were tested using a JEM-2010F transmission electron microscope at an accelerating voltage of 200 kV to obtain high-resolution internal structures of the materials. To carry out the study, a small amount of powdered material was dispersed in ethanol using an ultrasonic device. Then, the suspension was pipetted onto the test grid of the TEM device. The samples were examined after evaporation of the solvent and drying of the sample at room temperature.

2.2.2 Methods for determining the phase composition of samples and surface chemistry

X-ray diffraction analysis (XRD)

The monominerality of the materials and the qualitative composition of the modified samples obtained on its basis were controlled using X-ray diffraction analysis (X-ray diffractometer XD-8 with two Soller slits, filtered with $\text{CuK}\alpha$ radiation in the range $2\theta = 10 - 80^\circ$). The Match! software with an integrated international PDF-2 diffractogram database was used to interpret and decipher the results obtained.

X-ray photoelectron spectroscopy (XPS) analyses

The X-ray photoelectron spectroscopy (XPS) analyses were carried out with a PHI 5600 spectrometer using a monochromatic Al K (α) source. The instrument work function was calibrated to give a binding energy (BE) of 84 eV for the Au $4f_{7/2}$ line of metallic gold, and the spectrometer dispersion was adjusted to give a BE of 932.6 eV for the Cu $2p_{3/2}$ line of metallic copper. Survey scan analyses were carried out with a pass energy of 93.9 eV and a step size of 0.2 eV. The charge neutralization on the samples was adjusted to get the peak position of C 1s C-C peak at 284.8 eV.

Fourier-transform infrared spectroscopy (FTIR) analyses

The Fourier-transform infrared spectroscopy (FTIR) study was carried out in the wavelength range of $4000\text{--}400\text{ cm}^{-1}$ using a Fourier spectrometer Bruker Vertex 70 with the standard method of tableting with potassium bromide (KBr). The samples under study were thoroughly mixed with KBr powder in a mass ratio of 1:300, and the resulting mixture was pressed into transparent tablets with a diameter of 13 mm.

2.2.3 Methods for determining the parameters of the porous structure of samples

Method of low-temperature nitrogen adsorption-desorption (BET)

The method of low-temperature (-196 °C) nitrogen adsorption-desorption was used to study the surface parameters and porous structure of the synthesized samples. The samples were degassed in a vacuum before the measurement. The data obtained were processed using specialized software Quantachrome NovaWin version 11.04. The specific surface area (S_{BET} , m²/g) was calculated by the Brunauer-Emmett-Teller (BET) multipoint method, and the external pore surface (S_{ext} , m²/g) and micropore surface (S_{micro} , m²/g) were estimated by the t-method. The total pore volume (V_{Σ} , cm³/g) was determined by the maximum adsorbed volume of nitrogen at a relative pressure $p/p_0 \approx 1$ (0.99). The micropore volume (V_{micro} , cm³/g) was estimated by the t-method, and their percentage content (V_{micro} , %) was calculated using the following formula:

$$V_{\text{микро}} = \frac{V_{\text{микро}}}{V_{\Sigma}} \cdot 100 \quad (2.1)$$

The average pore radius (R , nm) was calculated using the following formula:

$$R = \frac{2V_{\Sigma}}{S_{BET}} \quad (2.2)$$

The micropore volume was estimated by the t-plot method, and their content was calculated using the following formula:

$$W_{\text{микро}} = \frac{V_{\text{микро}}}{V_{\Sigma}} \cdot 100 \quad (2.3)$$

2.2.4 Methods for determining the thermal stability of the materials

Thermal and thermogravimetric analysis (DTA/TG)

Differential thermal and thermogravimetric analysis (DTA/TG) was performed on a derivatograph in the temperature range from 20 °C to 1000 °C, with heating in air a rate of 5 °C/min. Al₂O₃ was used as a comparison sample.

The study of the structural and sorption characteristics and thermal stability of the granular materials based on biopolymers and clay minerals was carried out on samples, the initial data for which are presented in Table 2.5.

Table 2.5 - Initial data for obtaining granular samples

№	Sample name	*Mass ratio of saponite to sodium alginate, $m_{\text{sap}}/m_{\text{alg}}$	Volume of the added sodium alginate solution V_{alg} , cm ³	Mass fraction of saponite in the suspension W , %
1	Sap-Alg (6:1)	6	40	9
2	Sap.Fh-Alg (6:1)	6	40	9

*The calculation is made on a dry basis

2.2.5 Methods for determining the rheological characteristics of the suspensions

To study the rheological characteristics of the prepared suspensions with different mass ratios of saponite and biopolymer, a rotational viscometer (Rheotest-2, Germany) with a system of coaxial cylinders was used under thermostatic conditions at 25 °C (thermostat U8, Germany). The initial data for the preparation of suspensions are given in Table 2.6.

Table 2.6 - Initial data for the preparation of suspensions

	Sample name	*Mass ratio of saponite to sodium alginate, $m_{\text{sap}}/m_{\text{alg}}$	Volume of sodium alginate solution added, $V_{\text{alg}}, \text{cm}^3$	Mass fraction of saponite in the suspension, $W, \%$
1	Sap-Alg (16:1)	16	15	9
2	Sap-Alg (32:1)	32	15	18
3	Sap-Alg (48:1)	48	15	27

*The calculation is made on a dry basis

2.2.6 Methods for determining of the content of functional groups on the surface of samples

Determination of the content of functional groups (-OH)

The method of reverse titration of benzoic acid in 0.05 N toluene with KOH solution in the presence of bromothymol blue indicator was used to determine the total concentration of the main centers [B] [171]. A 100 mg sample of DMSN, pre-annealed and cooled to room temperature without exposure to moisture, was added with 10 ml of a 0.05 N solution of benzoic acid in toluene. After 30 minutes of stirring, a 3 ml aliquot of the sample was taken and titrated. The amount of adsorbed benzoic acid was calculated from the difference between the amount of acid taken and the amount determined after adsorption.

The content of amino (-NH₂) groups (meq/g) was determined by the acid-base back-titration method [173]. The *weighted DMSN-NH₂ sample (at least 100 mg)* was immersed in 20 ml HCl (0.1 N) for 24 h, and the resulting solution was titrated with KOH (0.1 N). The content of -NH₂ groups was calculated by the following Eq. 2.4:

$$\text{The content of NH}_2 \text{ groups} = \frac{V_{\text{HCl}}N_{\text{HCl}} - V_{\text{KOH}}N_{\text{KOH}}}{m} \quad (2.4)$$

where: V is the volume of acid and alkali taken for titration, ml; N is the equivalent concentration of acid and alkali taken for titration, N ; m is the mass of the sample, g.

2.2.7 Methods for determining of the stability of the granules in the aqueous medium

The stability of the obtained granules in the aqueous medium was determined visually by observing the behavior of the samples shaken on a shaker for a certain time. To do this, a sample of the granular material was placed in a 100 cm³ conical flask and filled with a solution that simulated water contaminated with Cu²⁺ ions with a pH of 5.6-5.8 and an ionic strength of $I = 0.01$ on NaCl. The ratio of solid to liquid phases was 1:500, and the concentration of Cu²⁺ was 5 mg/dm³. The shaking time of the obtained granules with the solution ranged from 15 minutes to 5 hours.

2.2.8 Methods for determining sorption characteristics

Adsorption of heavy metal ions in water

The adsorption capacity of the obtained samples was evaluated using model solutions contaminated with Cu(II) ions in the concentration range of 10-100 mg/l. (CuSO₄·5H₂O purchased from Sigma Aldrich (St. Louis, MO, USA) was employed as the source of Cu (II)).

The ionic strength ($I=0.01$) was adjusted with a 1 M NaCl solution. The pH value was adjusted with 0.1 M NaOH solution and controlled with a pH meter (ADWA AD1020).

Experimental studies of the effect of pH on the degree of purification of model solutions from Cu(II) ions were carried out in the pH range from 3 to 6, which corresponds to the range of pH values with the highest percentage of Cu²⁺ form. The removal efficiency (R , %) of copper (II) ions was estimated by Eq. 2.5:

$$R = \frac{C_{in} - C_{eq}}{C_{in}} \cdot 100\% \quad (2.5)$$

where: C_{in} and C_{eq} are representing the initial and equilibrium copper concentrations (mg/l).

To study the kinetics of the adsorption process, the contact time of the adsorbent with the model solution (20 mg/l) was varied in the range from 15 to 60 minutes. The analysis of the kinetic process parameters was carried out using pseudo-first-order (PFO) and pseudo-second-order (PSO) models, represented by Eq.2.6 and Eq.2.7, respectively:

$$\ln(a_e - a_t) = \ln a_e - k_1 t \quad (2.6)$$

$$\frac{t}{a_t} = \frac{1}{k_2 a_e^2} + \frac{t}{a_e} \quad (2.7)$$

where: a_e and a_t (mg/g) are the adsorption capacity at equilibrium and at any time (min), respectively; k_1 (min^{-1}) and k_2 ($\text{g/mg} \cdot \text{min}$) are the PFO and PSO rate constant, respectively.

All adsorption experiments were carried out under static conditions at 20 ± 2 °C and continuous shaking of the samples (Biosan OS-20). The solid-to-liquid phase ratio was 1:500. After the adsorption equilibrium was established, the liquid phase was separated by centrifugation (3600 rpm), and the equilibrium concentration of copper was determined by inductively coupled plasma atomic emission spectroscopy (Thermo Scientific iCAP 7400 ICP-OES).

The adsorption capacity (a , mg/g) of copper ions was estimated by Eq. 2.8:

$$a = \frac{(C_{in} - C_{eq}) \cdot V}{m} \quad (2.8)$$

where: C_{in} and C_{eq} represent the initial and equilibrium copper concentrations (mg/l), V is the solution volume (L), and m is the weight of the adsorbent (g).

The Langmuir (Eq. 2.9) and Freundlich (Eq. 2.10) equations were used to describe the experimental adsorption isotherms of Cu(II) ions:

$$a_e = \frac{a_{max} K_L C_{eq}}{1 + K_L C_{eq}} \quad (2.9)$$

$$a_e = K_F C_{eq}^{1/n} \quad (2.10)$$

where: a_e (mg/g) is the equilibrium adsorption capacity, C_{eq} (mg/l) denotes equilibrium concentration, a_{max} (mg/g) is the maximum adsorption capacity, K_L (l/mg) denotes the Langmuir equilibrium constant, and K_F ((mg/g)(l/mg)^{1/n}) and $1/n$ are Freundlich constants related to the adsorption capacity and adsorption intensity, respectively [173].

Adsorption of dye in water

In a typical adsorption experiment, a fixed amount of 0.1 g of the adsorbent was added to a series of conical flasks containing methylene blue (MB) solution and continuously shaken at room temperature. Different variables were investigated in the experiments, including the concentration of the MB solution, the contact time, and the pH value, which all affect the adsorption efficiency of the material. After the adsorption equilibrium was established, the liquid phase was separated from the solid phase by centrifugation, and the equilibrium concentration of the dye in the aqueous phase was determined spectrophotometrically. The optical density of the solutions was determined on UNICO-UV 2100 spectrophotometer (USA) at $\lambda=665$ nm and an absorbing layer thickness of 1 cm. The adsorption value (a , mg/g) of methylene blue was calculated by the formulas 2.8 – 2.10.

Conclusions to Chapter 2

The method of obtaining dendritic mesoporous silica nanoparticles (DMSN) and sorption materials based on them is described. The surface of DMSN was modified with zero-valent iron particles and organosilicon compounds. The method of applying nickel oxide to the surface of commercial silica gel is presented. It is shown how granular sorbents based on natural clay and biopolymers were obtained and how an adsorbent was synthesized using fly ash. To study the morphology, structural and sorption characteristics and physicochemical properties of the obtained adsorbents, modern instrumental research methods were used, which are also presented in this chapter.

CHAPTER 3

SILICA-BASED MESOPOROUS MATERIALS FOR AQUEOUS POLLUTANTS REMOVAL

3.1 Synthesis and characterization of dendritic mesoporous silica nanoparticles

In this work, we try to search for optimal parameters for easy synthesis of monodisperse silica microspheres with controlled structural and physicochemical characteristics. The aim was to study the effect of synthesis time on the formation of silica microspheres for control of their surface morphological properties. The synthesis was conducted by alkaline hydrolysis in an aqueous/alcohol solution using structure-directing agents, namely cetyltrimethylammonium bromide (CTAB) and sodium salicylate (NaSal), in conjunction with an inorganic precursor, namely tetraethoxysilane (TEOS). The synthesis time varied from 1.5 to 5 hours. The following methods were used to study the synthesised silica microspheres: X-ray powder diffraction (XRD), Fourier-transform infrared spectroscopy (FTIR), scanning electron microscopy (SEM) and low-temperature N₂ adsorption/desorption method [165].

In order to investigate the impact of synthesis time on the morphology and structural properties of the synthesised silica microspheres, a series of studies were conducted.

The analysis of the obtained samples diffractograms (Fig. 3.1) revealed the presence of a single, broad diffraction peak at $2\theta = 22^\circ$, indicative of amorphous silica (JCPDS card No. 29-0085).

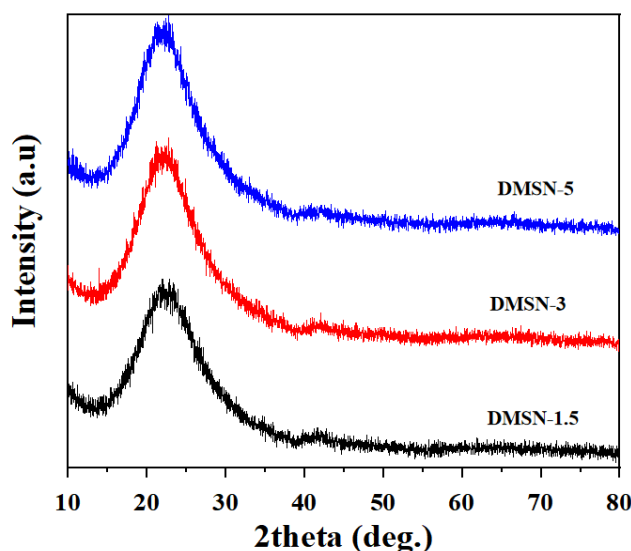


Fig. 3.1 - XRD diffraction patterns of synthesis silica materials

The analysis of structural features using infrared spectroscopy (Fig. 3.2) revealed that all samples exhibited a wide peak at 3433 cm^{-1} , which was identified as the antisymmetric stretching vibration peak of -OH group. The peak located at 1640 cm^{-1} was attributed to the bending vibrations of the water molecule [174]. Nevertheless, the intensity of these peaks is greatest for the DMSN-1.5 sample. This results from the fact that the calcination process produces a discontinuity in the dehydroxylation process. Once the hydrophobic surfactant molecules have been completely removed, the large surface area is then covered by silanol species, which immediately adsorb molecular water [174, 175]. The strong and wide band observed at 1093 cm^{-1} is attributed to the Si-O-Si antisymmetric stretching vibration. The peak observed at 966 cm^{-1} is attributed to the Si-O vibration bond of isolated Si-OH groups. The peak at 803 cm^{-1} is identified as the symmetric stretching vibration of the O-Si-O bond. Accordingly, the samples contain all the vibrational bands of Si-OH, O-Si-O and Si-O-Si, which are characteristic of amorphous DMSN [176, 177].

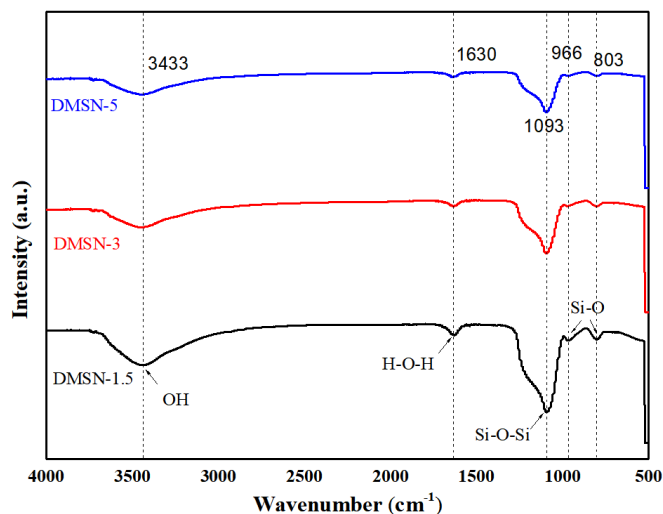


Fig. 3.2 - IR-spectra of synthesis silica materials

The morphology of silica is of critical importance in determining its properties and potential applications. The images obtained via scanning electron microscopy (Fig. 3.3) that silica microspheres, when subjected to varying reaction times, exhibit monodisperse spheres with a diameter of approximately 200 nm and evident pores. As illustrated in Fig. 3.3 (a, b), the spherical silica material subjected to a reaction time of 1.5 hours shows a nanoscale edge of approximately 7 nm and distinct mesopores. Furthermore, the high-magnification SEM image (Fig. 3.3a) reveals a substantial internal space within the silica spheres with acute edges. The spheres are observed to be isolated from one another, lacking any apparent bonding, which may facilitate the creation of a larger reaction area and the occurrence of specific reactions.

As illustrated in Fig. 3.3 (c, d), the reaction time of 3 hours results in a transformation of the silica spheres' edges from thin nanosheets to thicker strip-like edges. In particular, the dimensions of these edge nanosheets increase from 7 nm to 16 nm. Nevertheless, the edge shape and growth trend can still be discerned from the high-magnification SEM in Fig. 3.3 (c), indicating that it evolved from a thin edge. This

indicates that with an extended reaction time, the silica material continues to expand in the lateral direction rather than the longitudinal one. It is noteworthy that this change occurs solely in the thickness of the edges while the overall morphology with a 200 nm diameter is maintained.

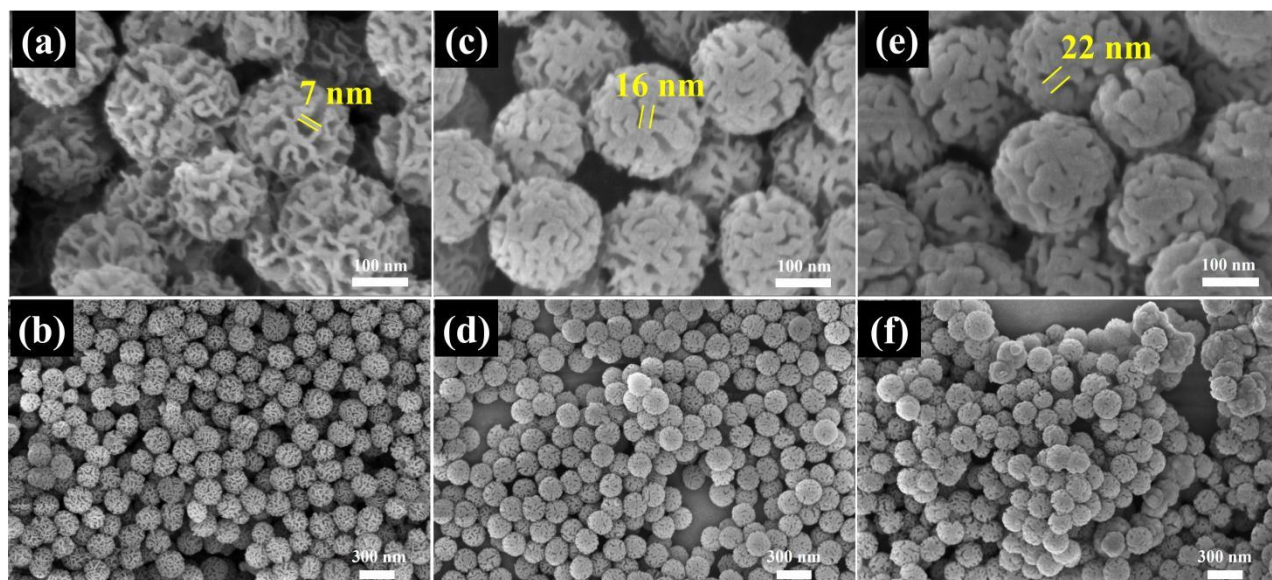


Fig. 3.3 - SEM images of silica microspheres (a, b – DMSN-1.5; c, d – DMSN-3; e,f – DMSN-5)

Upon reaching a reaction time of five hours (Fig. 3.3 e), while the overall size and morphology of the DMSN-5 material remain relatively consistent, exhibiting a spherical form with a porous structure, the edge widths continue to thicken, reaching up to 22 nm. At this juncture, the edges of the spherical silica are constituted entirely of nanostrips, and the presence of sharp edges is no longer discernible. At low magnification, as illustrated in Fig. 3.3 (f), the material begins to exhibit localized lumping or stacking. Consequently, a portion of the material loses its monodisperse nature, which leads us to conclude that further prolonging the reaction time is unnecessary.

The general principle of synthesis can be described as follows. In aqueous systems with CTAB and NaSal, the application of salicylate anion is role of form large pores, due to its superior micelle penetration effect. In particular, the strong electrostatic attraction and high miscibility of NaSal and CTAB result in a highly favourable interaction energetically. Sal^- anions ultimately migrate into CTA^+ micelles, with their hydrophobic portions inserted into the hydrophobic regions of the micelles. This results in an increase in the packing parameter, which induces a structural transition in the CTA^+ micelles from spherical to vesicular or lamellar, and subsequently to central radial [178]. An increase in the reaction time from 1.5 hours to 5 hours results in a slowing of the process, although it does not reach a complete halt.

The process of wall thickening of synthesised SiO_2 particles affects the overall textural parameters of the particles, including specific surface area, pore size and pore volume. As illustrated in Fig. 3.4, all samples of SiO_2 microspheres exhibited isotherms of low temperature nitrogen adsorption/desorption belong to the type IV isotherms with H3-type hysteresis loops according to the IUPAC classification. The nature of the hysteresis loop allows us to ascertain that the porous structure of all samples is constituted by spherical particles of homogeneous size, which is the same as commercial highpurity grade silica gel [179]. This type of isotherms is typical for materials with a mesoporous structure.

However, in comparison with the industrial silica sample, which exhibits a relatively narrow pore size distribution concentrated around 2.5-3 nm [179], the obtained samples (SiO_2 -1.5; SiO_2 -3; SiO_2 -5) display a considerably wider pore size distribution (Fig. 3.5). The pore sizes of all DMSN microspheres range from

approximately 5 to 50 nm.

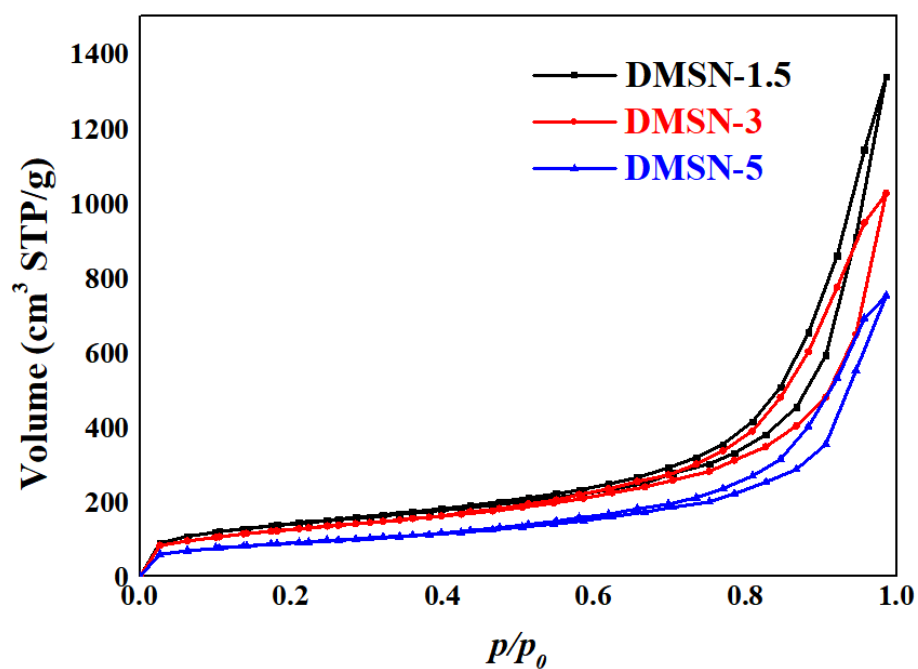


Fig. 3.4 - Isotherms of low-temperature N₂ adsorption/desorption of the synthesis DMSN

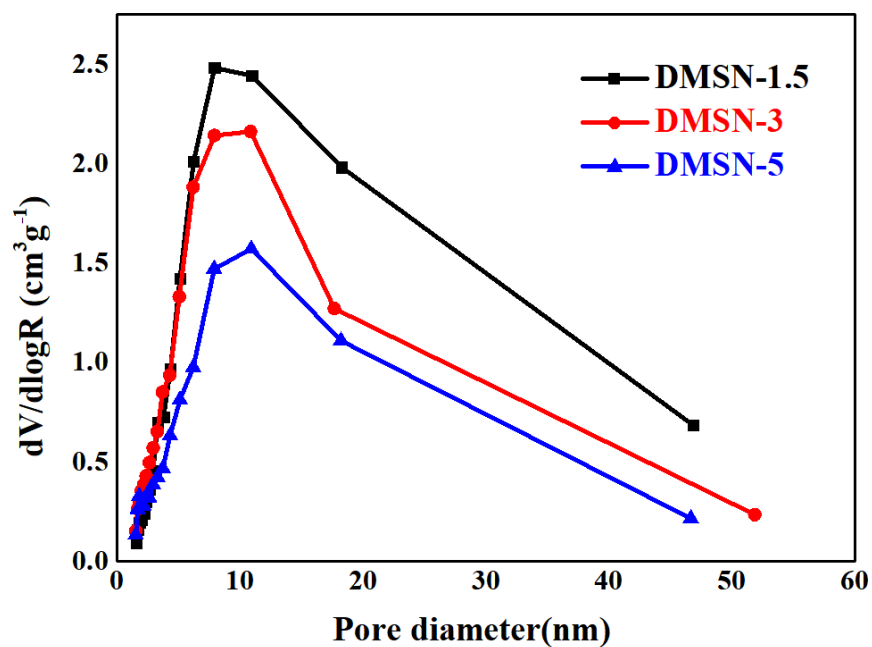


Fig. 3.5 - Pore size distribution by radius of the synthesis DMSN

The parameters of the porous structure of the investigated samples are presented in Table 3.1. As the synthesis time is increases, the specific surface area of the samples shows a gradual decrease of approximately 2 times. Concurrently, the total pore volume is observed to diminish. Among the synthesised samples, the DMSN-1.5 sample is the only one to show a microporous structure in addition to meso-structures.

Table 3.1 - Parameters of the porous structure of SiO₂ samples

Sample	S _{BET} , m ² /g	S _{ext} , m ² /g	S _{micro} , m ² /g	V _Σ , cm ³ /g	V _{micro} , cm ³ /g	V _{micro} , %	R, nm
DMSN-1.5	504	448	56	2.067	0.017	0.8	8.2
DMSN-3	452	452	-	1.586	-	-	7.02
DMSN-5	308	308	-	1.161	-	-	7.5

This effect due to the continued growth of the outer edges, thickening, and extrusion of the original pore space, that observation aligns with SEM images (Fig. 3.3).

The analysis conducted via XRD and FTIR corroborated the amorphous nature of the synthesised SiO₂ and the presence of characteristic Si-OH, O-Si-O, and Si-O-Si bands, which are indicative of amorphous silica structures. The IR-spectroscopy analysis demonstrated that shorter synthesis times resulted in incomplete hydrolysis of TEOS, as evidenced by the presence of free Si-OH groups in the SiO₂ -1.5 sample.

Across the full range of synthesis times, the diameter of the silica microspheres remained at approximately 200 nm. However, the edges of the nanosheets exhibited a gradual thickening as synthesis time was extended, increasing in width from 7 nm at 1.5 hours to 22 nm at 5 hours. This edge thickening affected the overall texture of the

samples.

All samples exhibited mesoporous structures with type IV isotherms and H3 hysteresis loops, indicative of uniform spherical particles with a wide range of pore sizes. The SiO₂-1.5 sample demonstrated the highest specific surface area (504 m²/g) and contained both mesoporous and microporous structures. With longer synthesis times, the specific surface area decreased as a result of pore space reduction caused by the thickening of the nanosheets.

The study revealed that a synthesis time of 1.5 hours is optimal for achieving a high specific surface area and morphology without significant pore coalescence or edge thickening. Prolonged synthesis times (up to 5 hours) resulted in the formation of materials with reduced surface area, pore volume, and aggregation of individual particles DMSN.

The results obtained show the effect of synthesis time on nanosheet thickness and specific surface area, thereby providing insights into the optimisation of the structural properties of silica spheres for potential applications in catalysis, adsorption, and material science.

3.2 Adsorption removal of copper (II) from water by zero-valent iron loaded dendritic mesoporous silica

In this work, to solve the drawbacks of the dendritic silica material's weak inherent ability to capture heavy metal ions in the water body, as well as the difficulty

of solid-liquid separation after adsorption, we introduced zero-valent iron as an additional adsorption site on the surface of the dendritic silica. [100].

Scanning electron microscopy (SEM) and transmission electron microscopy (TEM) were used to observe the macroscopic and microscopic morphology of DMSN and Fe⁰@DMSN adsorbents. Fig. 3.6 (a, b) show the SEM patterns of DMSN and Fe⁰@DMSN, and we can see that the DMSN material still maintains the dendritic morphology before and after Fe⁰ loading and the material is well dispersed with a diameter of around 200 nm. We also observed that its monodispersed distribution and internal mesoporous structure give it a larger specific surface area and more active sites compared to the traditional silica material, which will play a positive role in the adsorption capacity of the material. In Fig. 3.6 (b), the synthetic Fe⁰ loaded on the edge of DMSN can be observed in the form of small particles.

To further observe the microscopic morphology of Fe⁰@DMSN materials and the loading state of Fe⁰, we performed transmission electron microscopy (TEM) tests on Fe⁰@DMSN, and in the TEM patterns in Fig. 3.6(c, d), we can clearly see that Fe⁰ is tightly adhered to the surface of DMSN and aggregated into clusters to a small extent, which is due to the van der Waals forces and magnetic properties of Fe⁰ nanoparticles, the unsupported Fe⁰ tends to aggregate together [176]. In addition, aggregated Fe⁰ material is not observed in the blank area of Fig. 3.6 (c), indicating that Fe⁰ is successfully composited with DMSN and firmly linked together, rather than simply stacking.

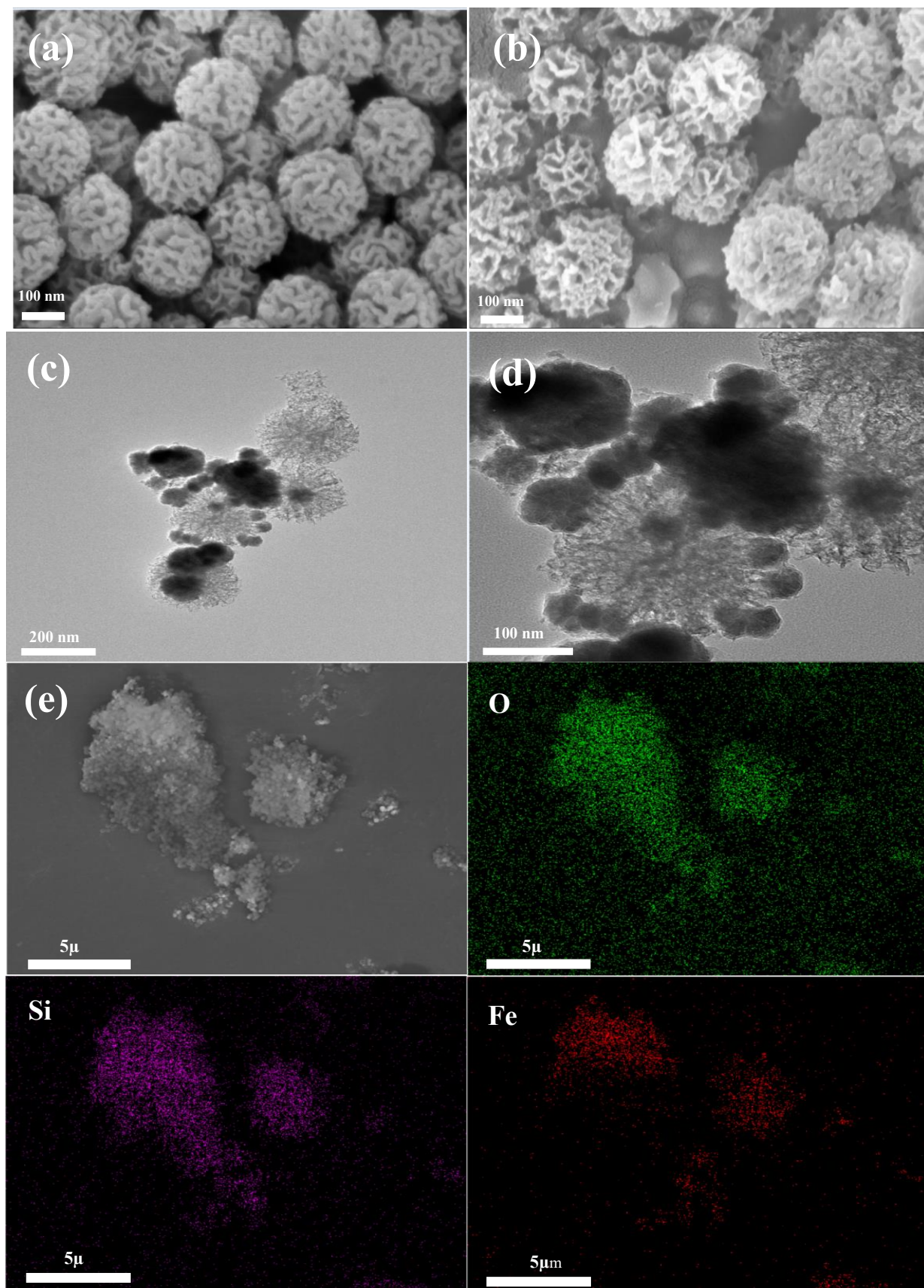


Fig. 3.6 - SEM images of DMSN (a), Fe⁰@DMSN (b), TEM image of Fe⁰@DMSN (c) and (d), EDS mapping characterization of Fe⁰@DMSN (e)

To observe the elemental distribution in the composites, the elemental distribution mapping test was carried out for $\text{Fe}^0\text{@DMSN}$ in Fig. 3.6 (e), and the results of the mapping test can be observed that the elements O, Si, and Fe are uniformly distributed in the materials, which further indicates the successful synthesis of $\text{Fe}^0\text{@DMSN}$ composites.

X-ray diffraction analyses of DMSN and $\text{Fe}^0\text{@DMSN}$ were carried out in Fig. 3.7.

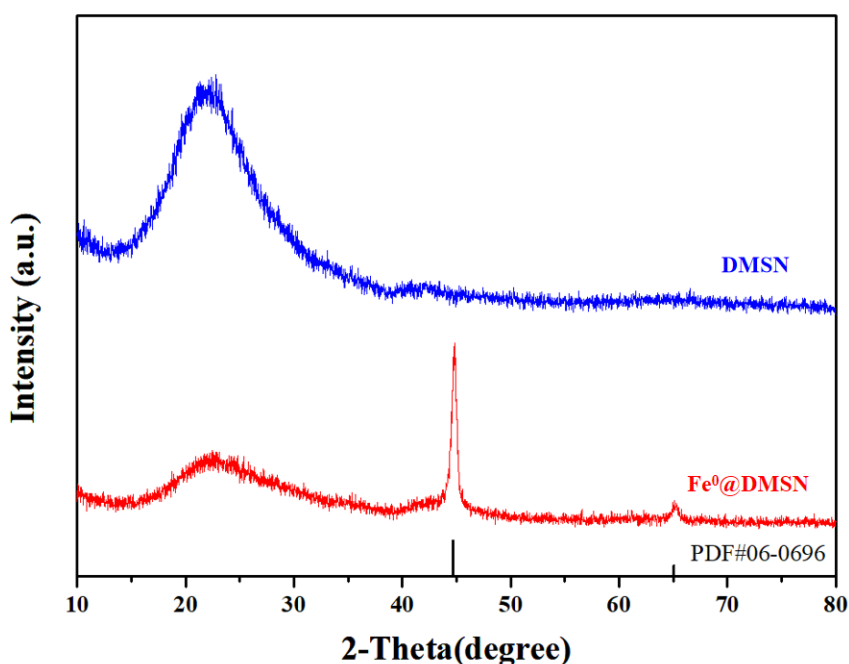


Fig. 3.7 - XRD images of DMSN (blue line) and $\text{Fe}^0\text{@DMSN}$ (red line).

A distinct broad peak was observed at around $2\theta = 24$ which is typical for amorphous silica materials. In the XRD pattern of the composite material $\text{Fe}^0\text{@DMSN}$, in addition to the observed broad diffraction peaks belonging to amorphous silica, two sharp peaks belonging to the (110) and (200) crystalline surfaces of Fe^0 are also revealed at $2\theta = 44.7$ and $2\theta = 65.0$, which is in agreement with the XRD card PDF#06-0696 of Fe^0 . The above results indicate that the Fe^0 is well crystallized and loaded onto

the DMSN material, and the $\text{Fe}^0\text{@DMSN}$ composite was successfully synthesized.

The surface functional group structures of DMSN and $\text{Fe}^0\text{@DMSN}$ were tested by FTIR spectroscopy, the results of which are shown in Fig. 3.8, where both materials show peaks at 3433, 1630, and 803, which corresponds to the -OH telescopic vibration, $\text{Si-H}_2\text{O}$ bending vibration, and O-Si-O bending, respectively.

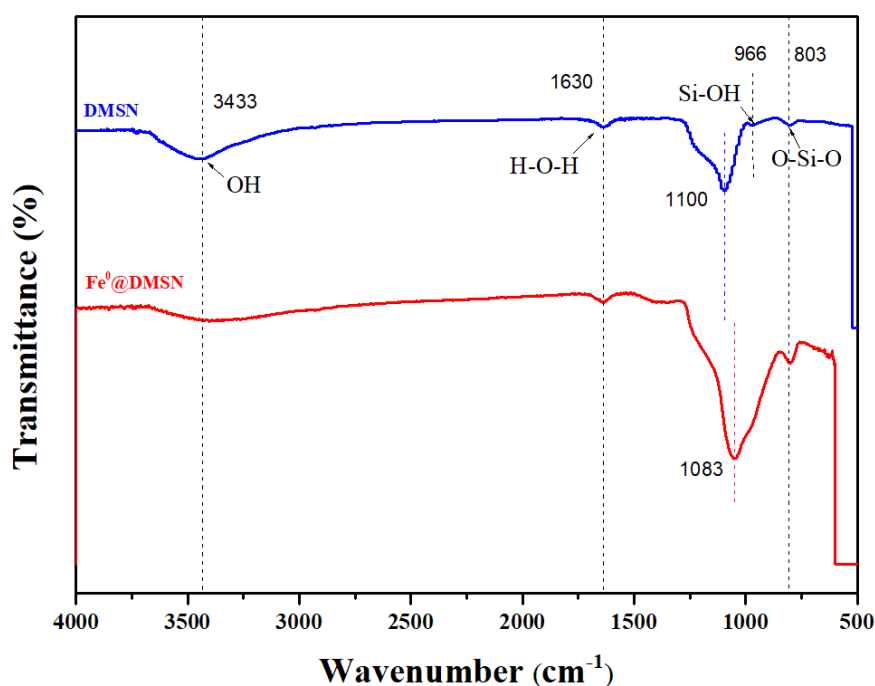


Fig. 3.8 - FTIR images of DMSN (blue line) and $\text{Fe}^0\text{@DMSN}$ (red line)

In particular, after the composite Fe^0 the Si-OH bending vibration peak at 966 cm^{-1} disappears in the FTIR spectra of $\text{Fe}^0\text{@DMSN}$, which may be attributed to the chemical bonding of Si-OH on the surface of DMSN with the iron atoms on the surface of Fe^0 to form Si-O-Fe [177]. In addition, the Si-O-Si vibration of the composite is red-shifted from 1100 to 1083 further indicating that the functional group structure of DMSN has changed. All these results indicate that Fe^0 was successfully dispersed in DMSN.

The obtained isotherms of low-temperature nitrogen adsorption/desorption (Fig. 3.9 a) of the studied samples belong to the type IV isotherms according to the IUPAC classification with a hysteresis loop of type H3, which is typical for mesoporous materials. The value of the specific surface area for the modified sample is almost half that of the synthesized DMSN, which may be due to the fact that nZVI occupies or partially blocks the DMSN's pore channels. The total pore volume has a similar trend. The distribution of pores by size (Fig. 3.9 b) shows a wide range of pore sizes in the range of 3-50 nm.

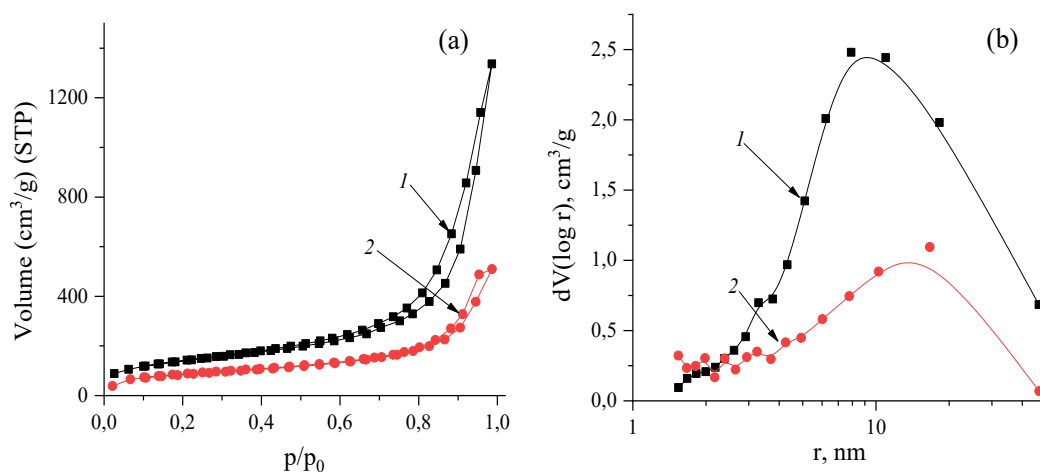


Fig 3.9 - Nitrogen adsorption/desorption isotherm (a) and pore radius distribution (b) of the studied samples (1 - DMSN, 2 - Fe⁰@DMSN)

The parameters of the porous structure are presented in Table 3.2.

Table 3.2 - Parameters of the porous structure of the investigated samples

Sample	S _{BET} , m ² /g	S _{ext} , m ² /g	S _{micro} , m ² /g	V _Σ , cm ³ /g	V _{micro} , cm ³ /g	V _{micro} , %	R, nm
1	504	448	56	2,067	0.017	0.82	8.2
2	312	251	61	0.788	0.021	2.66	5.1

In the adsorption reaction, the pH of the solution affects the functional groups of

the adsorbent and the solution's heavy metal ions, which in turn affects the actual adsorption effect of the adsorbent on the heavy metal solution. In addition, since copper ions in solution will precipitate as hydroxides under alkaline conditions, which will affect the accuracy of the adsorption experiments, we only considered the adsorption of copper ions by $\text{Fe}^0\text{@DMSN}$ at $\text{pH} \leq 6$.

In Fig. 3.10, we tested the adsorption capacity of $\text{Fe}^0\text{@DMSN}$ for copper ions at different pH (3~6), and the result shows that the composite material has the best adsorption effect when pH is equal to about 5, and the removal rate of copper ions in solution reaches 95.5%. This is the reason for the subsequent adsorption process, the solution pH was kept at 5.7 ± 0.1 .

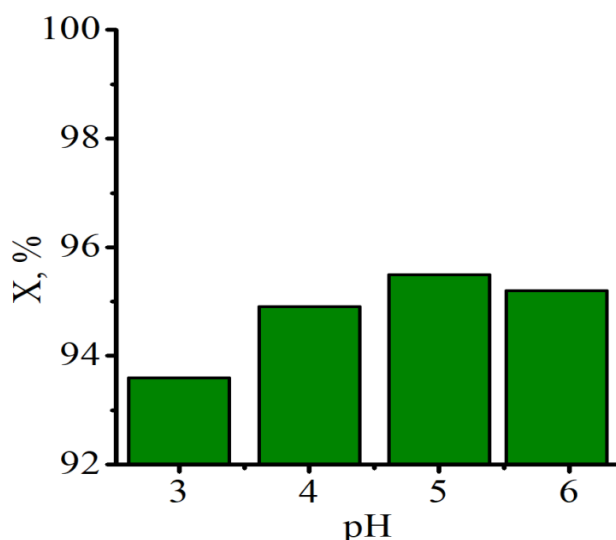
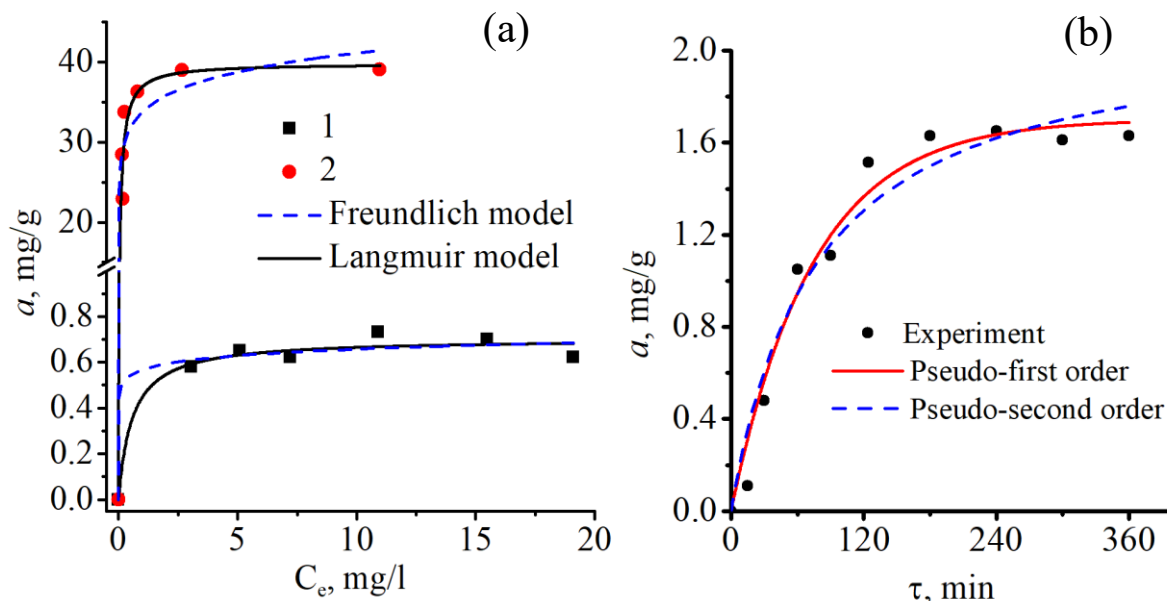


Fig 3.10 - Adsorption efficiency of Cu^{2+} by $\text{Fe}^0\text{@DMSN}$ materials under different pH. ($T = 298 \text{ K}$, $C_0(\text{Cu}^{2+}) = 20 \text{ mg/L}$, $t = 1 \text{ h}$)

To investigate the adsorption capacity of the materials, adsorption isotherms (Fig. 3.11(a)) were used to explore the interactions between the toxic heavy metals Cu^{2+} with DMSN and $\text{Fe}^0\text{@DMSN}$.



1 - DMSN, 2 - Fe⁰@DMSN

Fig 3.11 - Adsorption isotherms of (a); Adsorption kinetics of Fe⁰@DMSN (b)

(T= 298 K, pH = 5.7 ± 0.1)

The experimental data were tested using Langmuir and Freundlich models, respectively. The correlation parameters of the fitting results are shown in Table 3.3. The Langmuir model for the correlation coefficients of the two adsorbents (R^2 respectively DMSN > 0.97 and Fe⁰@DMSN > 0.96) fitted better with the experimental data as compared to the Freundlich model. This indicates that the adsorption process of heavy metal ions on both adsorbents is the same for homogeneous adsorption. The results of calculating the maximum adsorption (q_m) of Cu²⁺ on both adsorbent materials based on the Langmuir model showed that the adsorption capacity of DMSN for Cu ions was insignificant at around 0.7 mg·g⁻¹. However, after Fe⁰ modification on its surface, the maximum adsorption of Cu²⁺ by the composite material Fe⁰@DMSN increased significantly to 39.8 mg·g⁻¹, which is nearly 57 times higher than that of the

adsorption of the initial DMSN material. This confirms our view that nano-Fe⁰, as a newly introduced adsorption active site, significantly enhances the adsorption properties of the DMSN substrate for Cu²⁺.

Table 3.3 - Fitting parameters for Cu²⁺ adsorption removal isotherms for DMSN and Fe⁰@DMSN

Name	Langmuir			Freundlich		
	Q _m (mg·g ⁻¹)	K _L (L·mg ⁻¹)	R ²	K _f (mg ¹⁻ⁿ ·L ⁿ /g)	n	R ²
DMSN	0.702	1.754	0.969	0.567	15.73	0.963
Fe ⁰ @DMSN	39.804	12.720	0.955	33.76	11.71	0.922

The adsorption efficiency of Fe⁰@DMSN with Cu²⁺ was investigated using adsorption kinetics Fig. 3.11 (b), which showed that the composite reached equilibrium for the adsorption of Cu²⁺ ions at around 120 min. The kinetic data were fitted with pseudo-first and pseudo-second-order kinetic equations. According to the calculated constants (Table 3.4), the correlation coefficient of the pseudo-first-order kinetic model ($R^2 = 0.972$) is higher than that of the pseudo-second-order kinetic model ($R^2 = 0.951$), and the experimental value (q_e) is close to that calculated from the pseudo-second-order kinetic model so that the adsorption of Cu²⁺ by Fe⁰@DMSN is more suitable for the pseudo-first-order kinetic equation.

Table 3.4 - Kinetic parameters of Cu (II) adsorption on Fe⁰@DMSN

Name	Pseudo-first-order			Pseudo-second-order		
	Q _e (mg·g ⁻¹)	K ₁ (min ⁻¹)	R ²	Q _e (mg·g ⁻¹)	K ₂ (g·mg ⁻¹ ·min ⁻¹)	R ²
Fe ⁰ @DMSN	1.700	0.0136	0.972	2.129	0.0062	0.951

In summary, in this study, Fe⁰@DMSN composite adsorbent was successfully synthesized by reducing Fe³⁺ ion solution which contained DMSN material with sodium borohydride solution under a nitrogen environment. The material characterization confirmed that the material possessed a solid structure and abundant adsorption functional groups. In addition, its adsorption capacity for the toxic heavy metal Cu²⁺ in simulated wastewater was tested. The adsorption results showed that at pH = 5.7 ± 0.1 and 298 K, the maximum adsorption capacity was 39.8 mg·g⁻¹, which was about 57 times higher than that of the base DMSN material (0.7 mg·g⁻¹), and the kinetic process was described by a pseudo-first-order model. In addition, the adsorbed mixture could utilize an external magnetic field to achieve solid-liquid separation. All the results show that the Fe⁰@DMSN composite adsorbent is a promising adsorbent for the treatment of Cu²⁺-polluted wastewater.

3.3 Adsorption removal of copper (II) from water by amino-functionalized dendritic mesoporous silica nanoparticles

Amino groups (-NH₂) are particularly effective for removing heavy metal cations from aqueous media. Due to their lone electron pair and ability to act as Lewis bases,

they readily form coordinate bonds with heavy metal ions (Lewis acids). In most cases, amino silanes are used as modifiers for the grafting of amino groups onto various substrates [180, 181]. This approach can be applied to a wide range of materials, including aerosil, silica, silica gel, clay minerals, and even biosorbents [182-184].

Dendritic mesoporous silica nanoparticles (DMSN) are particularly attractive adsorbents due to their high specific surface area, uniform pore and particle size, chemical stability, and excellent surface functionalization capability [185]. Their unique dendritic-fiber morphology ensures that adsorption sites are easily accessible from all directions, further improving their efficiency in metal ion removal.

Therefore, in this study, we successfully synthesized a dendritic silica material with an amino-functionalized surface and applied it in the field of copper ion adsorption in wastewater [186].

The analysis of structural features by infrared (IR) spectroscopy showed that all the vibrational bands characteristic of amorphous silica are present in the studied samples, namely: the vibrational Si-O bond of isolated Si-OH groups (966 cm^{-1}), symmetrical valence vibrations (803 cm^{-1}), asymmetrical valence vibrations (1093 cm^{-1}) and bending vibrations (467 cm^{-1}) of the O-Si-O bond (Fig. 3.12) [187, 188].

The presence of new functional groups ($-\text{NH}_2$) was confirmed by the appearance of a shoulder of valence and deformation vibration bands at $\sim 1500\text{ cm}^{-1}$ [189]. In addition, the asymmetric and symmetric stretching modes of $-\text{CH}_2$ observed in the range of $\sim 2830 - 2990\text{ cm}^{-1}$ indicate the presence of APTES propyl chains [190]. The absence of a peak in the $\nu \sim 3000\text{ cm}^{-1}$ region, which belongs to the symmetrical stretching of the $-\text{N-H}$ bond, may be due to the low intensity of amine groups

originating from APTES functionalization [191].

The functionalization of the DMSN surface also transforms the peak in the $\nu \sim 3400 \text{ cm}^{-1}$ region from the low-frequency side and a shoulder appears in the range of $\sim 3200 - 3000 \text{ cm}^{-1}$. This peak corresponds to the asymmetric vibrations of the -OH group, namely partially hydrated silanols (Si-OH residue) and adsorbed molecular water [192, 193]. The peak at 1640 cm^{-1} characterizes the bending vibrations of the water molecule [192].

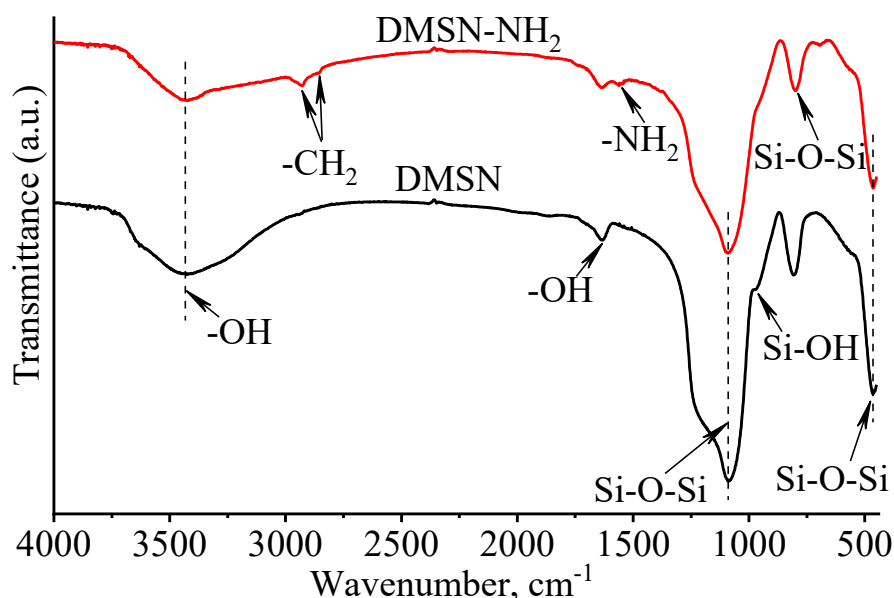


Fig. 3.12 - IR spectra of DMSN before and after surface functionalization with amino groups

The content of -OH groups in the initial DMSN sample was 0.16 meq/g. The content of NH_2 groups in the obtained sample, determined as the average of three titration results, was 2.03 meq/g. In the simplest case of functionalization, one hydroxyl group on the DMSN surface reacts with one triethoxysilyl group of APTES (Fig 3.13).

In this case, the equivalent content of amino groups in the modified sample should be equal to the equivalent content of hydroxyl groups in the initial DMSN. That is, 0.16 meq/g for NH_2 groups content. However, the content of amino groups in the resulting sample is significantly higher, which indicates a much more complex mechanism of DMSN modification by APTES. Such a mechanism could, for example, involve partial condensation of APTES with simultaneous functionalization of the DMSN surface (Fig 3.14).

The number of condensed APTES molecules (n in Scheme 3.2) in the resulting system is likely to vary significantly. Still, the average number n can be calculated by dividing the equivalent content of amino groups by the equivalent content of hydroxyl groups, which is 12.68.

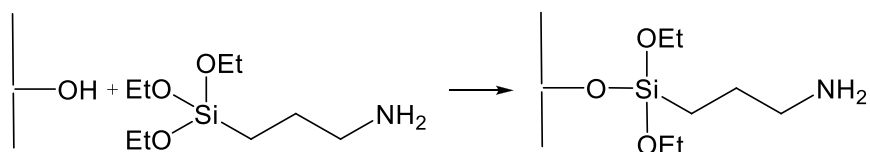


Fig 3.13 - The simplest scheme of interaction of surface -OH groups with APTES

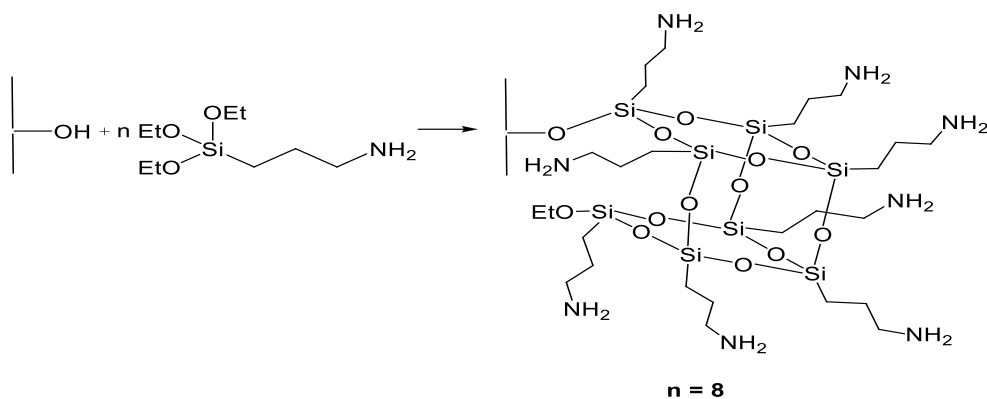


Fig 3.14 - The proposed mechanism of surface functionalization

Fig. 3.15 shows the DTA and TG curves for the DMSN sample before and after surface functionalization. The DTA curves of both samples show similar endo effects at temperatures from 40 to 110 °C, which correspond to the dehydration of the surface of silica particles. In this range, the mass loss (TG curve) is mainly due to the removal of physically bound water, i.e., adsorbed on the surface of the original and modified silica particles [144, 194].

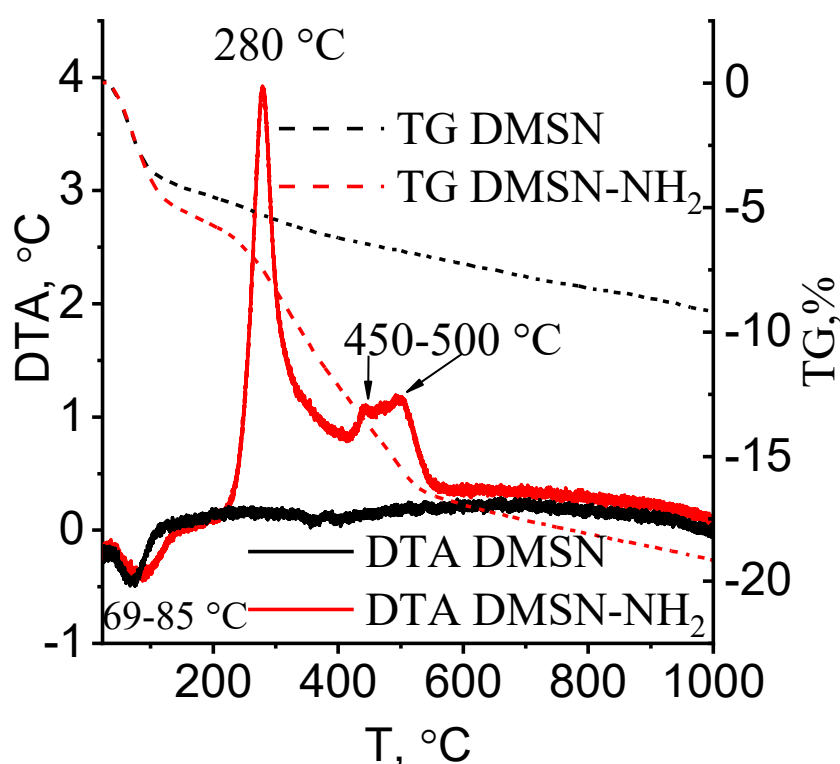


Fig. 3.15 - DTA and TG curves for DMSN before and after surface functionalization with amino groups

The maximum moisture removal rates differ between the original silica and the modified APTES. For the original sample, the maximum corresponds to the endo effect at 69 °C, and for the modified sample at higher temperatures up to 85 °C. This difference may be due to the influence of amino groups and the possible presence of

CO₂ adsorbed from the air, which shifts the maximum moisture removal rate to higher temperatures in the DMSN-NH₂ sample. The period of the second mass loss, between 120-200 °C, is explained by the removal of chemically bound water.

When the temperature exceeds 200 °C, the main contribution to the mass loss is due to the decomposition of organo-functional groups [195]. According to the literature [196], the boiling point of APTES is 217 °C, so it is assumed that physically adsorbed APTES will be completely removed from the matrix surface by 300 °C. Therefore, the maximum at 280 °C, which is present only in the DMSN-NH₂ sample, probably indicates the cleavage of the amino group in the form of ammonia or oxidation to nitrogen. In general, primary amines are characterized by a large number of possible reactions with the release of gaseous products [197].

In the temperature range above 450 - 500 °C, an exogenous effect is observed when residual alkyl groups that no longer contain nitrogen are oxidized to gaseous products (CO, CO₂). The DTA curve shows that the main decomposition ends by 500 °C. This temperature is consistent with the results of an article [198], which indicates that the C-Si bond begins to break at temperatures of 450-510 °C. The low-temperature nitrogen adsorption/desorption isotherms (Fig. 3.16 a) of both samples under study, according to the IUPAC classification, can be attributed to type IV with H₃ hysteresis loops. This type of isotherm is characteristic of materials with a mesoporous structure, which is confirmed by the obtained pore size distribution (Fig. 3.16 b).

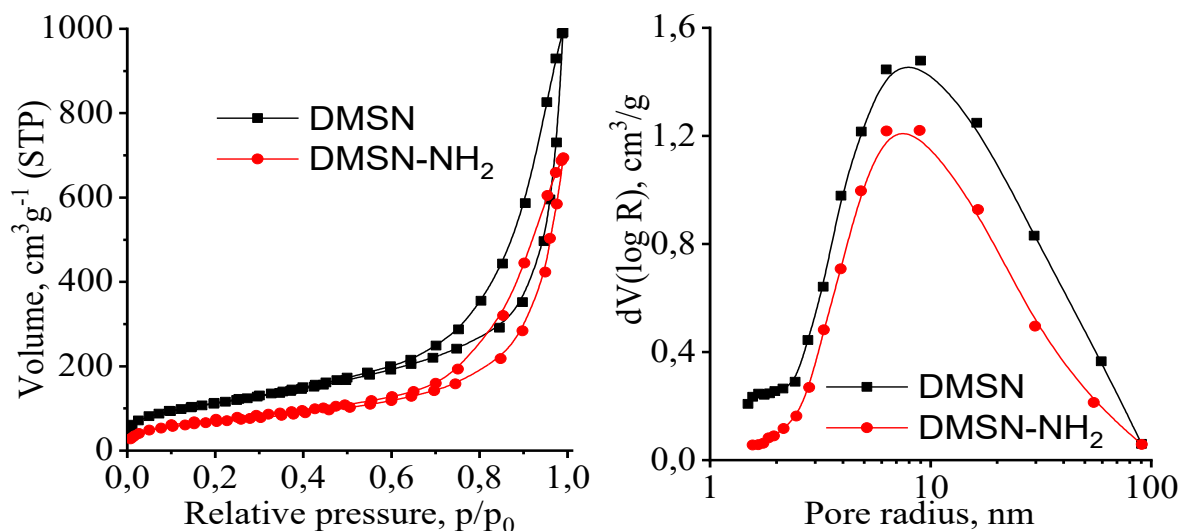


Fig. 3.16 - Isotherms of low-temperature nitrogen adsorption/desorption (a) and pore size distribution by radius (b) DMSN and DMSN-NH₂

The specific surface area of amino-functionalized DMSN (247 m²/g) is lower than that of the original sample's (404 m²/g). This decrease is due to the introduction of organic functional groups into the pores, which also reduces their volume. Consequently, the total pore volume decreases from 1.534 cm³/g to 1.073 cm³/g. At the same time, the average pore radius slightly increases from 7.6 nm to 8.7 nm, but before and after functionalization, the local maximum is observed in almost the same range. However, these changes in the pore structure after DMSN functionalization are insignificant. The obtained sample retains 80% of its structural characteristics and can be used as a potential adsorbent for the removal of heavy metal ions from aqueous media.

For the most part, wastewater contaminated with copper ions is acidic. In this case, the predominant form of copper is Cu²⁺. In addition, at pH 6, the processes of

precipitation of $\text{Cu}(\text{OH})_2$ from solution begin. Therefore, in this study, the effect of pH on the copper ion removal process was investigated in the range from 3 to 6 (Fig. 3.17).

The initial DMSN practically does not exhibit adsorption capacity, with a maximum purification efficiency at pH 6, reaches only 15%. In contrast, DMSN- NH_2 demonstrates highly efficient $\text{Cu}(\text{II})$ removal across the entire studied range, with a slight decrease in the degree of purification from 99% to 87% as the pH increase from 3 to 6. The ability of a potential adsorbent to absorb copper ions in an acidic environment is a key factor for the effective removal of $\text{Cu}(\text{II})$ from real water bodies, such as concentrated copper-containing wastewater. This is because, in highly concentrated solutions, copper complexes can precipitate at pH values below neutral below neutral [199]. Fig. 3.18 shows the time dependence of the $\text{Cu}(\text{II})$ adsorption process. In general, the establishment of adsorption equilibrium occurs quite quickly. Within 15 min for DMSN- NH_2 and 60 min for DMSN, the maximum removal of $\text{Cu}(\text{II})$ from the model solutions is achieved. Table 3.5 presents the calculated parameters of the pseudo-first and pseudo-second-order kinetic models of this process.

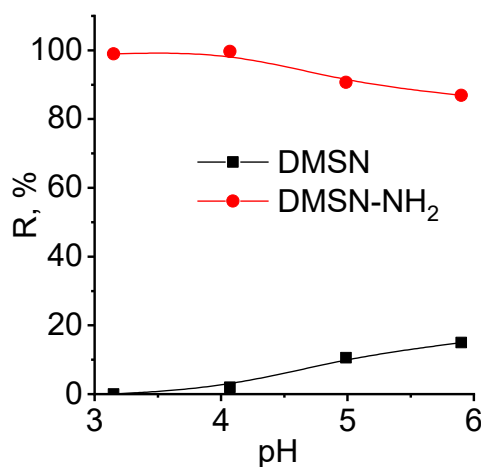


Fig. 3.17 - Dependence of the degree of $\text{Cu}(\text{II})$ ion removal on the pH of the aqueous medium by DMSN and DMSN- NH_2 samples

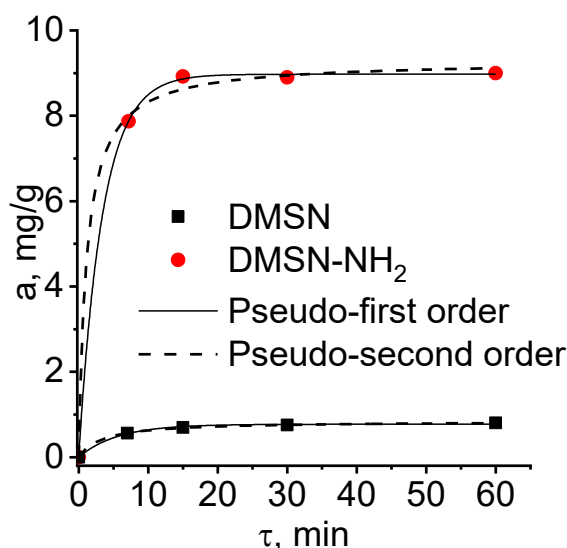


Figure 3.18 - Kinetics of Cu(II) adsorption on the studied samples

Table 3.5 - Coefficients of kinetic equations

Sample	Pseudo-first-order model			Pseudo-second-order model		
	Q_{eq} , mg/g	k_1 , min^{-1}	R^2	Q_{eq} , mg/g	k_2 , $\text{g/mg} \cdot \text{min}$	R^2
DMSN	0.77	0.17	0.9951	0.84	0.34	0.9992
DMSN-NH ₂	8.97	0.29	0.9998	9.29	0.09	0.9974

The kinetic curves are well described by both model, with ($R^2 > 0.99$). This suggests that the adsorption process may occur via a mixed mechanism. At the initial stages, adsorption is rapid due to a high concentration gradient, indicating physical adsorption during the first 10 minutes. As the Cu(II) concentration in the solution decreases, the process rate slows down, and adsorption increasingly involves chemical interactions, such as the formation of complexes or chemical bonds between Cu^{2+} ions

and active sites on the surface of the material. However, pseudokinetic models are only general tools for presenting kinetic results. They do not provide a clear physical description of the kinetic mechanism and do not determine which adsorption step is more important [200]. The equilibrium adsorption behavior of Cu^{2+} ions on DMSN and DMSN- NH_2 samples described by Langmuir and Freundlich adsorption models, is shown in Fig. 3.19. The results indicate that the adsorption capacity of the synthesized DMSN for copper ions is relatively low, reaching no more than 0.62 mg/g. For comparison, the adsorption of Cu(II) on commercial SiO_2 under similar conditions is 0.3 mg/g [179].

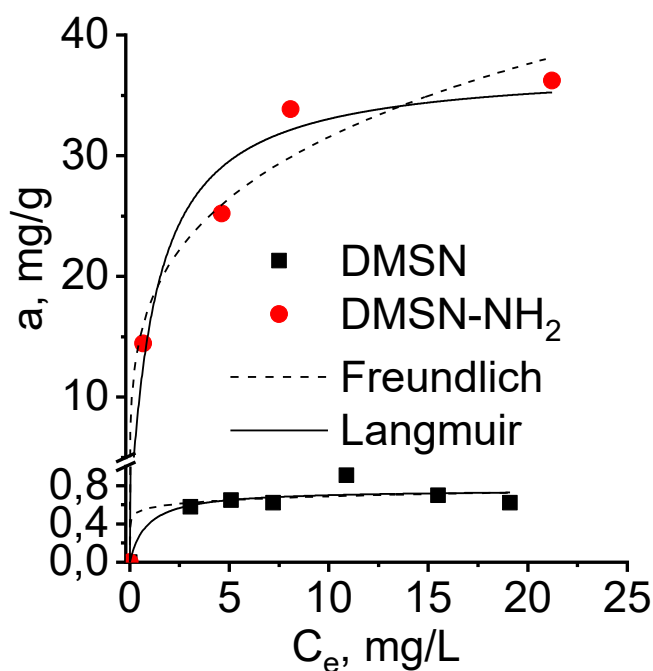


Figure 3.19. Adsorption isotherms of Cu(II) on DMSN samples before and after surface functionalization with amino groups

When the DMSN surface is modified with amino groups, the adsorption capacity

increase by a factor of 50. The calculated parameters of the adsorption equations are summarized in Table 3.6.

Table 3.6 - Coefficients of adsorption equations

Sample	Langmuir model			Freundlich model		
	Q_{\max}	K_L	R^2	K_F	n	R^2
DMSN	0.76	1.16	0.8517	0.56	11.7	0.8387
DMSN-NH ₂	37.5	0.74	0.9671	17.61	3.9	0.9667

The adsorption of Cu(II) on DMSN and DMSN-NH₂ samples is well described by both models, further confirms the combination of physical adsorption with chemisorption in the studied copper concentration range. To further investigate the mechanism of copper ions adsorption on the surface of amino-functionalized DMSN, XPS analysis of the sample before and after adsorption was performed (Fig. 3.20). The elemental composition of the initial and treated samples is shown in Table 3.7.

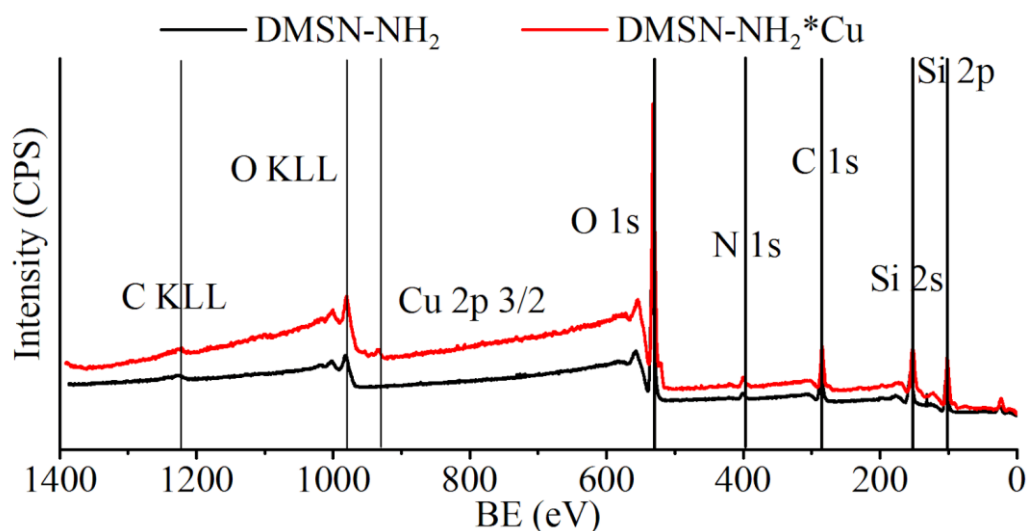


Figure 3.20 - XPS of amino-functionalized DMSN before and after sorption

The O1s maximum (about 532 eV), attributed to oxygen and surface hydroxyl groups (Si-OH), represents the main peak of the spectrum. The Si2p and Si2s peaks (about 100–160 eV) correspond to silicon present in the DMSN structure. The C1 peak, at 284 eV is associated with the carbon of the aminopropyl group ($-\text{C}_3\text{H}_6-\text{NH}_2$), while the N1 peak, at 400 eV corresponds to the nitrogen of the amino group.

The DMSN-NH₂ *Cu sample, with adsorbed copper ions has a characteristic Cu2p3/2 peak at 933.6 eV. Notably, the interaction between Cu²⁺ ions and amino groups leads to an increase in the intensity of the O1 and N1 peaks and their partial shift to the higher energy zone. In order to evaluate the possibility of reusing DMSN-NH₂, desorption experiments were conducted to determine its regeneration efficiency over three cycles of copper ion adsorption/desorption.

Table 3.7 - Elemental composition of the samples

Element	Initial	Treated
	Concentration, at. %	Concentration, at. %
C	22.83	18.57
N	2.96	2.28
O	49.47	51.91
Si	24.74	26.83
Cu	-	0.41

The adsorption of copper ions was carried out under the following optimal conditions: the solid-to-liquid phase ratio was 1:500, the interaction duration was 60 min, the concentration of the Cu(II) model solution was 100 mg/L, the ionic strength was 0.01, and the pH was 5.7. Copper ion desorption from the DMSN-NH₂ surface was achieved using 0.1 M HCl. Before this, the spent sample was washed several times with distilled water, followed by 60 minutes of stirring in 0.1 M HCl at a solid-to-liquid phase ratio of 1:500. After centrifugation, the copper ion concentration in the liquid phase was determined. The solid phase was then repeatedly washed with distilled water, and a single wash with 0.01 M NaOH solution was performed to activate the amino groups. Using 0.1 M HCl was found that the desorption capacity after each cycle was 10%, while the adsorption capacity of the material increased by 50%. The underlying reasons for this phenomenon – including the potential activation of novel adsorption centers, structural changes in DMSN, and modifications in the chemical properties of the -NH₂ groups – require further investigation.

The obtained results confirm the successful synthesis and amino-functionalization of dendritic mesoporous silica nanoparticles (DMSN). It was determined that the content of -NH_2 groups in the modified sample is significantly higher than the content of -OH groups in the initial sample – 2.03 meq/g and 0.16 meq/g, respectively. This confirms a complex modification mechanism involving partial condensation of APTES with simultaneous functionalization of the DMSN surface.

At the same time, the textural parameters of the material underwent notable changes, characterized by a decrease in specific surface area from $404 \text{ m}^2/\text{g}$ to $247 \text{ m}^2/\text{g}$ and a reduction in total pore volume from $1.534 \text{ cm}^3/\text{g}$ to $1.073 \text{ cm}^3/\text{g}$. Nevertheless, the mesoporous structure remained largely intact. Structural, morphological, and adsorption studies demonstrated that the modification of the DMSN surface with amino groups significantly enhances the efficiency of copper (Cu^{2+}) ion removal from aqueous solutions. DMSN- NH_2 exhibited high adsorption capacity (up to 99%) even in acidic environments, as confirmed by kinetic and isothermal adsorption models. The results of XPS analysis indicate the formation of coordination bonds between Cu^{2+} ions and amino groups, suggesting a combination of physical adsorption and chemisorption. Preliminary research on the regeneration and reuse of the material suggests that effective reuse is feasible. However, further research is needed to study the optimal conditions for this process in detail. The DMSN- NH_2 offers several advantages, including a simple synthesis process, control over particle size and texture parameters, and easy separation from the liquid phase. However, the material also has certain drawbacks, such as high dispersion, which may reduce accessibility to active sites.

Consequently, the modified DMSN-NH₂ are promising adsorbents for the effective treatment of wastewater contaminated with heavy metal ions.

Conclusions to Chapter 3

Amorphous dendritic mesoporous silica was synthesized and its morphology and structural and sorption characteristics were investigated. It was found that silica microspheres obtained as a result of synthesis carried out at 1, 3 and 5 hours are monodisperse spheres with a diameter of about 200 nm, the pore sizes of which are in the range from 5 to 50 nm, and the specific surface area is 504, 452 and 308 m²/g, respectively. It was determined that the synthesis time of 1.5 hours is optimal for achieving the high specific surface area and morphology without significant coalescence of pores or thickening of the edges.

The sorbent material was obtained by applying zero-valent iron particles to the surface of dendritic mesoporous silica. It was determined that applying a modifying layer of Fe⁰ particles leads to a decrease in the specific surface area almost half that of the original silica. It is shown that the maximum adsorption capacity of the adsorbent with respect to copper ions is 39.8 mg•g⁻¹, which is approximately 57 times higher than that of the starting material.

The amino-functionalized adsorbent was obtained by chemical modification of dendritic mesoporous silica with 3-aminopropyltriethoxysilane. It was found that the starting silica practically does not exhibit adsorption capacity for copper ions at pH 6, and the modified one demonstrates effective removal of Cu(II) in the entire studied pH

range. It is shown that the establishment of adsorption equilibrium occurs quite quickly. The results of X-ray photoelectron spectroscopy indicate the formation of coordination bonds between Cu^{2+} ions and amino groups, which indicates a combination of physical adsorption and chemisorption processes. Studies of the regeneration of the spent material indicate its possible reuse.

The results of this chapter were published in:

1. Tobilko, V. Y., **Yu, J.**, & Bondarieva, A. I. (2024). Effect of synthesis time on the morphology of monodisperse silica microspheres. *Journal of Chemistry and Technologies*, 32(4), 932-938. <https://doi.org/10.15421/jchemtech.v32i4.315165>

Журнал цитується у наукометричних базах даних Scopus (ISSN: 2663-2942). За даними SCImago Journal and Country Rank на момент публікації належить до квартиля Q4 (2024).

2. **Yu, J.**, & Tobilko, V. (2024). Absorption removal of copper (II) from water by zero valent iron loaded dendritic mesoporous silica. *Technology audit and production reserves*, 5(3 (79)), 6-12. <https://doi.org/10.15587/2706-5448.2024.314231>

3. **Junjie Yu**, Antonina Bondarieva, Ihor Pylypenko, Viktoriia Tobilko, Tomash Sabov, Mariana Gumenna, Tamara Tomila, Olena Inshyna (2025). Amino-functionalized dendritic mesoporous silica nanoparticles for removal of copper from aqueous solutions. *J. Ecol. Eng.*, 26(6), 365-377. <https://doi.org/10.12911/22998993/202979>.

4. **J. Yu**, V.Yu. Tobilko, A.I. Bondarieva. Synthesis of mesoporous silica

nanospheres. Book of abstracts of Ukrainian Conference with International Participation “Chemistry, Physics and Technology of Surface” (11-12 October 2023 p., Kyiv). P. 179.

5. **Yu Junjie**, Bondareva A.I., Tobilko V.Yu. Study of synthesis conditions on the structural properties of mesoporous silica nanospheres. Proceedings of the III All-Ukrainian Internet Conference of Young Scientists “Prospects of Chemistry in the Modern World” (November 22, 2023, Zhytomyr). P. 31-32 (in Ukraine).

CHAPTER 4

MODIFIED COMMERCIAL SILICA GEL USED FOR HEAVY METAL IONS AND ORGANIC DYES REMOVAL FROM AQUEOUS SOLUTIONS

4.1 Adsorption removal of copper (II) from water by NiO-modified silica gel

The treatment methods of heavy metals in the water environment mainly include adsorption, chemical precipitation, ion exchange, etc. [201, 202]. Some of these methods are not suitable for the treatment of heavy metals in the water environment or prohibitive due to their inability to meet water purification requirements or the high cost of the materials. Therefore, finding an efficient and clean water purification material with controllable cost has become the preferred goal of researchers. In recent years, it has been found that metal oxide-based adsorbents have unique physicochemical properties, including chemical stability, controllable morphology and size, and abundant surface active sites. They have potential applications in the removal of various heavy metal contaminants from water systems [203, 204]. For example, iron oxide (Fe_3O_4), which is common among metal oxides, has been shown to be effective in the removal of various heavy metals (including lead (Pb^{2+}), arsenic (As^{3+}) and mercury (Hg^{2+})) due to its magnetic properties and ease of separation from the adsorbed wastewater.[205 – 207]. Another example includes metal oxide composites using titanium dioxide (TiO_2), which is well known for its large specific surface area and stable properties [208, 209]. In addition, nickel oxide (NiO) stands out for its excellent physicochemical properties, with its high specific surface area, low cost, and natural

porosity [210 – 212], showing great potential for water treatment. These examples highlight that metal oxide nanoparticles and their complexes possess the potential to act as effective adsorbents for water purification.

Given these studies, we designed a silica (SiO_2)-based composite embedded with nickel oxide (NiO) particles based on several considerations. First, it is well known that the surface of SiO_2 is negatively charged in water, while the surface of NiO is positively charged, which allows the two to bond uniformly and tightly together due to charge attraction [213]. Silicon dioxide material serves as an excellent support substrate, and its chemical stability and high specific surface area can provide nickel oxide particles with a substrate bed that is stable and reactive in a variety of environments and can control the size of NiO particles to a certain extent, as well as enhance their dispersion and heavy metal adsorption capacity. In addition, NiO was selected for its special affinity for heavy metal ions, and the literature shows that it still maintains good adsorption performance in aqueous environments where a variety of heavy metal ions are present [214]. Therefore, modification of silica surface with nickel oxide particles can synergize the properties of the two materials, thus significantly improving the adsorption performance and reducing the cost of adsorption.

In this study, we prepared a simple, cost-controlled silica material embedded with nickel oxide particles and evaluated its ability to adsorb the removal of Cu^{2+} ions from aqueous solution by adsorption experiments (pH, Cu^{2+} ion concentration, time). By combining the physicochemical properties of NiO with the structural advantages of SiO_2 , this study contributes to the advancement of water purification technology and

provides a novel and effective solution to the pressing problem of heavy metal pollution in water resources [179].

When analyzing the XRD (X-Ray Diffraction Analysis) data for the $\text{SiO}_2@\text{NiO}$ sample (Fig. 4.1), 5 characteristic peaks were observed at $2\theta = 37^\circ, 43^\circ, 62^\circ, 75^\circ,$ and 79° , corresponding to the planes (222), (400), (440), (622), (444), respectively, and belonging to NiO (JCPDS database card No. 89-5881). The broad peak at $2\theta \approx 22^\circ$ is characteristic of SiO_2 in the amorphous phase. The $\text{SiO}_2@0.5\text{NiO}$ sample has a similar X-ray diffraction pattern, but the intensity of the main characteristic peaks is lower.

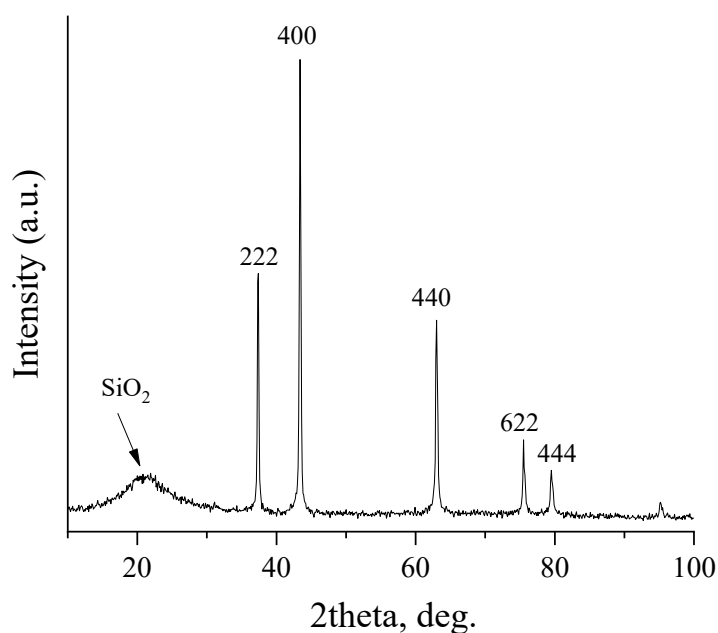


Fig. 4.1 - Diffraction pattern of the synthesized $\text{SiO}_2@\text{NiO}$

The obtained isotherms of low-temperature nitrogen adsorption/desorption (Fig. 4.2 a) belong to the type IV isotherms according to the IUPAC classification.

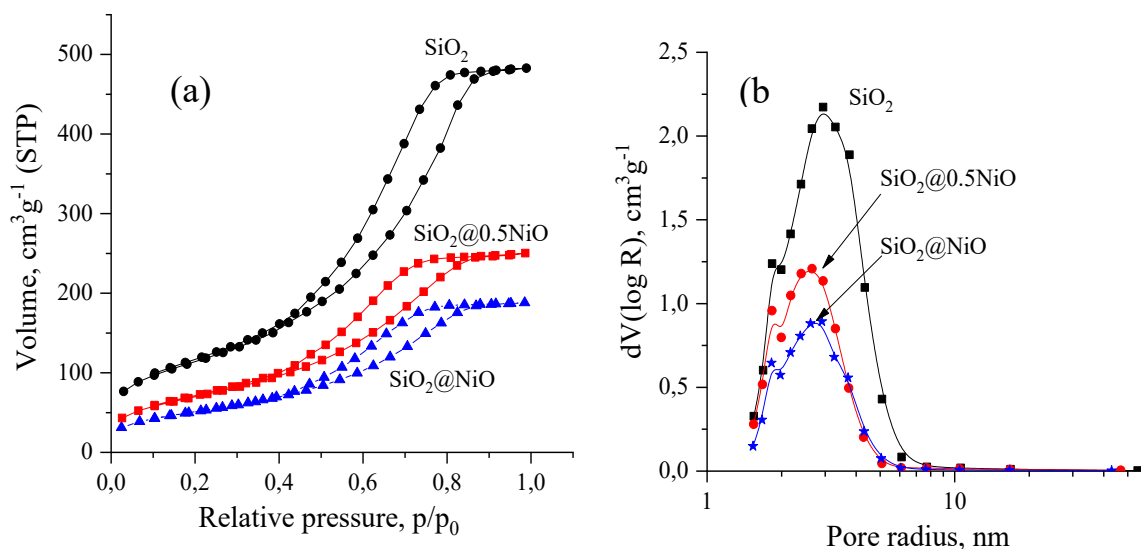


Fig. 4.2 - Isotherms of low-temperature N₂ adsorption/desorption of the pure and modified SiO₂ (a) and the distribution of pores by radius (b)

This type of isotherms is typical for materials with a mesoporous structure. The nature of the hysteresis loop allows us to determine that the porous structure of all samples is formed by spherical particles of similar size with homogeneous packing, forming cylindrical pore channels. Also, these materials have a narrow range of homogeneous mesopores concentrated around 2.5 – 3 nm, which is confirmed by the distribution of pores by radius (Fig. 4.2 b). The parameters of the porous structure of the investigated samples are presented in Table 4.1.

Table 4.1 - Parameters of the porous structure of SiO₂ samples before and after Ni-modified

Sample	S_{BET} , m ² /g	V_{Σ} , cm ³ /g	Pore radius $dV(r)$, nm
SiO ₂	411	0.746	2.653
SiO ₂ @0.5NiO	256	0.387	1.830
SiO ₂ @NiO	186	0.290	1.822

Note: S_{BET} – specific surface area, V_{Σ} – total pore volume, $dV(r)$ – average pore radius (BJH)

With an increase in the amount of the deposited NiO layer on the SiO₂ surface, the value of the specific surface area decreases by 1.5-2.5 times. In addition, the total volume of pores decreases, indicating that they are partially blocked by NiO particles or that NiO agglomerates are formed on the pore walls.

It is well established that the initial pH of a solution affects not only the protonation of the functional groups of adsorbents, but also the degree of ionization and speciation of toxicants in an aqueous solution. This, in turn, affects the interactions between the adsorbents and the adsorbate. Fig. 4.3 shows the distribution of copper ion forms in aqueous medium depending on pH (calculated using the software "The software Chemical Equilibrium Diagrams", Sweden).

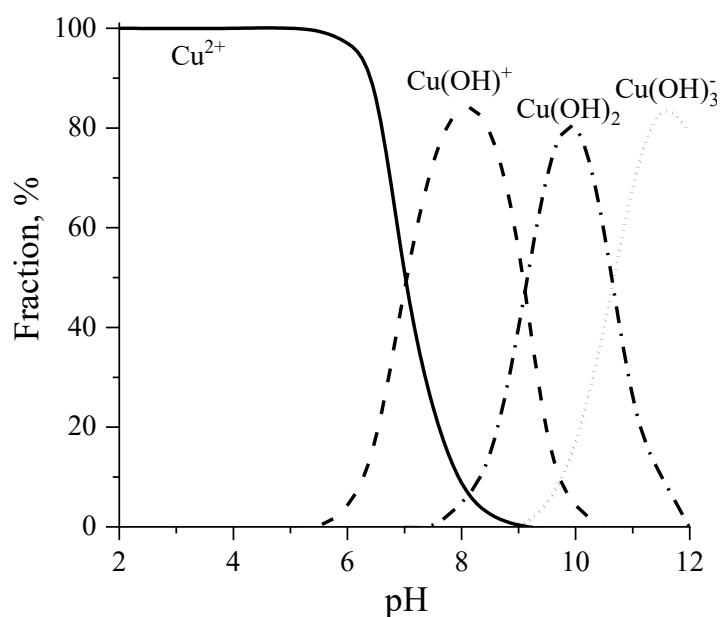


Fig. 4.3 - Diagram of the distribution of copper forms depending on pH of the aqueous solution

In an acidic environment (pH<6), copper is found mainly in the form of positively charged Cu²⁺ ions. When the pH shifts towards an alkaline environment,

copper is precipitated in the form of hydroxides. The dynamics of this process depends on the concentration of copper, the presence of other anions and cations, and temperature. Accordingly, in natural aqueous systems, copper hydroxocomplexes can be formed in the pH range of 6.5 and higher [215]. Therefore, the effect of pH on the adsorption of Cu (II) was studied in the pH range from 3 to 5.5 to avoid the precipitation of copper in the form of $\text{Cu}(\text{OH})_2$ at $\text{pH} > 6$.

According to the results obtained, commercial SiO_2 shows almost no sorption capacity for Cu (II) in the studied pH range, and the maximum sorption value is 0.2 mg/g at pH 5.5. For the modified samples, the degree of Cu^{2+} ion removal increases simultaneously with an increase in pH. Thus, the maximum sorption values are observed at pH 5.5 and are equal to 0.9 mg/g and 1.7 mg/g for the $\text{SiO}_2@0.5\text{NiO}$ and $\text{SiO}_2@\text{NiO}$ samples, respectively. That is why all subsequent sorption experiments were performed at $\text{pH } 5.5 \pm 0.1$.

The study of the influence of the contact time between the samples modified with nickel oxide and copper ions on the sorption process showed that their removal occurs quite quickly (Fig. 4.4).

The time for establishing sorption equilibrium in the system is 1 hour. At the same time, within the first 15 minutes, the degree of removal for the $\text{SiO}_2@\text{NiO}$ sample is 51%. At the same time, the $\text{SiO}_2@0.5\text{NiO}$ sample removes only 36% of copper ions, which is much higher than unmodified SiO_2 .

The analysis of the kinetics of copper ion sorption by the obtained sorbents was carried out using pseudo-first-order and pseudo-second order kinetic models. The calculated parameters of the kinetic models are shown in Table 4.2. The obtained data

indicate that the kinetic dependences of Cu (II) sorption are better described by the pseudo-second-order model, since the calculated values of sorption values ($a_{e, \text{cal}}$) coincide with the experimental data ($a_{e, \text{exp}}$) and the correlation coefficient is close to 1 ($R^2 > 0.99$).

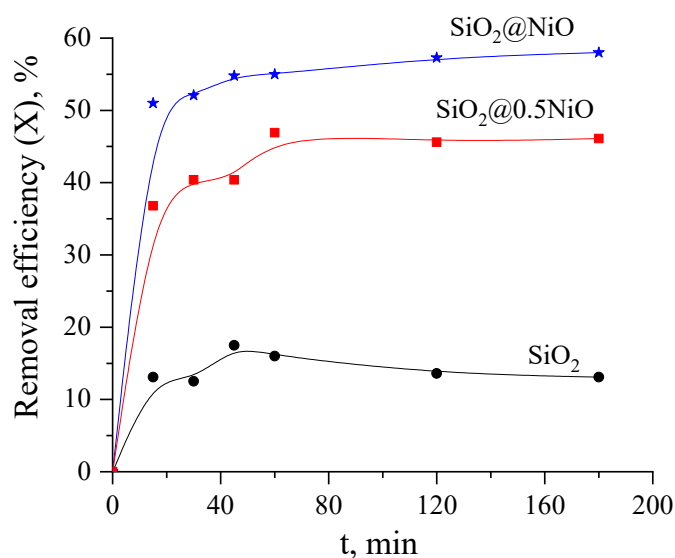


Fig. 4.4 - Kinetic curves of Cu (II) adsorption on the studied materials

Table 4.2 - Kinetic parameters of Cu (II) adsorption on Ni-modified silica gel

Sample	Parameters						
	$a_{e, \text{exp}}$, (mg/g)	Pseudo-first-order			Pseudo-second-order		
		$a_{e, \text{cal}}$, (mg/g)	k_1 , min ⁻¹	R^2	$a_{e, \text{cal}}$, (mg/g)	k_2 , g/mg min	R^2
SiO ₂ @0,5NiO	1.20	0.53	0.0085	0.554	1.20	0.2158	0.997
SiO ₂ @NiO	1.34	0.37	0.0192	0.786	1.33	0.3113	0.999

Fig. 4.3 shows the sorption isotherms of copper ions on pure commercial SiO_2 , and modified samples based on it.

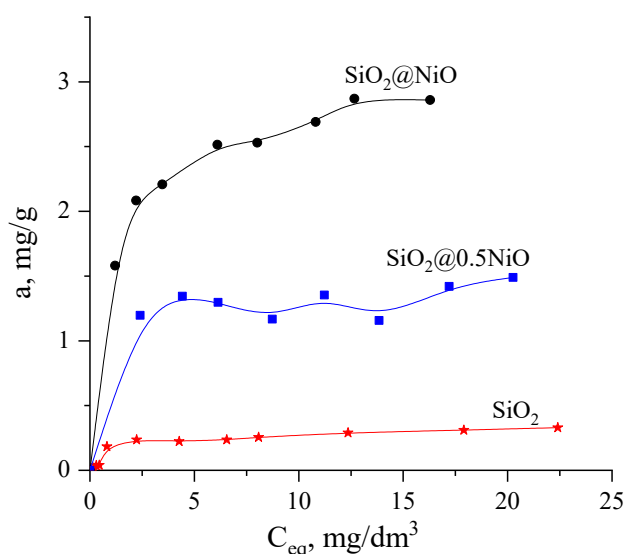


Fig. 4.5 - Isotherms of adsorption of Cu (II) by the pure and modified SiO_2 samples

The results obtained indicate that the sorption capacity of the original SiO_2 in relation to copper ions is insignificant and reaches no more than 0.3 mg/g. At the same time, after modifying its surface with nickel oxide, an increase in this indicator is observed. Thus, for the $\text{SiO}_2@0.5NiO$ sample, the increase in the maximum sorption value is almost 5 times, and for $\text{SiO}_2@NiO$, almost 10 times.

A range of materials, based on commercial silica gel and nickel oxide, was synthesised with differing mass ratios of the components. The analysis of the textural characteristics showed that the obtained samples retained the mesoporous structure of the original matrix, although the average pore radius a slight decline. Furthermore, in the series $\text{SiO}_2 > \text{SiO}_2@0.5NiO > \text{SiO}_2@NiO$, the specific surface area decreased from 411 m^2/g to 186 m^2/g .

4.2 Adsorption removal of methylene blue from water by NiO-modified silica gel

Many industries, such as textile, cosmetic, paper, printing, chemical, etc., use various synthetic dyes to dye their products. As a result, wastewater is formed, which is a potential hazard to the environment and poses a serious threat to human health and other living organisms [216]. Most organic dyes are toxic, have carcinogenic and mutagenic effects on living organisms and negatively affect the photosynthesis processes of aquatic biota [217 - 219]. Due to their limited biodegradability, organic dyes are mainly removed from the aquatic environment. Various technologies are used for this purpose, including ion exchange, chemical precipitation, biosorption, filtration, reverse osmosis, and adsorption [220, 221]. Among these methods, adsorption is widely used for the removal of dyes from water bodies due to its low cost and high efficiency.

Among inorganic materials, silicate-based sorbents can be included in a separate group. They are promising adsorbents for the removal of dyes due to their high chemical and mechanical stability, low cost, availability and structure, which allows modifying their surface by various methods to increase reactivity [222, 223]. It is known that metal oxides exhibit adsorption and photocatalytic ability to organic pollutants, including synthetic dyes [224 - 226]. There are also works that present the results of effective adsorption of dyes by composite materials based on metal oxides and silicates, including using amorphous forms of silica [227, 228].

Therefore, the aim of this study is to obtain an adsorbent based on commercial silica gel with a nickel oxide layer applied for the removal of the organic dye methylene blue from aqueous solutions. Studying the morphology, structural and sorption characteristics, and physicochemical features of the obtained materials will allow for their targeted synthesis, which will contribute to obtaining effective materials with unique properties [229].

Fig. 4.6 shows images of the microstructure of commercial SiO_2 and synthesized samples $\text{SiO}_2\text{-}0.5\text{NiO}$ and $\text{SiO}_2\text{-NiO}$.

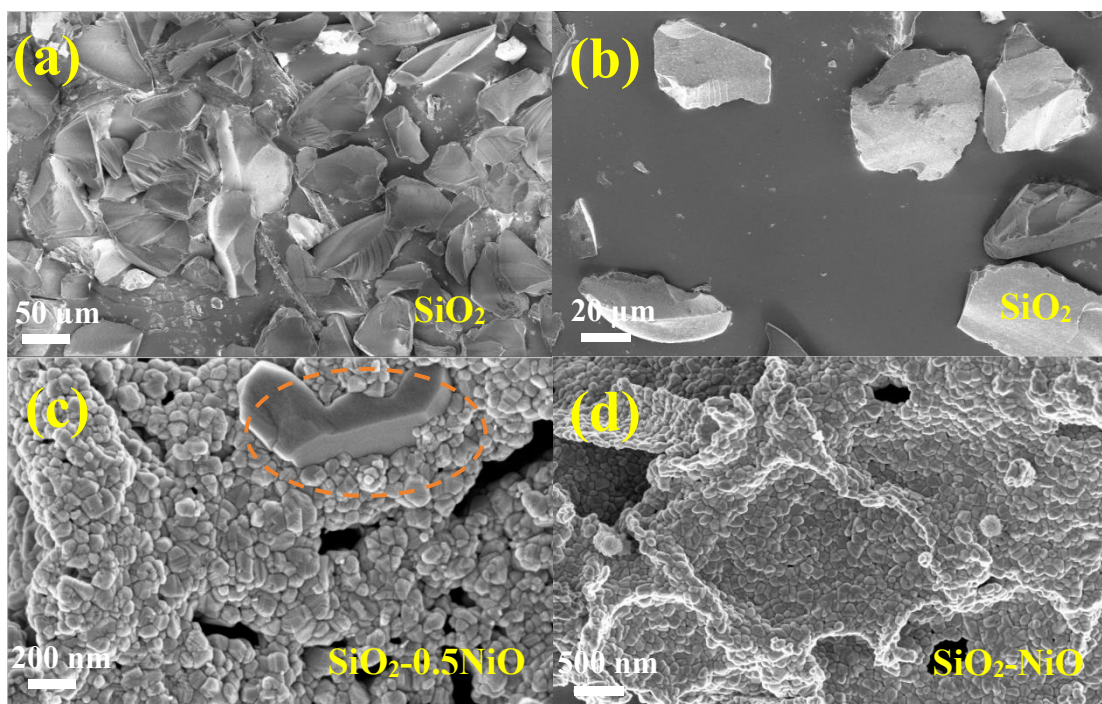


Fig. 4.6 - Characterization of the obtained materials:

a, b – SEM images of SiO_2 ; *c* – SEM images of $\text{SiO}_2\text{-}0.5\text{NiO}$;

d – SEM image of $\text{SiO}_2\text{-NiO}$

It can be seen that the particles of the initial silica gel do not stick together and

have an irregular shape (Fig. 4.6, *a, b*). After modifying its surface with nickel oxide ($\text{SiO}_2\text{-}0.5\text{NiO}$ sample), the formation of a NiO layer is observed (Fig. 4.6, *c*). The presence of this layer is possible due to the fact that SiO_2 and NiO are charged oppositely – negatively and positively, respectively, which allows nickel oxide particles to remain on the SiO_2 surface due to the attraction of charges [227]. It can also be seen that not the entire surface of the silica gel is completely covered with nickel oxide (Fig.4.6, *c*, highlighted in orange), due to which both silica gel and nickel oxide can participate in the dye adsorption process. With an increase in the amount of deposited NiO ($\text{SiO}_2\text{-NiO}$ sample in Fig.4.6,*d*) it is possible to observe an almost completely covered SiO_2 surface, which indicates that further increasing the amount of nickel oxide is no longer of practical importance.

Fig.4.7 shows the elemental analysis of the $\text{SiO}_2\text{-}0.5\text{NiO}$ sample. It can be seen that the element Ni is evenly distributed on the surface of the material, which indicates that nickel oxide is evenly deposited on the surface of the silica gel – silica composite material filled with nickel oxide.

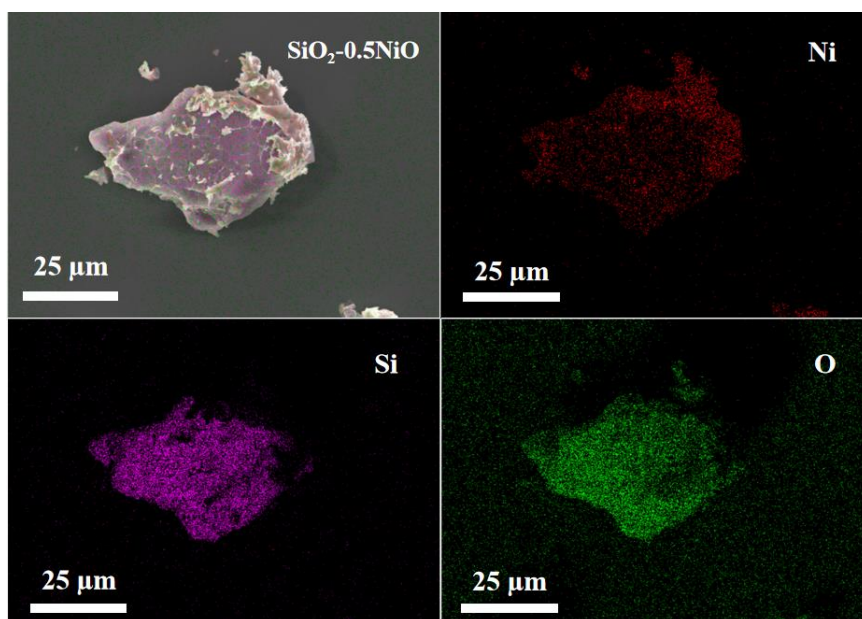


Fig. 4.7 - EDS mapping characterization of $\text{SiO}_2\text{-}0.5\text{NiO}$

In addition, all three elements Si, O are also evenly distributed in the composite sorption material, which further proves its successful synthesis.

To obtain information about the functional groups that are on the surface of the original silica gel and what changes occur to the surface during modification, IR spectra of the samples were obtained, which are presented in Fig.4.8.

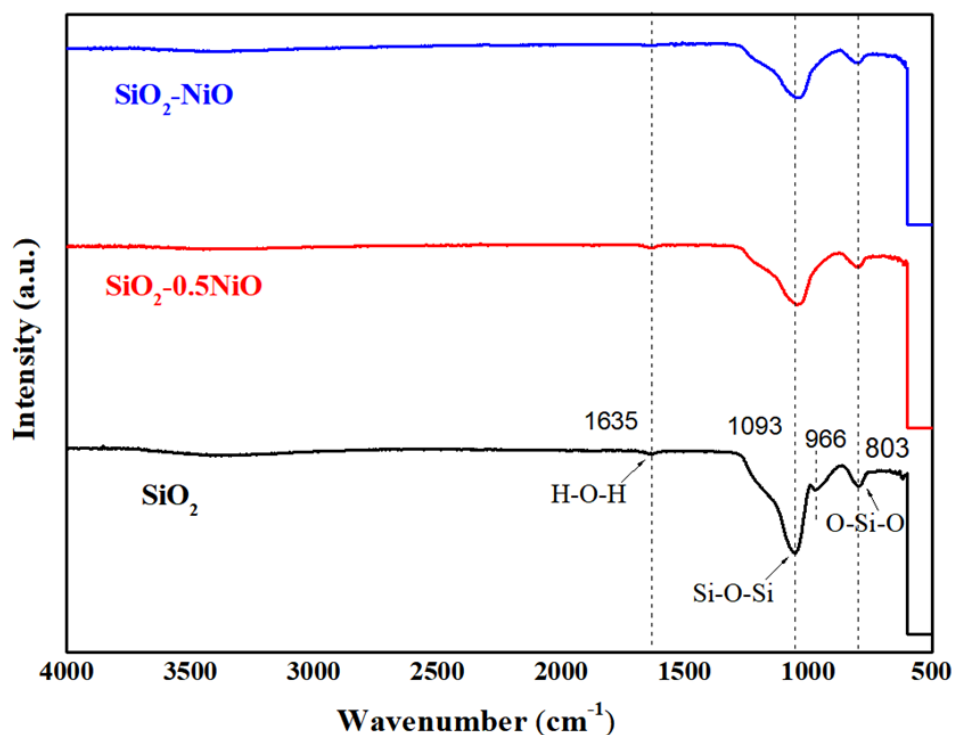


Fig. 4.8 - FTIR images of the obtained materials

It was found that all three materials are characterized by a weak peak at 1635 cm^{-1} , which is due to the vibrations of hydroxyl groups (H-O-H) [230]. In addition, the peaks shown at 1093 cm^{-1} and 803 cm^{-1} , on the other hand, correspond to asymmetric vibrations of Si-O-Si bonds [231]. Only in the IR spectrum of silica gel, a silica-specific peak of Si-OH bonds at 966 cm^{-1} is observed. For the composite samples

$\text{SiO}_2\text{-}0.5\text{NiO}$ and $\text{SiO}_2\text{-NiO}$, the intensity of this peak weakens with an increase in the amount of deposited NiO, which confirms the successful completion of the modification [232]. In addition, the presence of a crystalline phase of nickel oxide on the surface of silica gel is confirmed by X-ray phase analysis. For the $\text{SiO}_2\text{-}0.5\text{NiO}$ and $\text{SiO}_2\text{-NiO}$ samples, characteristic peaks for NiO are observed at $2\theta=37^\circ$, 43° , 62° , 75° and 79° , corresponding to the (222), (400), (440), (622), (444) planes, respectively (JCPDS database map No. 89-5881) and a broad peak at $2\theta\approx 22^\circ$ characteristic of SiO_2 in the amorphous phase [233].

Nitrogen adsorption-desorption isotherms on the original silica gel and modified samples belong to type IV isotherms according to the IUPAC classification, which is typical for materials with a mesoporous structure and a pore size in a narrow range, about 2.5–3 nm. It was found that after applying a nickel oxide layer to silica gel, the specific surface area and pore volume decrease significantly. Thus, SiO_2 has a specific surface area of $411 \text{ m}^2/\text{g}$ and a total pore volume of $0.746 \text{ cm}^3/\text{g}$. The same values for $\text{SiO}_2\text{-}0.5\text{NiO}$ and $\text{SiO}_2\text{-NiO}$ are $256 \text{ m}^2/\text{g}$ and $0.387 \text{ cm}^3/\text{g}$ and $186 \text{ m}^2/\text{g}$ and $0.290 \text{ cm}^3/\text{g}$, respectively, which indicates that the pores are partially blocked by NiO particles or NiO agglomerates are formed on the pore walls [233].

Fig.4.9 shows the dependences of the sorption values of methylene blue on the time of contact with the sorption materials.

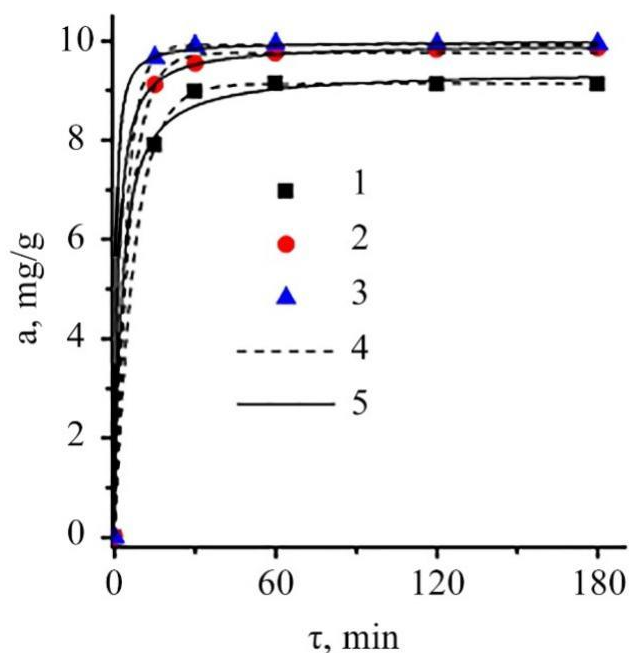


Fig. 4.9 - Adsorption kinetics of methylene blue adsorption by the obtained materials: 1 – SiO_2 ; 2 – $\text{SiO}_2\text{-NiO}$ (1:1); 3 – $\text{SiO}_2\text{-NiO}$ (1:0.5); 4 – pseudo-first-order; 5 – pseudo-second-order

The results indicate that at an initial dye concentration of 20 mg/dm^3 all the studied materials adsorb methylene blue cations quite quickly. The equilibrium state occurs practically within 15–30 minutes, and 1 hour is quite sufficient for adsorption experiments. The analysis of kinetic curves was carried out using pseudo-first and pseudo-second order kinetic models. Table 4.3 shows the calculated parameters of the corresponding equations. The obtained data show that the correlation coefficients of all materials have a very high correspondence to the kinetic models of both orders and are close to 1 ($R^2 > 0.99$).

Table 4.3 - Kinetic parameters adsorption of methylene blue on the obtained materials

Sample	Pseudo-first-order			Pseudo-second-order		
	q_e (mg·g ⁻¹)	K_1 (min ⁻¹)	R^2	q_e (mg·g ⁻¹)	K_2 (g·mg ⁻¹ ·min ⁻¹)	R^2
SiO ₂	9.1310	0.1338	0.999	9.394	0.0435	0.997
SiO ₂ -NiO (1:1)	9.7568	0.1796	0.999	9.940	0.0759	0.999
SiO ₂ -NiO (1:0.5)	9.9248	0.2388	0.999	9.992	0.2068	0.999

Fig.4.10 shows the adsorption isotherms of methylene blue on the original SiO₂ and modified samples based on it. The results obtained indicate that the sorption capacity of SiO₂ with respect to dye ions is somewhat lower than on composite sorbents. It is found that all materials effectively adsorb dye cations from the solution at low initial concentrations, which is due to the presence of a sufficient number of active adsorption centers on the surface. With an increase in the dye concentration in the solution, the surface of the sorbents gradually becomes saturated and at a certain content of the pollutant in the solution, the sorption value no longer increases. It is shown that the maximum adsorption capacity of silica composites after applying NiO increases compared to the original silica, and the efficiency of SiO₂-NiO (1:0.5) is higher than SiO₂-NiO (1:1).

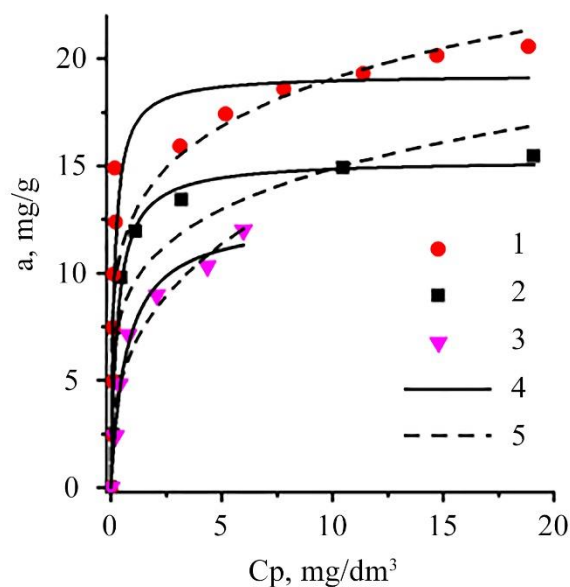


Fig. 4.10 - Adsorption isotherms of methylene blue by the investigated samples:

1 – $\text{SiO}_2\text{-NiO}$ (1:0.5); 2 – $\text{SiO}_2\text{-NiO}$ (1:1); 3 – SiO_2 ; 4 – Langmuir model;

5 - Freundlich model

The experimental data were tested using Langmuir and Freundlich models, respectively [179].

The Langmuir model, according to the calculated correlation coefficients, better describes the obtained isotherms than the Freundlich model (Table 4.4).

Table 4.4 - Fitting parameters for methylene blue adsorption removal isotherms for the investigated samples

Sample	Langmuir			Freundlich		
	q_m ($\text{mg}\cdot\text{g}^{-1}$)	K_L ($\text{l}\cdot\text{mg}^{-1}$)	R^2	K_F ($\text{mg}\cdot\text{g}^{-1}$)	n	R^2
SiO_2	12.636	1.426	0.983	6.528	2.91	0.959
$\text{SiO}_2\text{-NiO}$ (1:0,5)	19.259	6.613	0.876	12.670	5.63	0.836
$\text{SiO}_2\text{-NiO}$ (1:1)	15.286	3.459	0.974	9.458	5.09	0.869

This indicates that the surface of the obtained sorbents is energetically homogeneous and in the process of methylene blue adsorption, a monolayer of pollutant molecules is presumably formed on the surface.

Sorption materials based on commercial silica gel and nickel oxide with different mass ratios of components were obtained. Analysis of structural and sorption characteristics showed that the obtained samples retained the mesoporous structure of the original matrix after applying the modifier layer. At the same time, the specific surface area and average pore radius decreased slightly compared to the original sample. It was found that the removal of methylene blue from the solution by the synthesized materials occurs quite quickly, and the maximum adsorption capacity is possessed by $\text{SiO}_2\text{-NiO}$ (1:0.5). However, the issues of effective phase separation after sorption and the possibility of regeneration of the spent material remain unresolved.

Conclusions to Chapter 4

The mesoporous adsorbent based on commercial silica gel and nickel oxide with different mass ratios of components was obtained. It was shown that the adsorption capacity of silica gel after modification increases almost 10 times. It was established that the removal of methylene blue from the solution by modified silica gel occurs quite quickly, and the maximum adsorption capacity (19.3 mg/g) is possessed by the sample with a mass ratio of SiO_2 to NiO (1:0.5).

The results of this chapter were published in:

1. **Yu, J.**, Bondarieva, A., Tobilko, V., & Pavlenko, V. (2023). Adsorption removal of Cu (II) using Ni-modified silica gel. *Water and Water Purification Technologies*, 3(37), 3-12. <https://doi.org/10.20535/2218-930032023302423>
2. **Yu, J.**, & Tobilko, V. (2024). Removal of methylene blue from water by NiO-modified silica gel. *Technology audit and production reserves*, 6(3 (80)), 47-52. <https://doi.org/10.15587/2706-5448.2024.319822>

CHAPTER 5

MATERIALS BASED ON ALUMINOSILICATES FOR ADSORPTION REMOVAL HEAVY METAL IONS FROM AQUEOUS SOLUTIONS

5.1 Preparation of granular materials based on biopolymers and clay minerals for adsorption removal heavy metal ions from water

Recently, much of the attention of scientists has been focused on the development of so-called “low-cost” adsorbents based on available and inexpensive raw materials [234 - 236]. One of the most promising directions in water purification is the use of natural clay minerals, which, despite their sufficiently high efficiency, strength, chemical resistance and low cost in removing a wide range of pollutants from water, have not been widely used due to their high dispersibility in water, which is not conducive to their recovery [237]. In order to improve the recyclability of adsorbents based on silicate raw materials, powdered aluminosilicates are usually granulated using various binders, such as natural biopolymers - alginates [238]. Although the separation of granular silicate adsorbents from the solution is significantly simplified, on the other hand, the adsorption capacity of the particles decreases due to the reduction in specific surface area. Therefore, the surface modification of aluminosilicates with compounds with a high affinity for metal ions, in particular iron oxyhydroxide (ferrihydrite), has been shown to significantly improve the efficiency of such materials [239, 240].

One of the stages in the production of granular adsorbents based on clay minerals and sodium alginate is to obtain homogeneous suspensions with an optimal ratio of

solid and liquid phases so that the granules are stable in the aqueous medium for a certain time, have a particle shape as close to spherical as possible, and a size that ensures intensive kinetic processes. An unresolved part of the scientific problem is the study of the rheological behavior of such mixtures and the thermal stability of the resulting granules, because if we consider the prospect of using these adsorbents on an industrial scale, ensuring the continuity of the technological process of their production is quite important.

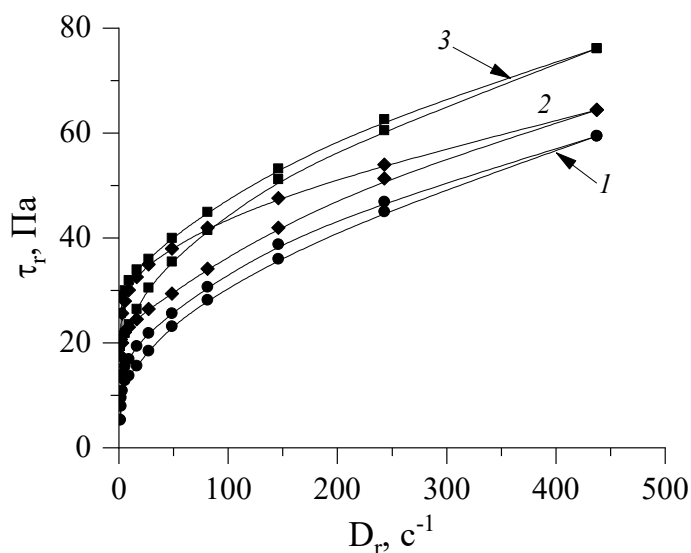
Granular adsorption materials are widely used in water treatment and water purification technologies. Ion-exchange resins [241], adsorbents based on activated carbon [242], natural and modified zeolites [243] are well known, which are highly effective in removing various pollutants from water. A significant number of studies in the field of obtaining granular materials using inorganic, including silicate, raw materials indicate a high interest of scientists in the development of adsorbents using affordable and cheap materials, including natural biopolymers (alginates), which show a high affinity for heavy metal ions and are biocompatible, biodegradable and safe for living organisms. Sorption materials can be produced using only sodium alginate, but such adsorbents have low mechanical strength and thermal stability. To avoid these disadvantages, various fillers are added during synthesis, in particular, organic molecules, polymers, biomass, or inorganic materials [244, 245], such as natural and artificial silicates, metal oxyhydroxides, etc. For example, granular adsorbents based on diatomite [246], silica modified with titanium oxide [247], artificial laponite silicate [248], natural bentonite [250, 251], and synthesized ferrihydrite [252] have been obtained. Given the above, it would be interesting to study the synthesis parameters,

rheological characteristics of clay suspensions with the addition of biopolymers, and thermal properties of granular materials based on modified layered aluminosilicates, which will have improved physical and chemical, including sorption, properties due to the increase of active reaction groups on their surface. Layered clay minerals, such as saponite from the Tashkivske deposit (Ukraine), which is an environmentally friendly mineral raw material with a wide range of applications in agriculture, chemical industry, medicine, and environmental protection, are promising in this area.

The aim of the work is to obtain granular adsorbents based on a natural clay mineral and a biopolymer that are stable in the water environment for water purification from heavy metal ions. To achieve this goal, it was necessary to investigate the rheological behavior of clay suspensions based on saponite and sodium alginate, to obtain granular alginate-containing adsorption materials using natural and modified saponite, and to study the structural, sorption, and thermal properties of the resulting granules [253].

Of particular importance for the preparation of granular adsorption materials based on clay minerals and biopolymers is the viscosity of the resulting suspensions, which is affected by both the content of the solid phase and the amount of sodium alginate solution added. Such mixtures must be aggregately stable for a given time and sufficiently fluid. This ensures favorable conditions for high-quality granulation of the samples.

The rheological behavior of suspensions based on saponite and sodium alginate was studied by obtaining flow curves (Fig. 5.1), i.e., the dependence of shear stress (τ_r) on shear rate (D_r) in the range up to 437 s^{-1} .



1 - Sap-Alg (16:1); 2 – Sap-Alg (32:1); 3 - Sap-Alg (48:1)

Fig. 5.1 - Rheological flow curves of suspensions

The rheological characteristics of the suspensions are presented in Table 5.1. The Bingham model was used to describe them:

$$\tau_r = \tau_c + \eta^* \cdot D_r, \quad (5.1)$$

where τ_r - the shear stress, Pa; τ_c – the ultimate shear stress, Pa; η^* - the plastic viscosity, Pa · s; D_r - the shear rate, c⁻¹.

Table 5.1 - Rheological characteristics of suspensions

№	Sample name	Low shear rates		High shear rates	
		Viscosity, Pa · s	Interval D_r , s ⁻¹	Bingham's equation	Interval D_r , s ⁻¹
1	Sap-Alg (16:1)	6,78	0 – 2	$\tau_r = 20,7 + 0,061 \cdot D_r$	130-437
2	Sap-Alg (32:1)	12,0	0 – 2	$\tau_r = 39,7 + 0,057 \cdot D_r$	160-437
3	Sap-Alg (48:1)	15,47	0 – 2	$\tau_r = 45,3 + 0,071 \cdot D_r$	210-437

After determining the conditions for granulation, a series of samples were obtained, the parameters of which are presented in Table 2.6 (Chapter 2).

The study of their stability in the aqueous medium showed that they completely disintegrated within 1 hour of shaking, which indicated an insufficient amount of added sodium alginate in the clay suspension.

The flow curves of saponite suspensions with sodium alginate (Fig. 5.1) have a typical appearance for clay dispersions with clearly defined hysteresis loops, indicating the formation of thixotropic structures with a predominant mechanism of interaction between the positively charged side surface of clay mineral particles and the negatively charged biopolymer anion [254]. The strength of the structure of the resulting suspensions increases with an increase in the mass ratio of saponite to sodium alginate. This may result from a specific interaction between aluminosilicate particles and the biopolymer, in particular, its possible adsorption by two clay mineral particles simultaneously with the formation of bonds between them, leading to the formation of spatial coagulation structures. In addition, the presence of a hysteresis loop in the flow curves obtained by increasing and decreasing the shear rate is due to the low rate of recovery of the destroyed coagulation structure of the suspension, the strength of which significantly depends on the content of the solid phase in it [255].

In the range of low shear rates (up to 2 s^{-1}), the curves are approximated by straight lines passing through the origin. In this case, the static shear stress (yield strength) is zero because the suspensions are not concentrated. The dependence of the shear stress on the shear rate is linear since in slow flow there is no or low rate of destruction of the suspension structure and coagulation contacts between particles have

time to recover under the influence of thermal motion. Thus, from a rheological point of view, at low shear rates, the investigated suspensions are Newtonian fluids. Under such conditions, they have the highest dynamic viscosity, which depends on the content of clay mineral and sodium alginate. The analysis of flow curves in the range of average shear rate (from 2 to 81 s⁻¹) showed that the effective viscosity of suspensions decreases due to the fact that the destruction of the structure prevails over its recovery.

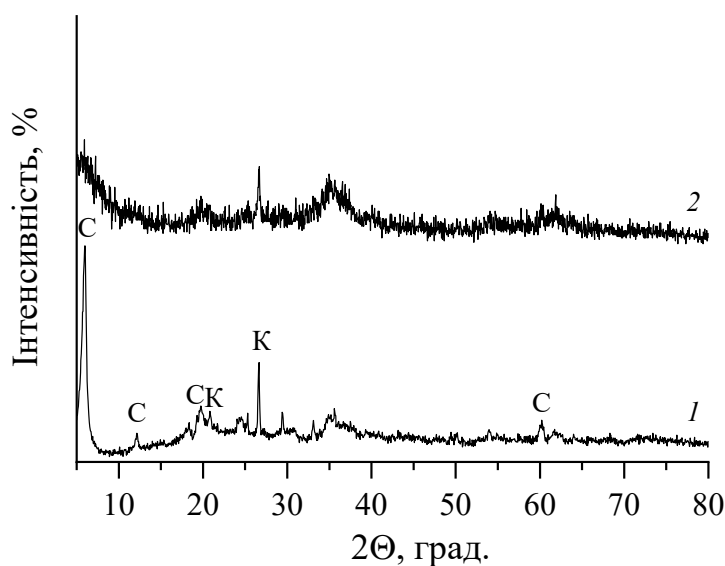
At the same time, it is also possible to orient the particles of the destroyed structure in the flow of the dispersion medium. The dependence of the shear stress, and thus the viscosity, on the shear rate is nonlinear. At high shear rates (interval from 81 to 437 s⁻¹), under the action of high shear stress, the suspension structure is completely destroyed, and the effective (Bingham's) viscosity is the lowest and remains practically unchanged throughout the interval, which creates the most favorable conditions for the implementation of the process of high-quality granulation.

Thus, the results of rheological studies indicate that these suspensions are thixotropic, and for high-quality granulation, it is necessary to carry out their continuous mixing with a shear rate in the range from 225 s⁻¹ to 437 s⁻¹. The necessary conditions can be met by using an orbital shaker and setting the mixing speed of clay dispersions to 150 rpm. At the same time, the suspensions have the necessary fluidity, which makes it easy to pump them with a supervolute pump for continuous feeding into the calcium chloride solution to form spherical granules.

Further studies have determined that in order to obtain stable granules that do not disintegrate during several hours of intense shaking, both based on natural saponite and its ferrihydrite-modified form, it is necessary to have a ratio of components with a

significantly higher content of biopolymer in relation to the clay mineral (see Table 2.5 (Chapter 2)). It should be noted that the synthesized granular adsorption materials Sap-Alg (6:1) and Sap.Fh-Alg (6:1) proved to be quite stable in the aqueous medium since no signs of their destruction were detected during 5 h of shaking on a shaker.

The X-ray diffraction patterns of the original saponite and its modified sample after ferrihydrite application are shown in Fig. 5.2.



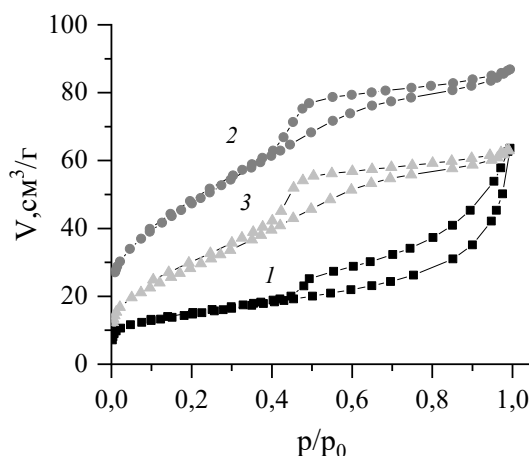
1 - original saponite (S - saponite, K - quartz); 2 - modified saponite

Fig. 5.2 - Diffractograms of powdered saponite

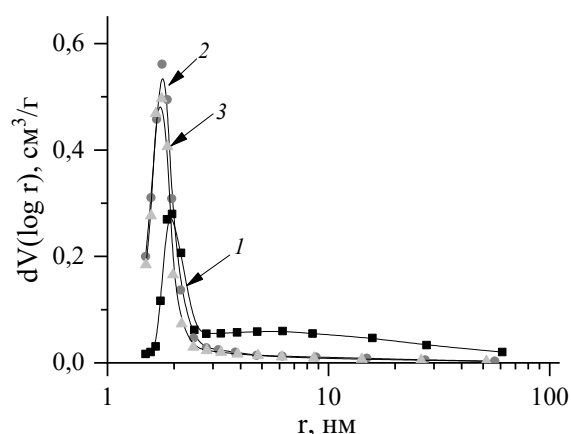
X-ray diffraction data (Fig. 5.2) indicate the practical monominerality of the initial saponite (curve 1) with diffraction peaks $2\theta = 6^\circ$ (1.46 nm), 12° (0.72 nm), 19° (0.45 nm), and 60° (0.15 nm) (PDF File No. 00-013-0305), which contains quartz impurities ($2\theta = 21^\circ$ (0.426 nm) and 27° (0.334 nm) (PDF File No. 01-083-2472)). The diffraction pattern of saponite after ferrihydrite is applied to its surface shows the appearance of an amorphous phase with weak signals characteristic of iron-containing compounds (FeO, Fe₂O₃, etc.). This confirms its successful modification with synthetic

iron oxyhydroxide.

The adsorption-desorption isotherms of nitrogen on natural and modified saponite are shown in Fig. 5.3, and the distribution of pores by size in Fig. 5.4, respectively.



1 - Sap, 2 - Sap-Fh, 3 - Sap.Fh-Alg



1 - Sap, 2 - Sap-Fh, 3 - Sap.Fh-Alg

Fig. 5.3 - Isotherms of low-temperature nitrogen adsorption/desorption of samples

Fig. 5.4 - Distribution of pores by size

The parameters of the porous structure of the test samples are given in Table 5.2.

Table 5.2 - Parameters of the porous structure of the tested samples

Sample	SSA, m ² /g	V _Σ , cm ³ /g	V _{micro} , cm ³ /g	W _{micro} , %	Average pore radius, r, nm
Sap	52	0,0984	0,00523	5,32	3,81
Sap-Fh(6:1)	173	0,134	0,00453	3,38	1,56
Sap.Fh-Alg(6:1)	109	0,0974	-	-	1,78

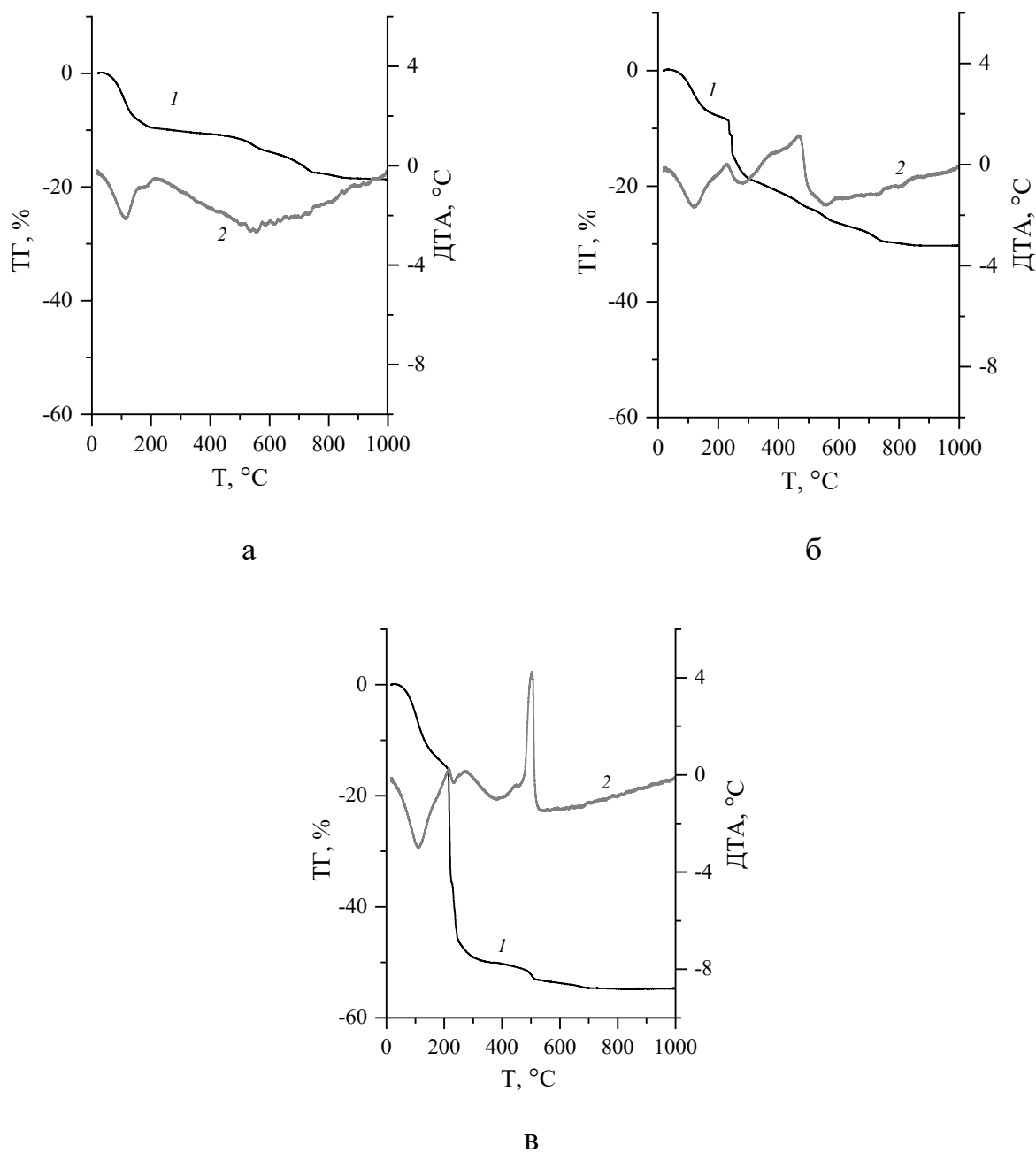
SSA – specific surface area, m²/g; *V_Σ* – total pore volume, cm³/g; *V_{micro}* – micropore volume, cm³/g; *W_{micro}* – micropore content, % *r* – average pore radius, nm

The obtained isotherms of low-temperature nitrogen adsorption/desorption (Fig. 5.3) belong to the type IV isotherms according to the IUPAC classification, which is typical for mesoporous materials. The hysteresis loop of type H4 indicates the presence of micropores in the studied samples, as well as pores with a predominantly slit shape, which is confirmed by the distribution of shapes by size (Fig. 5.4). It should be noted that for sample 3, the desorption branch is not completely closed in the medium and low-pressure region, which is characteristic of a microporous structure with narrow areas in the pore channels. This phenomenon may be due to the filling of free space with sodium alginate molecules. When a layer of amorphous ferrihydrite is applied to the surface of saponite, the specific surface area increases by a factor of 3. At the same time, due to an increase in the proportion of micropores from 21.5% to 42%, the total pore volume increases. During granulation, the specific surface area decreases from 173 m²/g (for the powdered sample) to 109 m²/g (for the granulated sample) but remains 2 times higher than that of the original mineral (Table 5.2).

Using the methods of differential thermal analysis (DTA) and thermogravimetric analysis (TG), we studied the phase transformations and mass changes that occur in granular samples based on clay minerals and biopolymers during heating. Fig. 5.5 shows the derivatograms of granules obtained based on natural (Sap-Alg (6:1)) and ferrihydrite-modified saponite (Sap.Fh-Alg (6:1)). For comparison, DTA and TG curves for the powdered clay mineral (Sap) are presented.

As can be seen from Fig. 5.5, in the temperature range from 20 °C to 170 °C, active mass loss is observed for all samples (see curves 1 for Fig. 5.5 (a, b, c)), which is due to the removal of physically adsorbed water, including its molecules that may be

in the interlayer space of saponite [144]. This is also confirmed by the endothermic effects in this temperature range, which can be observed in the DTA curves (see curves 2 of Fig. 5 (a, b, c)).



a – Sap, б – Sap-Alg(6:1), B – Sap.Fh-Alg (6:1)

1 – TG, %, 2 – DTA, °C

Fig. 5.5 - Derivatograms of samples

At the same time, the results of thermogravimetric analysis (Table 5.3) indicate a gradual increase in the mass loss of granular samples “Sap-Alg(6:1)” and “Sap. Fh - Alg(6:1)” from 7.3% and 12.9%, respectively.

Table 5.3 - Results of differential thermal and thermogravimetric analysis of samples

Sample	Temperature range, °C	Peak temperature of the thermal effect , °C	Mass loss in the temperature range, %	Total mass loss, %
Sap	20 - 170	120	8,3	18,5
	500 - 580	550	1,9	
	700 - 750	-	1,6	
Sap-Alg(6:1)	20 - 170	120	7,3	31,0
	240 - 280	240	9,6	
	480 - 550	480	2,1	
	700 - 750	720	1,5	
Sap.Fh-Alg(6:1)	20 - 170	120	12,9	54,6
	220 - 280	240	44,1	
	480 - 540	500	2,0	
	700 - 750	-	-	

With further heating (in the temperature range from 220 °C to 280 °C), a sharp mass loss is observed for the Sap-Alg(6:1) and Sap.Fh-Alg(6:1) granules, which are not observed for the natural saponite sample. This is due to the dehydration processes that occur in sodium alginate [256] and ferrihydrite [257] at these temperatures. Thus, for the sample Sap.Fh-Alg(6:1), the mass loss is 44.1 %, which is significantly higher

than that for Sap-Alg(6:1) (Table 5.3). These processes are confirmed by the DTA curves, which show end-effects in a given temperature range (Fig. 5.5, b and c, curves 2). With further heating (480 °C - 500 °C), the TG curves for all samples show a slow mass loss, a slight acceleration of which begins at 580 °C, due to the removal of crystallization water and dehydroxylation processes. At the same time, for the granular samples Sap-Alg(6:1) and Sap.Fh-Alg(6:1), this process is superimposed on the burnout of alginate [258] and phase transformations of ferrihydrite [257], respectively, which is confirmed by the exo-effects on the DTA curves (Fig. 5.5 b, c).

Thus, the results obtained indicate that when the obtained granules are heated to a temperature above 200 °C, mass loss occurs due to the processes that take place during the heat treatment of both clay minerals and the burning of sodium alginate and phase transformations of ferrihydrite. However, given the drying regime of granular materials Sap. Fh-Alg(6:1) granular materials proposed in this work (no more than 105 °C), it can be noted that the obtained samples will exhibit high adsorption capacity for heavy metal ions compared to the Sap-Alg(6:1) adsorbent due to the fact that under these synthesis conditions, materials based on modified saponite will have improved physicochemical properties due to an increase in the number of reactive groups introduced by sodium alginate and ferrihydrite.

The rheological behavior of suspensions based on saponite and sodium alginate with different mass ratios of components was investigated. It was found that these systems are thixotropic and their viscosity at the introduction of the same amount of biopolymer depends on the content of the solid phase. Based on these data, the necessary conditions for granulation were selected and samples were obtained using

natural and ferrihydrite-modified saponite. It was found that the stability of granules in an aqueous medium is significantly affected by the amount of sodium alginate added to the suspension. The structural and sorption characteristics and thermal properties of the obtained granular adsorbents were studied and the prospects of their application in water purification from heavy metal ions pollution were shown.

5.2 Adsorption removal of copper (II) from water by mesoporous adsorbents from coal fly ash

Fly ashes formed at thermal power plants during coal combustion (cenospheres) are considered by researchers as a cheap and available raw material for obtaining artificial zeolites. Due to their unique microspherical design and chemical composition, similar to low-modulus zeolites, energy ash cenospheres are a promising base for producing microspherical zeolites that combine a specific zeolite structure with the preserved spherical shape of the original cenospheres. In this work, the method of precipitation was chosen, meaning the synthesis of a zeolite phase on the surface of aluminosilicate microspheres. It is essential that after modification the material retains its original spherical form. In this process the aluminosilicate microspheres act not only as a matrix (core) for the creation of the new material but also as an additional source of silicon and aluminum necessary for building the zeolite framework.

Fig. 5.6 shows the X-ray diffraction patterns of the initial fly ash microspheres (FAM) and the sample with the deposited zeolite layer (z/FAM).

According to the results of the X-ray diffraction analysis (Fig. 5.6), the main

phases of the initial microspheres (FAM) are mullite (PDF File No. 00-015-0776) and quartz (PDF File No. 00-046-1045). As a result of interaction with a sodium aluminate solution, a zeolite phase forms on the surface of the FAM, which is represented by jadeite (PDF File. No. 00-022-1338). Based on calculations, the mineral composition of z/FAM is as follows: jadeite-type zeolite – 45–50%, mullite – 25–27%, and silicon dioxide – up to 20%. For comparison, the FAM consists of 45% mullite and 45% silicon dioxide, the latter including quartz and a significant amount of amorphous SiO₂.

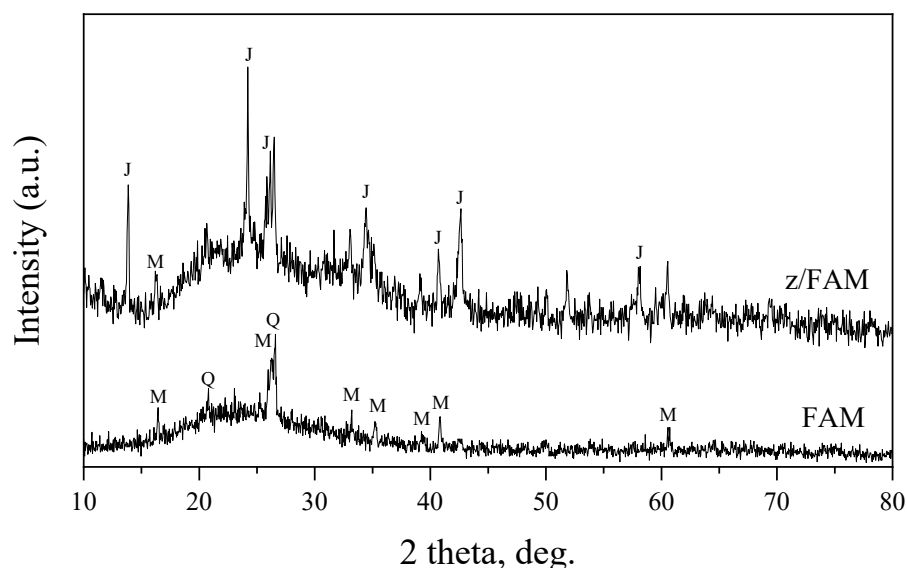


Fig. 5.6 – X-ray patterns of fly ash microspheres (FAM) and zeolite-modified fly ash microspheres (z/FAM): J - jadeite, M – mullite, Q - quartz

SEM images of the initial microspheres and synthesized samples are shown in Fig. 5.7 (a, b) and Fig. 5.7 (c, d), respectively.

Analysis of the SEM images (Fig. 5.7) allows estimation of the average particle size of the initial cenospheres (Figs. 5.7 a and 5.7 b), which is 172.2 μm and agrees

with literature data [259]. The fairly smooth surface structure of the FAM grains, without significant distortions or cracks, indicates the probable absence of micropores. The modified samples (Figs. 5.7 c and 5.7 d) retain the hollow spherical structure of the FAM and possess a secondary external zeolite layer in the form of petal-like spheres ($\sim 2\text{--}2.5\ \mu\text{m}$).

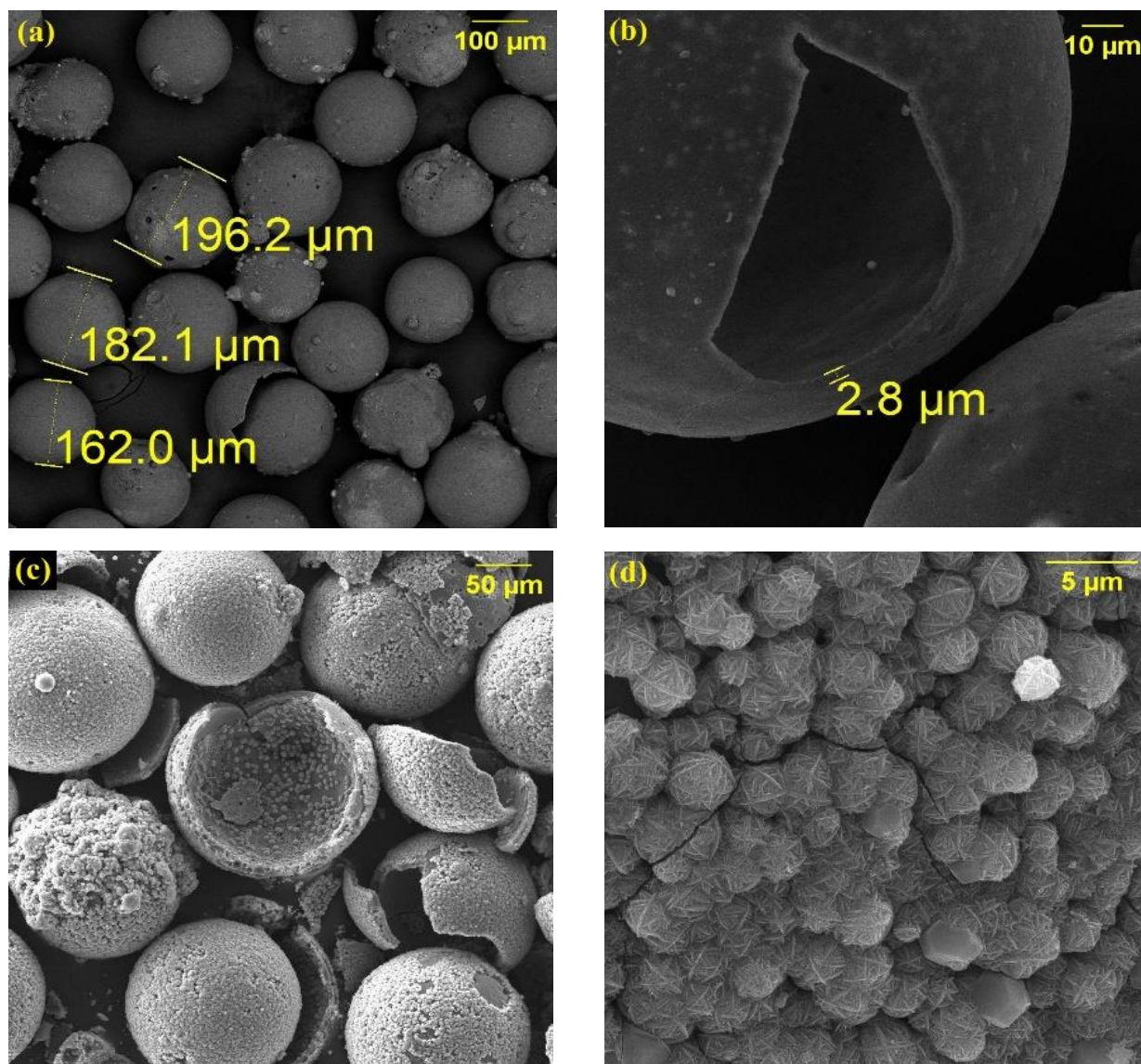


Fig. 5.7 – SEM images of the original microspheres (a, b) and synthesized samples (c, d)

Fig. 5.8 presents EDS spectra of the original microspheres, and Table 5.4 shows

the elemental analysis of the original and modified microspheres.

As can be seen (Fig. 5.8), the spectrum shows clear peaks corresponding to the elements Si, Al, O, and Na. Additionally, the presence of other elements (Mg, K, Ca, Ti, Fe, C) is recorded, confirming the quantitative elemental analysis (Table 5.4).

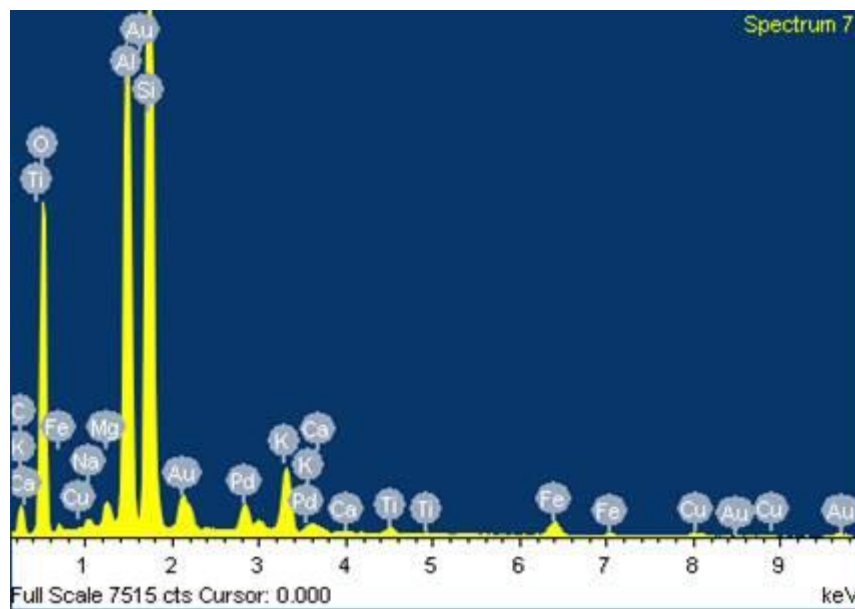


Fig. 5.8 – EDS spectra of the original microspheres

Table 5.4 – Elemental analysis of the original and modified microspheres (EDS results)

Samples	Content (wt.%)			
	Si	Al	Na	Others*
FAM	22,11	13,59	0,37	63,93
z/FAM	14,66	14,44	10,77	60,13

*Mg, K, Ca, Ti, Fe, C

The presence of gold and palladium peaks is due to surface treatment prior to analysis. It is worth noting that after treating FAM with sodium aluminate solution, the Na content in the z/FAM sample significantly increased, while the Si content decreased, with the Al content remaining nearly unchanged. This indicates that a chemical reaction occurred between the FAM components and the alkaline sodium aluminate solution, resulting in a zeolite phase deposited on the surface of the original microspheres.

Nitrogen adsorption-desorption isotherms for FAM and z/FAM samples and their pore size distributions are shown in Fig. 5.9 and 5.10, respectively. Table 5.5 provides the main porous structure parameters of the studied materials.

As a result of FAM zeolitization, the specific surface area increased more than tenfold; the number and total volume of pores also increased. The shape of the isotherm for the initial microspheres (Fig. 5.9 a) indicates the presence of primarily macropores and a small number of micropores, which aligns with SEM observations.

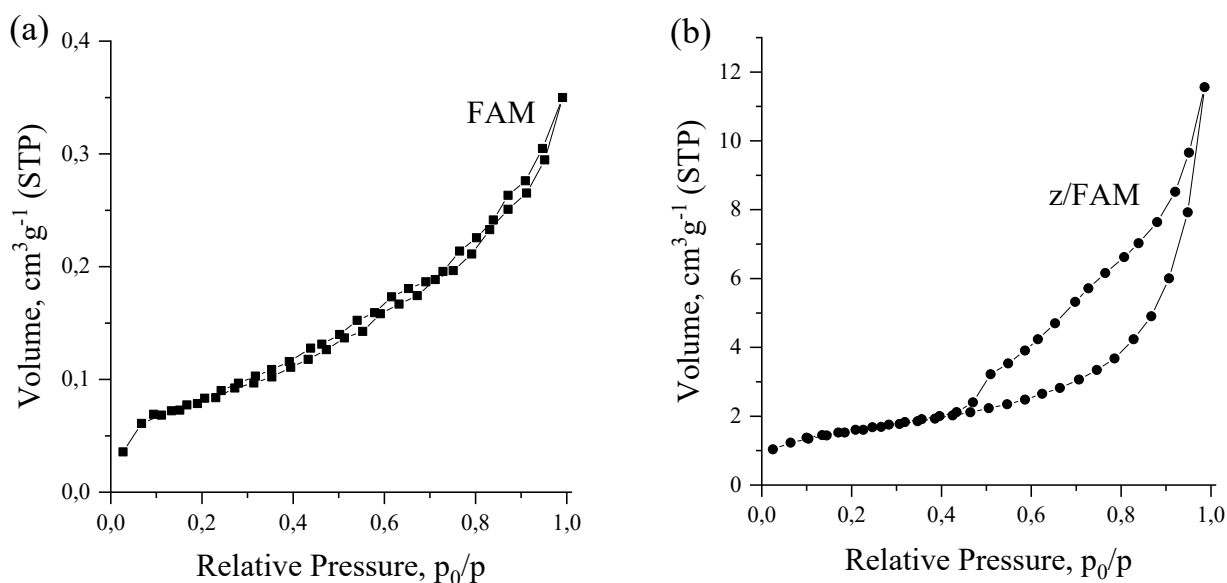


Fig. 5.9 – Nitrogen adsorption/desorption isotherms for original (FAM) and modified (z/FAM) microspheres

For the modified microspheres (Fig. 5.9 b), the isotherm displays a pronounced hysteresis loop in the relative pressure range from 0.45 to 1, indicating a mesoporous structure. This change in porous structure is also confirmed by Fig. 5.10. While the FAM shows several local pore maxima below 10 nm with a small volume (Fig. 5.10 a), the z/FAM displays a wide pore size distribution starting from 2 nm with a stable volume (Fig. 5.10 b).

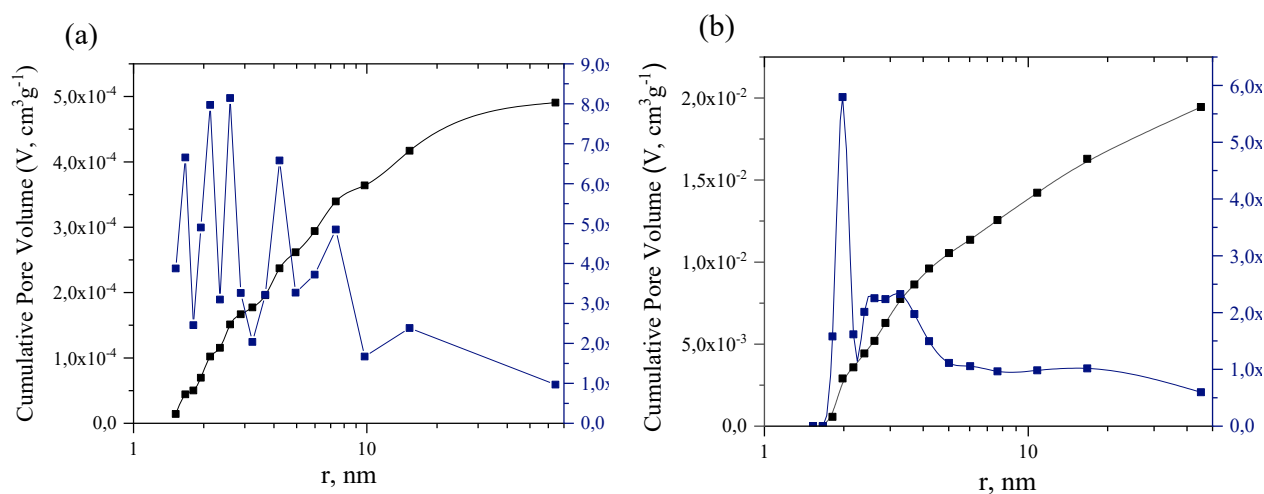


Fig. 5.10 – Pore size distribution of original (a) and modified (b) microspheres by BJH method

Table 5.5 – Porous structure parameters of the studied materials

Parameters	Materials	
	FAM	z/FAM
Specific surface area (S_{BET}), $m^2 g^{-1}$	0,4	6
External surface area, $m^2 g^{-1}$	0,17	5
Total pore volume (V_{Σ}), $cm^3 g^{-1}$	$5,415 \cdot 10^{-4}$	$1,788 \cdot 10^{-2}$
Volume of micropores (V_{μ}), $cm^3 g^{-1}$	$7,693 \cdot 10^{-5}$	$1,544 \cdot 10^{-4}$
Content of micropores (V_{μ}), %	1,75	21,4
Average pore radius, nm	2,615	6,489

To determine the efficiency of the synthesized zeolite-coated sample for removing heavy metal ions from water, the main physicochemical features of copper ion removal from model solutions were studied.

The study of contact time between solid and liquid phases showed that copper cation removal by z/FAM occurs quite rapidly. At an initial Cu^{2+} concentration of 5 mg/L and a pH of 5.6, more than 85% of the contaminant is removed within 1 hour.

Fig. 5.11 shows the dependence of copper ion removal efficiency on the pH of the water. As can be seen, with increasing pH, the adsorption capacity increases, which is related to both the speciation of copper ions in water and the surface chemistry of the samples. It is known that up to pH 5.8, copper exists as positively charged ions Cu^{2+} and $\text{Cu}(\text{OH})_2^{2+}$ [179], and the Cu^{2+} content decreases as pH approaches 6. The study was conducted in the pH range 3.2–5.8 to avoid copper hydroxide precipitation. For z/FAM, the copper removal efficiency exceeds 70% already at pH ~ 3 , and at pH 4 or higher it reaches about 90% and remains stable up to pH 5.8. This indicates that the obtained sorbent material can effectively remove metal cations in acidic and mildly acidic environments.

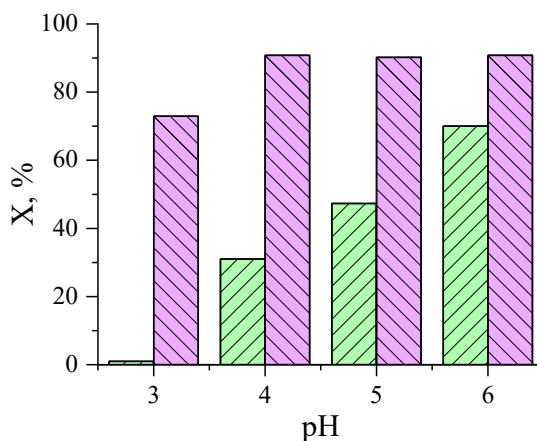


Fig. 5.11 – Influence of pH on copper ion removal efficiency (green – original

microspheres, purple – modified)

Results of copper adsorption capacity studies of the obtained zeolite materials are presented in Fig. 5.12. The study was conducted in the Cu^{2+} concentration range of 5–25 mg/l, pH = 5.7, and mixing time of 1 hour.

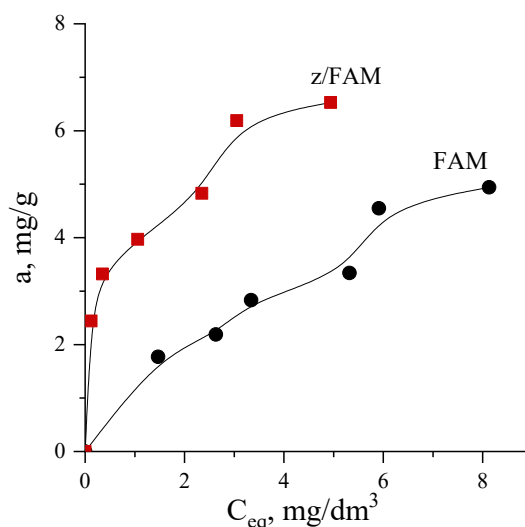


Fig. 5.12 – Copper adsorption isotherms on FAM and z/FAM samples

The obtained data indicate that the deposition of a zeolite phase on FAM increases copper sorption capacity from 4.94 mg/g to 6.53 mg/g. Thus, the research shows that synthetic zeolites have good sorption capacities for Cu(II) ions at low concentration levels. The affinity of Cu(II) ions for synthetic zeolites (z/FAM) was significantly higher than for fly ash microspheres (FAM). Consequently, they should be considered effective and economical sorbents for water and wastewater treatment.

Conclusions to Chapter 5

Stable in an aqueous environment, low-cost granular adsorption materials were

obtained using saponite modified with ferrihydrite and sodium alginate. Based on the study of the rheological properties of suspensions and thermal characteristics of granules, the optimal conditions for their production were determined. The perspective of their use in water purification from heavy metal ion contamination has been established.

It was shown that using fly ash, it is possible to obtain adsorption materials for the removal of heavy metal ions from water. It was established that the deposition of the zeolite phase on the surface of microspheres increases their sorption capacity with respect to copper ions from 4.94 mg/g to 6.53 mg/g, but to increase efficiency, it is necessary to carry out a longer synthesis at a higher temperature.

The results of this chapter were published in:

1. Fomenko, O., Makovetskyi, O., Bondarieva, A., Tobilko, V., & **Yu, J.** (2024). Obtaining granular adsorbents based on biopolymers and clay minerals. Bulletin of NTUU «Igor Sikorsky Kyiv Polytechnic Institute», Series «Chemical Engineering, Ecology and Resource Saving», (3), 93–103. <https://doi.org/10.20535/2617-9741.3.2024.312425> (in Ukraine).
2. Bondarieva, A., **Yu, J.**, Tobilko, V. (2022). Saponite based composite materials for removal of inorganic toxicants. Abstract Book of participants of the International research and practice conference «Nanotechnology and nanomaterials» (NANO-2022). Lviv, Ukraine, August 25-27, 2022, P. 276.

CONCLUSIONS

An analytical review of the literature was conducted regarding adsorption materials used for the protection of water environments from contamination by heavy metal ions and organic dyes. Methods for obtaining mesoporous adsorbents based on synthetic silicates (silicas) and natural and artificial aluminosilicate materials were analyzed, and various approaches to their chemical modification were considered.

Amorphous dendritic mesoporous silica was synthesized. The surface morphology was studied, revealing that the silica microspheres obtained from syntheses conducted over 1, 3, and 5 hours are monodisperse spheres with diameters of approximately 200 nm, pore sizes ranging from 5 to 50 nm, and specific surface areas of 504, 452, and 308 m²/g, respectively. It was determined that a synthesis duration of 1.5 hours is optimal for achieving a high specific surface area and favorable morphology without significant pore coalescence or edge thickening.

An adsorbing material was obtained by depositing zero-valent iron (Fe⁰) particles onto the surface of the dendritic mesoporous silica. It was found that the specific surface area of the modified sample is nearly half that of the original silica, which may be attributed to Fe⁰ particles occupying or partially blocking the pore channels. It was demonstrated that the maximum adsorption capacity of the modified adsorbent for copper ions is 39.8 mg·g⁻¹, which is approximately 57 times higher than that of the unmodified material.

An aminofunctionalized adsorbent was obtained by chemically modifying dendritic mesoporous silica with 3-aminopropyltriethoxysilane. It was found that the

content of -NH_2 groups in the modified sample is significantly higher than the content of -OH groups in the unmodified material - 2.03 meq/g versus 0.16 meq/g, respectively. It was established that the original silica exhibits virtually no adsorption capacity for copper ions at pH 6, whereas the modified material demonstrates efficient removal of Cu(II) across the entire studied pH range. It was shown that adsorption equilibrium is reached relatively quickly. X-ray photoelectron spectroscopy results indicate the formation of coordination bonds between Cu^{2+} ions and amino groups, which confirms the involvement of both physisorption and chemisorption processes. Studies on the regeneration of the spent material show that it can be reused.

An adsorbent based on commercial silica gel and nickel oxide with varying mass ratios of the components was obtained. It was found that this material has a mesoporous structure formed by uniformly packed spherical particles of the same size. The results show that the adsorption capacity of silica gel increases nearly tenfold after surface modification with nickel oxide, reaching about 3 mg/g. It was demonstrated that the removal of methylene blue from solution by the modified silica gel occurs rapidly, with the highest adsorption capacity (19.3 mg/g) observed for the sample with a SiO_2 to NiO mass ratio of 1:0.5.

Water-stable low-cost granulated adsorbent materials were obtained using aluminosilicate (saponite) modified with ferrihydrite and the natural biopolymer sodium alginate. Based on the study of the rheological properties of the suspensions and the thermal characteristics of the granules, optimal conditions for their preparation were determined. The materials showed promising potential for use in the removal of heavy metal ions from water.

It was shown that adsorption materials for heavy metal ion removal from water can also be obtained using technogenic aluminosilicate waste (fly ash). It was found that the deposition of a zeolite phase on the surface of microspheres increases their sorption capacity for copper ions from 4.94 mg/g to 6.53 mg/g. However, to improve effectiveness, a longer synthesis time at a higher temperature is necessary.

REFERENCES

1. Mishra, R. K. (2023). Fresh water availability and its global challenge. *British Journal of Multidisciplinary and Advanced Studies*, 4(3), 1-78. <https://doi.org/10.37745/bjmas.2022.0208>
2. Zhou, Q., Yang, N., Li, Y., Ren, B., Ding, X., Bian, H., & Yao, X. (2020). Total concentrations and sources of heavy metal pollution in global river and lake water bodies from 1972 to 2017. *Global Ecology and Conservation*, 22, e00925. <https://doi.org/10.1016/j.gecco.2020.e00925>
3. Adesibikan, A. A., Emmanuel, S. S., Olawoyin, C. O., & Ndungu, P. (2024). Cellulosic metallic nanocomposites for photocatalytic degradation of persistent dye pollutants in aquatic bodies: a pragmatic review. *Journal of Organometallic Chemistry*, 123087. <https://doi.org/10.1016/j.jorganchem.2024.123087>
4. Rad, S. M., Ray, A. K., & Barghi, S. (2022). Water pollution and agriculture pesticide. *CleanTechnologies*, 4(4), 1088-1102. <https://doi.org/10.3390/cleantechnol4040066>
5. Wu, L., Qiu, X. W., Wang, T., Tao, K., Bao, L. J., & Zeng, E. Y. (2022). Water quality and organic pollution with health risk assessment in China: a short review. *ACS ES&T Water*, 2(8), 1279-1288. <https://doi.org/10.1021/acsestwater.2c00137>
6. Verma, R., & Kumar, S. (2023). Research on the Impact of River Pollution on Water Quality. *Social Science Journal for Advanced Research*, 3(4), 6-11. <https://doi.org/10.54741/ssjar.3.4.3>
7. Dahiya, V. (2022). Heavy metal toxicity of drinking water: A silent killer. *GSC Biological and Pharmaceutical Sciences*, 19(1), 020-025.

<https://doi.org/10.30574/gscbps.2022.19.1.0107>

8. Kaji, Masanori (2019)."6. Cadmium Poisoning in Japan: Itai-itai Disease and Beyond". *Hazardous Chemicals: Agents of Risk and Change, 1800-2000*, edited by Ernst Homburg and Elisabeth Vaupel, New York, Oxford: Berghahn Books, , pp. 211-234. <https://doi.org/10.1515/9781789203202-010>
9. Xia, S., Song, Z., Zhao, X., & Li, J. (2023). Review of the recent advances in the prevention, treatment, and resource recovery of acid mine wastewater discharged in coal mines. *Journal of Water Process Engineering*, 52, 103555. <https://doi.org/10.1016/j.jwpe.2023.103555>
10. Bhupendra Koul, Dhananjay Yadav, Swati Singh, Manoj Kumar, Minseok Song (2022). Insights into the Domestic Wastewater Treatment (DWWT) Regimes: A Review. *Water*, 14(21), 3542. <https://doi.org/10.3390/w14213542>
11. Khatun, J., Intekhab, A., & Dhak, D. (2022). Effect of uncontrolled fertilization and heavy metal toxicity associated with arsenic (As), lead (Pb) and cadmium (Cd), and possible remediation. *Toxicology*, 477, 153274. <https://doi.org/10.1016/j.tox.2022.153274>
12. Maheshwari, K., Agrawal, M., Gupta, A.B. (2021). Dye Pollution in Water and Wastewater. In: Muthu, S.S., Khadir, A. (eds) *Novel Materials for Dye-containing Wastewater Treatment . Sustainable Textiles: Production, Processing, Manufacturing & Chemistry*. Springer, Singapore. https://doi.org/10.1007/978-981-16-2892-4_1
13. Ismail, M., Akhtar, K., Khan, M. I. et al. (2019). Pollution, toxicity and carcinogenicity of organic dyes and their catalytic bio-remediation. *Current pharmaceutical design*, 25(34), 3645-3663.

<https://doi.org/10.2174/1381612825666191021142026>

14. Shabir, M., Yasin, M., Hussain, M. et al. (2022). A review on recent advances in the treatment of dye-polluted wastewater. *Journal of Industrial and Engineering Chemistry*, 112, 1-19. <https://doi.org/10.1016/j.jiec.2022.05.013>

15. Chakraborty, D., Mukhopadhyay, K., Chakraborty, D., & Mukhopadhyay, K. (2014). Status of water pollution in India and other countries of Asia. *Water Pollution and Abatement Policy in India: A Study from an Economic Perspective*, 23-45. https://doi.org/10.1007/978-94-017-8929-5_2

16. Shan, V., Singh, S.K., Haritash, A.K. (2020). Water Crisis in the Asian Countries: Status and Future Trends. In: Kumar, M., Munoz-Arriola, F., Furumai, H., Chaminda, T. (eds) *Resilience, Response, and Risk in Water Systems*. Springer Transactions in Civil and Environmental Engineering. Springer, Singapore. https://doi.org/10.1007/978-981-15-4668-6_10

17. Rather, L. J., Akhter, S., Padder, R. A., Hassan, Q. P., Hussain, M., Khan, M. A., & Mohammad, F. (2017). Colorful and semi durable antioxidant finish of woolen yarn with tannin rich extract of *Acacia nilotica* natural dye. *Dyes and Pigments*, 139, 812-819. <https://doi.org/10.1016/j.dyepig.2017.01.018>

18. Shanker, U., Rani, M., & Jassal, V. (2017). Degradation of hazardous organic dyes in water by nanomaterials. *Environmental chemistry letters*, 15, 623-642. <https://doi.org/10.1007/s10311-017-0650-2>

19. Han, S., Xing, Z., Jiang, H., Li, W., & Huang, W. (2021). Biological adaptive mechanisms displayed by a freshwater plant to live in aquatic and terrestrial environments. *Environmental and Experimental Botany*, 191, 104623.

<https://doi.org/10.1016/j.envexpbot.2021.104623>

20. Sharma, J., Sharma, S., & Soni, V. (2021). Classification and impact of synthetic textile dyes on Aquatic Flora: A review. *Regional Studies in Marine Science*, 45, 101802. <https://doi.org/10.1016/j.rsma.2021.101802>

21. Selvaraj, V., Karthika, T. S., Mansiya, C., & Alagar, M. (2021). An over review on recently developed techniques, mechanisms and intermediate involved in the advanced azo dye degradation for industrial applications. *Journal of molecular structure*, 1224, 129195. <https://doi.org/10.1016/j.molstruc.2020.129195>

22. Danilov-Danilyan, V. I., Polyanin, V. O., Fashchevskaya, T. B., Kirpichnikova, N. V., Kozlova, M. A., & Venitsianov, E. V. (2020). The Problem of Reducing the Diffuse Pollution of Water Bodies and Improving the Efficiency of Water Protection Programs. *Water Resources*, 47, 691-701. <https://doi.org/10.1134/S009780782005005X>

23. Mushtaq, N., Singh, D. V., Bhat, R. A., Dervash, M. A., & Hameed, O. B. (2020). Freshwater contamination: sources and hazards to aquatic biota. *Fresh water pollution dynamics and remediation*, 27-50.. https://doi.org/10.1007/978-981-13-8277-2_3

24. Rathi, B. S., & Kumar, P. S. (2021). Application of adsorption process for effective removal of emerging contaminants from water and wastewater. *Environmental Pollution*, 280, 116995. <https://doi.org/10.1016/j.envpol.2021.116995>

25. Liu, Y., Zhang, X., & Wang, J. (2022). A critical review of various adsorbents for selective removal of nitrate from water: Structure, performance and mechanism. *Chemosphere*, 291, 132728. <https://doi.org/10.1016/j.chemosphere.2021.132728>

26. Khojastehnezhad, A., Moeinpour, F., Jafari, M., Shehab, M. K., Samih ElDouhaibi, A., El-Kaderi, H. M., & Siaj, M. (2023). Postsynthetic modification of core-shell magnetic covalent organic frameworks for the selective removal of mercury. *ACS Applied Materials & Interfaces*, 15(23), 28476-28490. <https://doi.org/10.1021/acsami.3c02914>
27. Gkika, D. A., Mitropoulos, A. C., & Kyzas, G. Z. (2022). Why reuse spent adsorbents? The latest challenges and limitations. *Science of the Total Environment*, 822, 153612. <https://doi.org/10.1016/j.scitotenv.2022.153612>
28. Bera, S. P., Godhaniya, M., & Kothari, C. (2022). Emerging and advanced membrane technology for wastewater treatment: A review. *Journal of Basic Microbiology*, 62(3-4), 245-259. <https://doi.org/10.1002/jobm.202100259>
29. Men, Y., Li, Z., Zhu, L., Wang, X., Cheng, S., & Lyu, Y. (2023). New insights into membrane fouling during direct membrane filtration of municipal wastewater and fouling control with mechanical strategies. *Science of the Total Environment*, 869, 161775. <https://doi.org/10.1016/j.scitotenv.2023.161775>
30. Jasim, A. Q., & Ajjam, S. K. A. (2024). Heavy Metal Removal Technologies with Details of Ion Exchange: Review study. *Journal of University of Babylon for Engineering Sciences*, 32(4), 116-132. <https://doi.org/10.29196/qnf7aa96>
31. Ren, Y., Han, Y., Lei, X., Lu, C., Liu, J., Zhang, G., ... & Zhang, Q. (2020). A magnetic ion exchange resin with high efficiency of removing Cr (VI). *Colloids and Surfaces A: Physicochemical and Engineering Aspects*, 604, 125279. <https://doi.org/10.1016/j.colsurfa.2020.125279>
32. Mudgal, V., Raninga, M., Patel, D., Ankoliya, D., & Mudgal, A. (2023). A review

on Phytoremediation: Sustainable method for removal of heavy metals. *Materials Today: Proceedings*, 77, 201-208. <https://doi.org/10.1016/j.matpr.2022.11.261>

33. Saleh, T. A., Mustaqeem, M., & Khaled, M. (2022). Water treatment technologies in removing heavy metal ions from wastewater: A review. *Environmental Nanotechnology, Monitoring & Management*, 17, 100617. <https://doi.org/10.1016/j.enmm.2021.100617>

34. Ahmad, K. (2023). Feasibility of the adsorption as a process for its large scale adoption across industries for the treatment of wastewater: Research gaps and economic assessment. *Journal of Cleaner Production*, 388, 136014. <https://doi.org/10.1016/j.jclepro.2023.136014>

35. Lei, X., Lian, Q., Zhang, X., Karsili, T. K., Holmes, W., Chen, Y., ... & Gang, D. D. (2023). A review of PFAS adsorption from aqueous solutions: Current approaches, engineering applications, challenges, and opportunities. *Environmental Pollution*, 321, 121138. <https://doi.org/10.1016/j.envpol.2023.121138>

36. Pourret, O., Bollinger, J. C., Hursthouse, A., & van Hullebusch, E. D. (2022). Sorption vs adsorption: The words they are a-changin', not the phenomena. *Science of the Total Environment*, 838, 156545. <https://doi.org/10.1016/j.scitotenv.2022.156545>

37. Tran, H. N., Tomul, F., Ha, N. T. H., Nguyen, D. T., Lima, E. C., Le, G. T., ... & Woo, S. H. (2020). Innovative spherical biochar for pharmaceutical removal from water: Insight into adsorption mechanism. *Journal of hazardous materials*, 394, 122255. <https://doi.org/10.1016/j.jhazmat.2020.122255>

38. Wang, J., & Guo, X. (2020). Adsorption isotherm models: Classification, physical meaning, application and solving method. *Chemosphere*, 258, 127279.

<https://doi.org/10.1016/j.chemosphere.2020.127279>

39. Gusain, R., Kumar, N., & Ray, S. S. (2020). Recent advances in carbon nanomaterial-based adsorbents for water purification. *Coordination Chemistry Reviews*, 405, 213111. <https://doi.org/10.1016/j.ccr.2019.213111>
40. Inglezakis, V. J., & Zorpas, A. A. (2012). Heat of adsorption, adsorption energy and activation energy in adsorption and ion exchange systems. *Desalination and water treatment*, 39(1-3), 149-157. <https://doi.org/10.1080/19443994.2012.669169>
41. Gong, H., Tan, Z., Zhang, L., & Huang, Q. (2019). Preparation of biochar with high absorbability and its nutrient adsorption–desorption behaviour. *Science of the Total Environment*, 694, 133728. <https://doi.org/10.1016/j.scitotenv.2019.133728>
42. Xia, M., Chen, Z., Li, Y., Li, C., Ahmad, N. M., Cheema, W. A., & Zhu, S. (2019). Removal of Hg (II) in aqueous solutions through physical and chemical adsorption principles. *RSC advances*, 9(36), 20941-20953. <https://doi.org/10.1039/C9RA01924C>
43. Inglezakis, V. J., & Zorpas, A. A. (2012). Heat of adsorption, adsorption energy and activation energy in adsorption and ion exchange systems. *Desalination and water treatment*, 39(1-3), 149-157. <https://doi.org/10.1080/19443994.2012.669169>
44. Siu, B., Chowdhury, A. R., Yan, Z., Humphrey, S. M., & Hutter, T. (2023). Selective adsorption of volatile organic compounds in metal-organic frameworks (MOFs). *Coordination Chemistry Reviews*, 485, 215119. <https://doi.org/10.1016/j.ccr.2023.215119>
45. Ewis, D., Ba-Abbad, M. M., Benamor, A., & El-Naas, M. H. (2022). Adsorption of organic water pollutants by clays and clay minerals composites: A comprehensive review. *Applied Clay Science*, 229, 106686. <https://doi.org/10.1016/j.clay.2022.106686>

46. Liu, S., Huang, J., Zhang, W., Shi, L., Yi, K., Yu, H., ... & Li, J. (2022). Microplastics as a vehicle of heavy metals in aquatic environments: A review of adsorption factors, mechanisms, and biological effects. *Journal of Environmental Management*, 302, 113995. <https://doi.org/10.1016/j.jenvman.2021.113995>
47. Jung, Y. E., Kang, S. W., & Yim, M. S. (2021). Feasibility study of using Bi-mna metal–organic frameworks as adsorbents for radioiodine capture at high temperature. *Industrial & Engineering Chemistry Research*, 60(16), 5964-5975. <https://doi.org/10.1021/acs.iecr.1c00450>
48. Hussain, S., Kamran, M., Khan, S. A., Shaheen, K., Shah, Z., Suo, H., ... & Ghani, U. (2021). Adsorption, kinetics and thermodynamics studies of methyl orange dye sequestration through chitosan composites films. *International Journal of Biological Macromolecules*, 168, 383-394. <https://doi.org/10.1016/j.ijbiomac.2020.12.054>
49. Chen, L., Zhu, Y., Cui, Y., Dai, R., Shan, Z., & Chen, H. (2021). Fabrication of starch-based high-performance adsorptive hydrogels using a novel effective pretreatment and adsorption for cationic methylene blue dye: Behavior and mechanism. *Chemical Engineering Journal*, 405, 126953. <https://doi.org/10.1016/j.cej.2020.126953>
50. Huang, W. H., Chang, Y. J., Wu, R. M., Chang, J. S., Chuang, X. Y., & Lee, D. J. (2023). Type-wide biochars loaded with Mg/Al layered double hydroxide as adsorbent for phosphate and mixed heavy metal ions in water. *Environmental Research*, 224, 115520. <https://doi.org/10.1016/j.envres.2023.115520>
51. Feng, C., Huang, M., & Huang, C. P. (2023). Specific chemical adsorption of selected divalent heavy metal ions onto hydrous γ -Fe₂O₃-biochar from dilute aqueous

- solutions with pH as a master variable. *Chemical Engineering Journal*, 451, 138921. <https://doi.org/10.1016/j.cej.2022.138921>
52. Acosta-Herrera, A. A., Hernández-Montoya, V., Tovar-Gómez, R., Pérez-Cruz, M. A., Montes-Morán, M. A., Rangel-Vázquez, N. A., & Cervantes, F. J. (2023). Water reclamation from anodizing wastewaters by removing reactive silica with adsorption and precipitation methods. *Journal of environmental management*, 326, 116683. <https://doi.org/10.1016/j.jenvman.2022.116683>
53. Liu, Y., Zhong, D., Xu, Y., Chang, H., Dong, L., Han, Z., ... & Zhong, N. (2023). Adsorption of phosphate in water by La/Al bimetallic-organic frameworks-chitosan composite with wide adaptable pH range. *Journal of Environmental Chemical Engineering*, 11(5), 110309. <https://doi.org/10.1016/j.jece.2023.110309>
54. Huang, J., Cao, Y., Shao, Q., Peng, X., & Guo, Z. (2017). Magnetic nanocarbon adsorbents with enhanced hexavalent chromium removal: morphology dependence of fibrillar vs particulate structures. *Industrial & Engineering Chemistry Research*, 56(38), 10689-10701. <https://doi.org/10.1021/acs.iecr.7b02835>
55. Yang, S., Li, X., Li, Q., Gu, P., Liu, X., & Yang, G. (2019). Competitive adsorption of metal ions at smectite/water interfaces: Mechanistic aspects, and impacts of co-ions, charge densities, and charge locations. *The Journal of Physical Chemistry C*, 124(2), 1500-1510. <https://doi.org/10.1021/acs.jpcc.9b10341>
56. Wang, Y. Y., Liu, Y. X., Lu, H. H., Yang, R. Q., & Yang, S. M. (2018). Competitive adsorption of Pb (II), Cu (II), and Zn (II) ions onto hydroxyapatite-biochar nanocomposite in aqueous solutions. *Journal of Solid State Chemistry*, 261, 53-61. <https://doi.org/10.1016/j.jssc.2018.02.010>

57. Aziz, S., Mazhar, A. R., Ubaid, A., Shah, S. M. H., Riaz, Y., Talha, T., & Jung, D. W. (2024). A comprehensive review of membrane-based water filtration techniques. *Applied Water Science*, 14(8), 169. <https://doi.org/10.1007/s13201-024-02226-y>
58. Liu, Z., Yang, F., Zhai, T., Yu, J., Wang, C., Liu, Z., & Yang, M. (2024). Removal of PFOA from water by activated carbon adsorption: Influence of pore structure. *Journal of Environmental Chemical Engineering*, 12(5), 113923. <https://doi.org/10.1016/j.jece.2024.113923>
59. Sarita Alhan, Monika Nehra, Neeraj Dilbaghi et al. (2019). Potential use of ZnO@activated carbon nanocomposites for the adsorptive removal of Cd²⁺ ions in aqueous solutions, *Environmental Research*, 173, 411-418, <https://doi.org/10.1016/j.envres.2019.03.061>.
60. Lv, D., Liu, Y., Zhou, J., Yang, K., Lou, Z., Baig, S. A., & Xu, X. (2018). Application of EDTA-functionalized bamboo activated carbon (BAC) for Pb (II) and Cu (II) removal from aqueous solutions. *Applied Surface Science*, 428, 648-658. <https://doi.org/10.1016/j.apsusc.2017.09.151>
61. Wei, Y. S., Zhang, M., Zou, R., & Xu, Q. (2020). Metal–organic framework-based catalysts with single metal sites. *Chemical Reviews*, 120(21), 12089-12174. <https://doi.org/10.1021/acs.chemrev.9b00757>
62. Robson, R. (2024). The Historical Development of the Concepts Underlying the Design and Construction of Targeted Coordination Polymers/MOFs: A Personal Account. *The Chemical Record*, e202400038. <https://doi.org/10.1002/tcr.202400038>
63. Huang, L., He, M., Chen, B., & Hu, B. (2018). Magnetic Zr-MOFs nanocomposites for rapid removal of heavy metal ions and dyes from water. *Chemosphere*, 199, 435-

444. <https://doi.org/10.1016/j.chemosphere.2018.02.019>

64. Tripathy, J., Mishra, A., Pandey, M., Thakur, R. R., Chand, S., Rout, P. R., & Shahid, M. K. (2024). Advances in Nanoparticles and Nanocomposites for Water and Wastewater Treatment: A Review. *Water*, 16(11), 1481. <https://doi.org/10.3390/w16111481>

65. Zangiabadi, M., & Yazdapanah, N. (2021). Removal of zinc and cadmium heavy metals from industrial wastewater using organic and nano oxide adsorbents. *Journal of Soil Management and Sustainable Production*, 10(4), 119-136. <https://doi.org/10.22069/EJSMS.2021.16088.1858>

66. Hirpo Hinsene, Nakara Bhawawet, Apichat Imyim (2024). Rice husk biochar doped with deep eutectic solvent and Fe₃O₄/ZnO nanoparticles for heavy metal and diclofenac removal from water, *Separation and Purification Technology*, 339:126638 <https://doi.org/10.1016/j.seppur.2024.126638>

67. Zhou, C. H., Zhou, Q., Wu, Q. Q., Petit, S., Jiang, X. C., Xia, S. T., & Yu, W. H. (2019). Modification, hybridization and applications of saponite: An overview. *Applied Clay Science*, 168, 136-154. <https://doi.org/10.1016/j.clay.2018.11.002>

68. Elboughdiri, N. (2020). The use of natural zeolite to remove heavy metals Cu (II), Pb (II) and Cd (II), from industrial wastewater. *Cogent Engineering*, 7(1), 1782623. <https://doi.org/10.1080/23311916.2020.1782623>

69. Esmacili, A., Mobini, M., & Eslami, H. (2019). Removal of heavy metals from acid mine drainage by native natural clay minerals, batch and continuous studies. *Applied Water Science*, 9(4), 97. <https://doi.org/10.1007/s13201-019-0977-x>

70. Truong, H. B., Ike, I. A., Ok, Y. S., & Hur, J. (2020). Polyethyleneimine

modification of activated fly ash and biochar for enhanced removal of natural organic matter from water via adsorption. *Chemosphere*, 243, 125454.

<https://doi.org/10.1016/j.chemosphere.2019.125454>

71. Stephen, S., Gorain, B., Choudhury, H., & Chatterjee, B. (2022). Exploring the role of mesoporous silica nanoparticle in the development of novel drug delivery systems. *Drug delivery and translational research*, 1-19.

<https://doi.org/10.1007/s13346-021-00935-4>

72. Kresge, A. C., Leonowicz, M. E., Roth, W. J., Vartuli, J. C., & Beck, J. S. (1992). Ordered mesoporous molecular sieves synthesized by a liquid-crystal template mechanism. *nature*, 359(6397), 710-712. <https://doi.org/10.1038/359710a0>

73. Liu, T., & Liu, G. (2020). Porous organic materials offer vast future opportunities. *Nature Communications*, 11(1), 4984. <https://doi.org/10.1038/s41467-020-15911-8>

74. Zhao, D., Feng, J., Huo, Q., Melosh, N., Fredrickson, G. H., Chmelka, B. F., & Stucky, G. D. (1998). Triblock copolymer syntheses of mesoporous silica with periodic 50 to 300 angstrom pores. *science*, 279(5350), 548-552. DOI: [10.1126/science.279.5350.548](https://doi.org/10.1126/science.279.5350.548)

75. Gao, D., Duan, A., Zhang, X., Chi, K., Zhao, Z., Li, J., ... & Xu, C. (2015). Self-assembly of monodispersed hierarchically porous Beta-SBA-15 with different morphologies and its hydro-upgrading performances for FCC gasoline. *Journal of Materials Chemistry A*, 3(32), 16501-16512. <https://doi.org/10.1039/C5TA03671B>

76. Qu, Q., Zhou, G., Ding, Y., Feng, S., & Gu, Z. (2014). Adjustment of the morphology of MCM-41 silica in basic solution. *Journal of non-crystalline solids*, 405,

104-115. <https://doi.org/10.1016/j.jnoncrysol.2014.09.012>

77. Zhang, X., & Du, T. (2022). Study of rice husk ash derived MCM-41-type materials on pore expansion, Al incorporation, PEI impregnation, and CO₂ adsorption. *Korean Journal of Chemical Engineering*, 39(3), 736-759. <https://doi.org/10.1007/s11814-021-0904-3>

78. Li, S., Wang, L., Lu, P., Li, Y., Li, Y., Wang, Y., & Qiu, D. (2025). Nanoconfined polyethyleneimine in mesoporous MCM-41 silica for heavy metal ions removal. *Separation and Purification Technology*, 353, 128421. <https://doi.org/10.1016/j.seppur.2024.128421>

79. Şimşek, V., Yarbay, R. Z., Marttin, V., & Gül, Ü. D. (2023). Treatment of textile dye via economic fungi/MCM-41 bio-based adsorbent: application of neural network approach. *Journal of Cleaner Production*, 421, 138448. <https://doi.org/10.1016/j.jclepro.2023.138448>

80. Vieira, J. C., Priebe, V. E., Wust, K. M., Benvenuti, E. V., Villetti, M. A., Bender, C. R., & Frizzo, C. P. (2023). Adsorption and release of diphenhydraminium ibuprofenate from SBA-15 and MCM-41 explained by intermolecular interactions. *Journal of Materials Science*, 58(16), 6998-7010. <https://doi.org/10.1007/s10853-023-08457-9>

81. Vinogradov, N. A., Pimerzin, A. A., Vutolkina, A. V., & Glotov, A. P. (2024). CoMoS HDS catalysts supported on hierarchical halloysite and MCM-41 core-shell composite: Structural features and catalytic behavior study. *Materials Today Chemistry*, 36, 101941. <https://doi.org/10.1016/j.mtchem.2024.101941>

82. Bhattacharyya, S., Lelong, G., & Saboungi, M. L. (2006). Recent progress in the

synthesis and selected applications of MCM-41: a short review. *Journal of Experimental Nanoscience*, 1(3), 375-395.

<https://doi.org/10.1080/17458080600812757>

83. Shende, R. A., & Chaudhari, B. P. (2023). Robust Optimization and Characterization of MCM-41 Nanoparticle Synthesis using Modified Sol-Gel Method. *Chemistry Select*, 8(11), e202204968. <https://doi.org/10.1002/slct.202204968>

84. Sayari, A., Liu, P., Kruk, M., & Jaroniec, M. (1997). Characterization of large-pore MCM-41 molecular sieves obtained via hydrothermal restructuring. *Chemistry of Materials*, 9(11), 2499-2506. <https://doi.org/10.1021/cm970128o>

85. Dhal, J. P., Dash, T., & Hota, G. (2020). Iron oxide impregnated mesoporous MCM-41: synthesis, characterization and adsorption studies. *Journal of Porous Materials*, 27, 205-216. <https://doi.org/10.1007/s10934-019-00803-0>

86. Verma, P., Kuwahara, Y., Mori, K., Raja, R., & Yamashita, H. (2020). Functionalized mesoporous SBA-15 silica: recent trends and catalytic applications. *Nanoscale*, 12(21), 11333-11363. <https://doi.org/10.1039/D0NR00732C>

87. Marcucci, S. M. P., Zanin, G. M., & Arroyo, P. A. (2022). Synthesis of SBA-15 and pore-expanded SBA-15 and surface modification with tin for covalent lipase immobilization. *Microporous and Mesoporous Materials*, 337, 111951. <https://doi.org/10.1016/j.micromeso.2022.111951>

88. Pirez, C., Morin, J. C., Manayil, J. C., Lee, A. F., & Wilson, K. (2018). Sol-gel synthesis of SBA-15: Impact of HCl on surface chemistry. *Microporous and Mesoporous Materials*, 271, 196-202.

<https://doi.org/10.1016/j.micromeso.2018.05.043>

89. Norsuraya, S., Fazlena, H., & Norhasyimi, R. (2016). Sugarcane bagasse as a renewable source of silica to synthesize Santa Barbara Amorphous-15 (SBA-15). *Procedia Engineering*, 148, 839-846.
<https://doi.org/10.1016/j.proeng.2016.06.627>
90. Chaudhary, V., & Sharma, S. (2017). An overview of ordered mesoporous material SBA-15: synthesis, functionalization and application in oxidation reactions. *Journal of Porous Materials*, 24, 741-749. <https://doi.org/10.1007/s10934-016-0311-z>
91. Jana, S., Dutta, B., Honda, H., & Koner, S. (2011). Mesoporous silica MCM-41 with rod-shaped morphology: Synthesis and characterization. *Applied clay science*, 54(2), 138-143. <https://doi.org/10.1016/j.clay.2011.07.018>
92. Giglio, V., Varela-Aramburu, S., Travaglini, L., Fiorini, F., Seeberger, P. H., Maggini, L., & De Cola, L. (2018). Reshaping silica particles: Mesoporous nanodiscs for bimodal delivery and improved cellular uptake. *Chemical Engineering Journal*, 340, 148-154. <https://doi.org/10.1016/j.cej.2018.01.059>
93. Almethen, A. A., Alotaibi, K. M., Alhumud, H. S., & Alswieleh, A. M. (2022). Highly efficient and rapid removal of methylene blue from aqueous solution using folic acid-conjugated dendritic mesoporous silica nanoparticles. *Processes*, 10(4), 705. <https://doi.org/10.3390/pr10040705>
94. Cai, Q., Luo, Z. S., Pang, W. Q., Fan, Y. W., Chen, X. H., & Cui, F. Z. (2001). Dilute solution routes to various controllable morphologies of MCM-41 silica with a basic medium. *Chemistry of materials*, 13(2), 258-263. <https://doi.org/10.1021/cm990661z>
95. Trewyn, B. G., Slowing, I. I., Giri, S., Chen, H. T., & Lin, V. S. Y. (2007). Synthesis and functionalization of a mesoporous silica nanoparticle based on the sol-gel process

- and applications in controlled release. *Accounts of chemical research*, 40(9), 846-853.
<https://doi.org/10.1021/ar600032u>
96. Yadav, S., Choudhary, N., Sonpal, V., & Paital, A. R. (2023). Engineering excitation-independent turn-on fluorescent probe for mercury: Functionalized dendritic silica doped with red-emissive carbon dots towards simultaneous detection and remediation with biosensing application. *Chemical Engineering Journal*, 471, 144715.
<https://doi.org/10.1016/j.cej.2023.144715>
97. Wan, M., Zhao, Y., Li, H., Zou, X., & Sun, L. (2023). pH and NIR responsive polydopamine-doped dendritic silica carriers for pesticide delivery. *Journal of Colloid and Interface Science*, 632, 19-34. <https://doi.org/10.1016/j.jcis.2022.11.009>
98. Jin, Z., Sheng, W., Ren, L., Bai, D., Sun, M., Wang, S., & Wang, Z. (2024). Homogeneous fluorescence immunoassay based on AuNPs quenching dendritic silica assembled with multicolor QDs for the simultaneous determination of four mycotoxins in cereals. *Chemical Engineering Journal*, 480, 148247.
<https://doi.org/10.1016/j.cej.2023.148247>
99. Hao, P., Peng, B., Shan, B. Q., Yang, T. Q., & Zhang, K. (2020). Comprehensive understanding of the synthesis and formation mechanism of dendritic mesoporous silica nanospheres. *Nanoscale Advances*, 2(5), 1792-1810.
<https://doi.org/10.1039/D0NA00219D>
100. Yu, J., & Tobilko, V. (2024). Absorption removal of copper (II) from water by zero valent iron loaded dendritic mesoporous silica. *Technology audit and production reserves*, 5(3 (79)), 6-12. <https://doi.org/10.15587/2706-5448.2024.314231>
101. Zhao, S. N., Tang, R. H., Deng, S. J., Chen, G. E., Ye, J., & Xu, Z. L. (2023). Dual

gatekeepers-modified dendritic mesoporous silica nanoparticles for controlled drug release. *Journal of Materials Science*, 58(46), 17610-17622.

<https://doi.org/10.1007/s10853-023-09128-5>

102. Sen, D., Maity, A., Bahadur, J., Das, A., & Polshettiwar, V. (2021). Unravelling the structural hierarchy in microemulsion droplet templated dendritic fibrous nano silica. *Microporous and Mesoporous Materials*, 323(33), 111234.

<https://doi.org/10.1016/j.micromeso.2021.111234>

103. Du, X., & Qiao, S. Z. (2014). Dendritic silica particles with center-radial pore channels: promising platforms for catalysis and biomedical applications. *Small*, 11(4), 392-413.

<https://doi.org/10.1002/sml.201401201>

104. Ren, D., Xu, J., Chen, N., Ye, Z., Li, X., Chen, Q., & Ma, S. (2021). Controlled synthesis of mesoporous silica nanoparticles with tunable architectures via oil-water microemulsion assembly process. *Colloids and Surfaces A: Physicochemical and Engineering Aspects*, 611, 125773.

<https://doi.org/10.1016/j.colsurfa.2020.125773>

105. Dang, M., Li, W., Zheng, Y., Su, X., Ma, X., Zhang, Y., & Wang, L. (2017). Mesoporous organosilica nanoparticles with large radial pores via an assembly-reconstruction process in bi-phase. *Journal of Materials Chemistry B*, 5(14), 2625-2634.

<https://doi.org/10.1039/C6TB03327J>

106. Wang, X., Liu, Y., Xu, H., Dai, M., Qiao, P., Wang, W., & Song, H. (2022). Preparation of surface-decorated mesoporous dendritic fibrous nanosilica/TiO₂ for use

in phenol degradation. *Applied Surface Science*, 603, 154414.

<https://doi.org/10.1016/j.apsusc.2022.154414>

107. Yang, J., Chen, W., Shen, D., Wei, Y., Ran, X., Teng, W., ... & Zhao, D. (2014). Controllable fabrication of dendritic mesoporous silica–carbon nanospheres for anthracene removal. *Journal of Materials Chemistry A*, 2(29), 11045-11048. <https://doi.org/10.1039/C4TA01516A>
108. Liu, P. C., Yu, Y. J., Peng, B., Ma, S. Y., Ning, T. Y., Shan, B. Q. & Wu, P. (2017). A dual-templating strategy for the scale-up synthesis of dendritic mesoporous silica nanospheres. *Green Chemistry*, 19(23), 5575-5581. <https://doi.org/10.1039/C7GC02139A>
109. Khantan, N., Shadjou, N., & Hasanzadeh, M. (2019). Synthesize of dendritic fibrous nano-silica functionalized by cysteine and its application as advanced adsorbent. *Nanocomposites*, 5(4), 104-113. <https://doi.org/10.1080/20550324.2019.1669925>
110. Malekmohammadi, S., Mohammed, R. U. R., Samadian, H., Zarebkohan, A., García-Fernández, A., Kokil, G. R., & Martínez-Máñez, R. (2022). Nonordered dendritic mesoporous silica nanoparticles as promising platforms for advanced methods of diagnosis and therapies. *Materials Today Chemistry*, 26, 101144. <https://doi.org/10.1016/j.mtchem.2022.101144>
111. Moon, D. S., & Lee, J. K. (2012). Tunable synthesis of hierarchical mesoporous silica nanoparticles with radial wrinkle structure. *Langmuir*, 28(33), 12341-12347. <https://doi.org/10.1021/la302145j>
112. Shan, B. Q., Xing, J. L., Yang, T. Q., Peng, B., Hao, P., Zong, Y. X. & Wu, P. (2019). One-pot co-condensation strategy for dendritic mesoporous organosilica nanospheres with fine size and morphology control. *CrystEngComm*, 21(27), 4030-

4035. <https://doi.org/10.1039/c9ce00593e>

113. Gisbert-Garzarán, M., & Vallet-Regí, M. (2020). Influence of the surface functionalization on the fate and performance of mesoporous silica nanoparticles. *Nanomaterials*, 10(5), 916. <https://doi.org/10.3390/nano10050916>

114. Shao, P., Liang, D., Yang, L., Shi, H., Xiong, Z., Ding, L., ... & Luo, X. (2020). Evaluating the adsorptivity of organo-functionalized silica nanoparticles towards heavy metals: quantitative comparison and mechanistic insight. *Journal of hazardous materials*, 387, 121676. <https://doi.org/10.1016/j.jhazmat.2019.121676>

115. Liu, L., Liu, J., Li, T., Yang, G., Tang, A., & Ling, Y. (2018). Adsorption efficiency, thermodynamics, and kinetics of amino-functionalized mesoporous calcium silicate for the removal of heavy metal ions. *Desalination and Water Treatment*, 107, 165-181. <https://doi.org/10.5004/dwt.2018.22138>

116. Li, P., Wang, J., Li, X., Zhu, W., He, S., Han, C., ... & Dionysiou, D. D. (2019). Facile synthesis of amino-functional large-size mesoporous silica sphere and its application for Pb²⁺ removal. *Journal of hazardous materials*, 378, 120664. <https://doi.org/10.1016/j.jhazmat.2019.05.057>

117. Soltani, R., Marjani, A., & Shirazian, S. (2019). Facile one-pot synthesis of thiol-functionalized mesoporous silica submicrospheres for Tl (I) adsorption: Isotherm, kinetic and thermodynamic studies. *Journal of hazardous materials*, 371, 146-155. <https://doi.org/10.1016/j.jhazmat.2019.02.076>

118. Castillo, R. R., Lozano, D., & Vallet-Regí, M. (2020). Mesoporous silica nanoparticles as carriers for therapeutic biomolecules. *Pharmaceutics*, 12(5), 432. <https://doi.org/10.3390/pharmaceutics12050432>

119. Tang, X., Feng, Q., Liu, K., Luo, X., Huang, J., & Li, Z. (2018). A simple and innovative route to remarkably enhance the photocatalytic performance of TiO₂: Using micro-meso porous silica nanofibers as carrier to support highly-dispersed TiO₂ nanoparticles. *Microporous and Mesoporous Materials*, 258, 251-261. <https://doi.org/10.1016/j.micromeso.2017.09.024>
120. Yang, C., Li, K., Wang, J., & Zhou, S. (2021). Selective hydrogenation of phenol to cyclohexanone over Pd nanoparticles encaged hollow mesoporous silica catalytic nanoreactors. *Applied Catalysis A: General*, 610, 117961. <https://doi.org/10.1016/j.apcata.2020.117961>
121. Nicola, R., Muntean, S. G., Nistor, M. A., Putz, A. M., Almásy, L., & Săcărescu, L. (2020). Highly efficient and fast removal of colored pollutants from single and binary systems, using magnetic mesoporous silica. *Chemosphere*, 261, 127737. <https://doi.org/10.1016/j.chemosphere.2020.127737>
122. Wawrzekiewicz, M., Wiśniewska, M., Wołowicz, A., Gun'ko, V. M., & Zarko, V. I. (2017). Mixed silica-alumina oxide as sorbent for dyes and metal ions removal from aqueous solutions and wastewaters. *Microporous and Mesoporous Materials*, 250, 128-147. <https://doi.org/10.1016/j.micromeso.2017.05.016>
123. Zauška, L., Volavka, D., Lisnichuk, M., Zelenka, T., Kinnertová, E., Zelenková, G., & Almáši, M. (2024). Tuning the photocatalytic performance of mesoporous silica-titanium dioxide and cobalt titanate for methylene blue and Congo red adsorption/photodegradation: Impact of azo dyes concentration, catalyst mass, wavelength, reusability and kinetic properties. *Journal of Photochemistry and Photobiology A: Chemistry*, 451, 115522.

<https://doi.org/10.1016/j.jphotochem.2024.115522>

124. Gisbert-Garzarán, M., Lozano, D., & Vallet-Regí, M. (2020). Mesoporous silica nanoparticles for targeting subcellular organelles. *International journal of molecular sciences*, 21(24), 9696. <https://doi.org/10.3390/ijms21249696>

125. Abdo, G. G., Zagho, M. M., & Khalil, A. (2020). Recent advances in stimuli-responsive drug release and targeting concepts using mesoporous silica nanoparticles. *Emergent Materials*, 3(3), 407-425. <https://doi.org/10.1007/s42247-020-00109-x>

126. Tran, V. A., Vo, V. G., Shim, K., Lee, S. W., & An, S. S. A. (2020). Multimodal mesoporous silica nanocarriers for dual stimuli-responsive drug release and excellent photothermal ablation of cancer cells. *International journal of nanomedicine*, 7667-7685. <https://doi.org/10.2147/IJN.S254344>

127. Vandghanooni, S., Barar, J., Eskandani, M. & Omid, Y. (2020). Aptamer-conjugated mesoporous silica nanoparticles for simultaneous imaging and therapy of cancer. *TrAC Trends in Analytical Chemistry*, 123, 115759. <https://doi.org/10.1016/j.trac.2019.115759>

128. Feng, Y., Liao, Z., Li, M., Zhang, H., Li, T., Qin, X. & Liu, Y. (2023). Mesoporous silica nanoparticles-based nanoplatfroms: basic construction, current state, and emerging applications in anticancer therapeutics. *Advanced Healthcare Materials*, 12(16), 2201884. <https://doi.org/10.1002/adhm.202201884>

129. Lu, D., Xu, S., Qiu, W., Sun, Y., Liu, X., Yang, J., & Ma, J. (2020). Adsorption and desorption behaviors of antibiotic ciprofloxacin on functionalized spherical MCM-41 for water treatment. *Journal of Cleaner Production*, 264, 121644.

<https://doi.org/10.1016/j.jclepro.2020.121644>

130. Deng, J., Li, X., Wei, X., Liu, Y., Liang, J., Song, B. & Huang, W. (2020). Hybrid silicate-hydrochar composite for highly efficient removal of heavy metal and antibiotics: Coadsorption and mechanism. *Chemical engineering journal*, 387, 124097.

<https://doi.org/10.1016/j.cej.2020.124097>

131. Li, S., Li, S., Wen, N., Wei, D., & Zhang, Y. (2021). Highly effective removal of lead and cadmium ions from wastewater by bifunctional magnetic mesoporous silica. *Separation and Purification Technology*, 265, 118341.

<https://doi.org/10.1016/j.seppur.2021.118341>

132. Yu, X., & Williams, C. T. (2022). Recent advances in the applications of mesoporous silica in heterogeneous catalysis. *Catalysis science & technology*, 12(19), 5765-5794. <https://doi.org/10.1039/D2CY00001F>

133. Liu, S., Liu, L., Wang, Y., Ouyang, Y., Li, N., Hu, Z., & Chen, S. (2023). Inorganic-organic composite membranes containing amino-functionalized mesoporous silica loaded phosphotungstic acid with enhanced fuel cell performance and stability. *International Journal of Hydrogen Energy*, 48(25), 9436-9450.

<https://doi.org/10.1016/j.ijhydene.2022.12.162>

134. Wu, X., Tan, L., Li, Y., Liu, W., Peng, Z., Dong, Y. & Liang, Y. (2023). Novel sensor array distinguishes heavy metal ions based on multiple fluorescence channels from dendritic mesoporous silica nanoparticles. *Analytica Chimica Acta*, 1240, 340749.

<https://doi.org/10.1016/j.aca.2022.340749>

135. Patnaik, S., Sahoo, D. P., & Parida, K. M. (2020). Bimetallic co-effect of Au-Pd alloyed nanoparticles on mesoporous silica modified g-C₃N₄ for single and

simultaneous photocatalytic oxidation of phenol and reduction of hexavalent chromium. *Journal of colloid and interface science*, 560, 519-535.

<https://doi.org/10.1016/j.jcis.2019.09.041>

136. Lu, S., Wang, D., Jiang, S. P., Xiang, Y., Lu, J., & Zeng, J. (2010). HPW/MCM-41 phosphotungstic acid/mesoporous silica composites as novel proton-exchange membranes for elevated-temperature fuel cells. *Advanced Materials*, 22(9), 971-976.

<https://doi.org/10.1002/adma.200903091>

137. Qiu, Z., Shu, J., & Tang, D. (2017). Bioresponsive release system for visual fluorescence detection of carcinoembryonic antigen from mesoporous silica nanocontainers mediated optical color on quantum dot-enzyme-impregnated paper.

Analytical chemistry, 89(9), 5152-5160.

<https://doi.org/10.1021/acs.analchem.7b00989>

138. Foroutan, R., Mohammadi, R., Adeleye, A. S., et al. (2019). Efficient arsenic (V) removal from contaminated water using natural clay and clay composite adsorbents.

Environmental Science and Pollution Research. 26(29), 29748-29762.

<https://doi.org/10.1007/s11356-019-06070-5>

139. Aziz, B. K, Shwan, D. M. S., Kaufhold S. (2020). Characterization of Tagaran natural clay and its efficiency for removal of cadmium (II) from Sulaymaniyah industrial zone sewage. *Environmental Science and Pollution Research*. 27(31):

38384-38396. <https://doi.org/10.1007/s11356-019-06995-x>

140. Rao Rifaqat Ali Khan , Kashifuddin M. (2016). Adsorption studies of Cd (II) on Ball Clay: comparison with other natural clays. *Arabian Journal of Chemistry*. 9:

S1233-S1241. <https://doi.org/10.1016/j.arabjc.2012.01.010>

141. Es-Sahbany, H., Berradi, M., Nkhili, S. et al. (2019). Removal of heavy metals (nickel) contained in wastewater-models by the adsorption technique on natural clay. *Materials Today: Proceedings*. 13:866-875. <https://doi.org/10.1016/j.matpr.2019.04.050>
142. Tamjidi, S., Moghadas, B. K., Esmaeili, H., et al. (2021). Improving the surface properties of adsorbents by surfactants and their role in the removal of toxic metals from wastewater: A review study. *Process Safety and Environmental Protection*. 148: 775-795. <https://doi.org/10.1016/j.pserp.2021.02.003>
143. Zhang, T., Wang, W., Zhao, Y., et al. (2021). Removal of heavy metals and dyes by clay-based adsorbents: From natural clays to 1D and 2D nano-composites. *Chemical Engineering Journal*. 420: 127574. <https://doi.org/10.1016/j.cej.2020.127574>
144. Handbook of Clay Science, F. Bergaya, B.K.G. Theng, G. Lagaly Elsevier, Amsterdam (2006), 1224 pp., ISBN: 978-0-08-044183-2.
145. Chengxu Liao, Xiaotan Wu, Li Zou, Yawen Liu & Zhihui Chen (2022). Research Progress on the Modification Methods of Clay Minerals. *Applied Science and Innovative Research*. 6 (4): 35-44. <http://doi.org/10.22158/asir.v6n4p35>
146. Adel Mokhtar Boubekour Asli ,Soumia Abdelkrim ,Mohammed Hachemaoui, Bouhadjar Boukoussa, Mohammed Sassi ,Gianluca Viscusi and Mohamed Abboud. Polymer/Clay Nanocomposites as Advanced Adsorbents for Textile Wastewater Treatment (2024). *Minerals*. 14(12): 1216. <https://doi.org/10.3390/min14121216>
147. Huang, Z., Wu, P., Gong, B., et al. (2016). Efficient removal of Co^{2+} from aqueous solution by 3-aminopropyltriethoxysilane functionalized montmorillonite with

- enhanced adsorption capacity. *PLoS one*. 11(7): e0159802.
<https://doi.org/10.1371/journal.pone.0159802>
148. Liu, C., Liu, S., Wu, P., et al. (2016). Enhancing the adsorption behavior and mechanism of Sr (II) by functionalized montmorillonite with different 3-aminopropyltriethoxysilane (APTES) ratios. *RSC advances*. 6(86): 83288-83295.
<https://doi.org/10.1039/C6RA19362E>
149. Ahmed, Z., Wu, P., Xu, Y., et al. (2021). Enhanced Single and Simultaneous As (III) Adsorption in Pearl River Delta Water by Hexylamine Functionalized Vermiculite. *Water*. 13(17): 2412. <https://doi.org/10.3390/w13172412>
150. Long, H., Wu, P., Yang, L., et al. (2014). Efficient removal of cesium from aqueous solution with vermiculite of enhanced adsorption property through surface modification by ethylamine. *Journal of colloid and interface science*. 428: 295-301.
<https://doi.org/10.1016/j.jcis.2014.05.001>
151. Chen, M., Guo, Q., Pei, F. et al. (2020). The role of Fe (III) in enhancement of interaction between chitosan and vermiculite for synergistic co-removal of Cr (VI) and Cd (II). *Colloids and Surfaces A: Physicochemical and Engineering Aspects*. 606: 125356. <https://doi.org/10.1016/j.colsurfa.2020.125356>
152. Yang, F., Sun, S., Chen, X., et al. (2016). Mg–Al layered double hydroxides modified clay adsorbents for efficient removal of Pb²⁺, Cu²⁺ and Ni²⁺ from water. *Applied Clay Science*. 123: 134-140. <https://doi.org/10.1016/j.clay.2016.01.026>
153. Mnasri-Ghnimi, S., Frini-Srasra, N. (2019). Removal of heavy metals from aqueous solutions by adsorption using single and mixed pillared clays. *Applied Clay Science*, 179: 105151. <https://doi.org/10.1016/j.clay.2019.105151>

154. Maleki, A., Hajizadeh, Z., Sharifi, V., et al. (2019). A green, porous and eco-friendly magnetic geopolymer adsorbent for heavy metals removal from aqueous solutions. *Journal of cleaner production*. 215: 1233-1245. <https://doi.org/10.1016/j.jclepro.2019.01.084>
155. Awwad A. M., Amer M. W. and Al-aqarbeh M. M. (2020). TiO₂-kaolinite nanocomposite prepared from the Jordanian Kaolin clay: Adsorption and thermodynamics of Pb(II) and Cd(II) ions in aqueous solution. *Chemistry International*. 6(4) 168-178. <https://doi.org/10.5281/zenodo.3597558>
156. Liu C, Wu P, Zhu Y, et al. (2016). Simultaneous adsorption of Cd²⁺ and BPA on amphoteric surfactant activated montmorillonite. *Chemosphere*. 144: 1026-1032. <https://doi.org/10.1016/j.chemosphere.2015.09.063>
157. Kordala, N., Wyszowski, M. (2024). Zeolite Properties, Methods of Synthesis, and Selected Applications. *Molecules*. 29, 1069. <https://doi.org/10.3390/molecules29051069>
158. Shishkin, A., Abramovskis, V., Zalite, I., Singh, A.K., Mezinskis, G., Popov, V., Ozolins, J. (2023). Physical, Thermal, and Chemical Properties of Fly Ash Cenospheres Obtained from Different Sources. *Materials*. 16, 2035. <https://doi.org/10.3390/ma16052035>
159. Sofi Buzukashvili, Roberto Sommerville, Weiqing Hu, Oliver Brooks, Ozan Kökkılıç, Philippe Ouzilleau, Neil A. Rowson, Kristian E. (2024). Waters Zeolite synthesis from coal fly ash and its application to heavy metals remediation from water contaminated with Pb, Cu, Zn and Ni ions. *Minerals Engineering*. 209: 108619 <https://doi.org/10.1016/j.mineng.2024.108619>

160. Piyush Gupta, Garima Nagpal, Namrata Gupta (2021). Fly ash-based geopolymers: an emerging sustainable solution for heavy metal remediation from aqueous medium. *Beni-Suef Univ J Basic Appl Sci.* 10:89 <https://doi.org/10.1186/s43088-021-00179-8>
161. Yuan, N., Xu, H., Liu, Y., Tan, K., Bao, Y. (2023). Synthesis and Environmental Applications of Nanoporous Materials Derived from Coal Fly Ash. *Sustainability.* 15, 16851. <https://doi.org/10.3390/su152416851>
162. Zhang, K., Xu, L. L., Jiang, J. G., Calin, N., Lam, K. F., Zhang, S. J., ... & Wu, P. (2013). Facile large-scale synthesis of monodisperse mesoporous silica nanospheres with tunable pore structure. *Journal of the American Chemical Society*, 135(7), 2427-2430. <https://doi.org/10.1021/ja3116873>
163. Gao, F., Lei, C., Liu, Y., Song, H., Kong, Y., Wan, J., & Yu, C. (2021). Rational design of dendritic mesoporous silica nanoparticles' surface chemistry for quantum dot enrichment and an ultrasensitive lateral flow immunoassay. *ACS Applied Materials & Interfaces*, 13(18), 21507-21515. <https://doi.org/10.1021/acsami.1c02149>
164. Shi, L. N., Lin, Y. M., Zhang, X., & Chen, Z. L. (2011). Synthesis, characterization and kinetics of bentonite supported nZVI for the removal of Cr (VI) from aqueous solution. *Chemical Engineering Journal*, 171(2), 612-617. <https://doi.org/10.1016/j.cej.2011.04.038>
165. Yu, J., Bondarieva, A.I. & Tobilko, V. Yu. (2024). Effect of synthesis time on the morphology of monodisperse silica microspheres. *Journal of Chemistry and Technologies*, 32(4), 932-938. <https://doi.org/10.15421/jchemtech.v32i4.315165>
166. Tobilko, V., Spasonova, L., Kovalchuk, I., Kornilovych, B. & Kholodko, Yu.

- (2019). Adsorption of Uranium (VI) from Aqueous Solutions by Amino-functionalized Clay Minerals. *Colloids and Interfaces*, 3(1), 41. <https://doi.org/10.3390/colloids3010041>
167. Bhanita Goswami, Debajyoti Mahanta (2019). Polyaniline coated nickel oxide nanoparticles for the removal of phenolic compounds: Equilibrium, kinetics and thermodynamic studies. *Colloids and Surfaces A*, 582, 123843. <https://doi.org/10.1016/j.colsurfa.2019.123843>
168. Bondarieva, A., Tobilko, V., Kholodko, Y., & Kornilovych, B. (2019). Obtaining of iron-containing silicate composites for contaminated water purification from arsenic compounds. *Technology audit and production reserves*, 3(3 (47)), 14-19. <https://doi.org/10.15587/2312-8372.2019.173710>
169. Tzu, T. W., Tsuritani, T., & Sato, K. (2013). Sorption of Pb (II), Cd (II), and Ni (II) toxic metal ions by alginate-bentonite. *Journal of Environmental Protection*, 4(1B), 51. <https://doi.org/10.4236/jep.2013.41b010>
170. Łętocha, A., Miastkowska, M., & Sikora, E. (2022). Preparation and characteristics of alginate microparticles for food, pharmaceutical and cosmetic applications. *Polymers*, 14(18), 3834. <https://doi.org/10.3390/polym14183834>
171. Tanabe, K., Misono, M., Hattori, H., & Ono, Y. (1990). *New solid acids and bases: their catalytic properties*. Elsevier, 300 p.
172. Moaseri, E., Baniadam, M., Maghrebi, M. & Karimi, M. (2013). A simple recoverable titration method for quantitative characterization of amine-functionalized carbon nanotubes. *Chemical Physics Letters*, 555, 164-167. <https://doi.org/10.1016/j.cplett.2012.10.064>

173. Choi, W. S., Lee, H. J. (2022). Nanostructured materials for water purification: Adsorption of heavy metal ions and organic dyes. *Polymers*, 14(11), 2183. <https://doi.org/10.3390/polym14112183>
174. Innocenzi, P., Falcaro, P., Grosso, D., Babonneau, F. (2003). Order-disorder transitions and evolution of silica structure in self-assembled mesostructured silica films studied through FTIR spectroscopy. *The Journal of Physical Chemistry B*, 107(20), 4711-4717. <https://doi.org/10.1021/jp026609z>
175. Lei, Z., Pang, X., Li, Na, Lin, L., Li, Y. (2009). A novel two-step modifying process for preparation of chitosan-coated Fe₃O₄/SiO₂ microspheres. *Journal of Materials Processing Technology*, 209(7), 3218-3225. <https://doi.org/10.1016/j.jmatprotec.2008.07.044>
176. Dong, K., Wu, S., Chang, B., Sun, T. (2023). Zero-valent iron supported by dendritic mesoporous silica nanoparticles to purify dye wastewater. *Journal of Environmental Chemical Engineering*, 11(5), 110434. <https://doi.org/10.1016/j.jece.2023.110434>
177. Li, H., Si, R., Wang, W., Huang, Y., Xiang, M., Wang, C., Chen, S., Cao, W., Lu, Z., Huang, M. (2021). Sulfidated nanoscale zero-valent iron dispersed in dendritic mesoporous silica nanospheres for degrading tetrabromobisphenol A. *Colloids and Surfaces A: Physicochemical and Engineering Aspects*, 621, 126586. <https://doi.org/10.1016/j.colsurfa.2021.126586>
178. Yang, Y., Bernardi, S., Song, H., Zhang, J., Yu, M., Reid, J.C., Strounina, E., Searles, D.J., Yu, C. (2016). Anion assisted synthesis of large pore hollow dendritic mesoporous organosilica nanoparticles: understanding the composition gradient.

Chemistry of Materials, 28(3), 704-707.

<https://doi.org/10.1021/acs.chemmater.5b03963>

179. Yu, J., Bondarieva, A., Tobilko, V., Pavlenko, V. (2023). Adsorption removal of Cu(II) using Ni-modified silica gel. *Water and Water Purification Technologies. Scientific and Technical News*, 37(3), 3-12. <https://doi.org/10.20535/2218-930032023302423>

180. Wamba, A.G.N., Kofa, G.P., Koungou, S.N., Thue, P.S., Lima, E.C., Reis, G.S. et al. (2018). Grafting of Amine functional group on silicate based material as adsorbent for water purification: A short review. *Journal of Environmental Chemical Engineering*, 6(2), 3192-3203. <https://doi.org/10.1016/j.jece.2018.04.062>

181. Kostenko, L.S., Tomashchuk, I.I., Kovalchuk, T.V. & Zaporozhets, O.A. (2019). Bentonites with grafted aminogroups: Synthesis, protolytic properties and assessing Cu(II), Cd(II) and Pb(II) adsorption capacity. *Applied Clay Science*, 172, 49-56. <https://doi.org/10.1016/j.clay.2019.02.009>

182. Arce, V.B., Gargarello, R.M., Ortega, F., Romañano, V., Mizrahi, M. et al. (2015). EXAFS and DFT study of the cadmium and lead adsorption on modified silica nanoparticles. *Spectrochimica Acta Part A: Molecular and Biomolecular Spectroscopy*, 151, 156-163. <https://doi.org/10.1016/j.saa.2015.06.093>

183. Najafi, M., Yousefi, Y. & Rafati, A.A. (2012). Synthesis, characterization and adsorption studies of several heavy metal ions on amino-functionalized silica nano hollow sphere and silica gel. *Separation and Purification Technology*, 85, 193-205. <https://doi.org/10.1016/j.seppur.2011.10.011>

184. Yang, Z., Chen, X., Li, S., Ma, W., Li, Y., He, Z. et al. (2020). Effective removal

of Cr(VI) from aqueous solution based on APTES modified nanoporous silicon prepared from kerf loss silicon waste. *Environmental Science and Pollution Research*, 27, 10899-10909. <https://doi.org/10.1007/s11356-019-07427-6>

185. Xu, C., Lei, C., Wang, Y. & Yu, C. (2022). Dendritic Mesoporous Nanoparticles: Structure, Synthesis and Properties. *Angewandte Chemie International Edition*, 61(12), e202112752. <https://doi.org/10.1002/anie.202112752>

186. Yu, J., Bondarieva, A., Pylypenko, I., Tobilko, V., Sabov, T., Gumenna, M., Tomila, T., Inshyna, O. (2025). Amino-functionalized dendritic mesoporous silica nanoparticles for removal of copper from aqueous solutions. *J. Ecol. Eng.*, 26(6), 365-377. <https://doi.org/10.12911/22998993/202979>

187. Dong, K., Wu, S., Chang, B. & Sun, T. (2023). Zero-valent iron supported by dendritic mesoporous silica nanoparticles to purify dye wastewater. *Journal of Environmental Chemical Engineering*, 11(5), 110434. <https://doi.org/10.1016/j.jece.2023.110434>

188. Li, H., Si, R., Wang, W., Huang, Y., Xiang, M., Wang, C. et al. (2021). Sulfidated nanoscale zero-valent iron dispersed in dendritic mesoporous silica nanospheres for degrading tetrabromobisphenol A. *Colloids and Surfaces A: Physicochemical and Engineering Aspects*, 621, 126586. <https://doi.org/10.1016/j.colsurfa.2021.126586>

189. Dhaffouli, A., Salazar-Carballo, P.A., Carinelli, S., Holzinger, M. & Barhoumi, H. (2024). Improved electrochemical sensor using functionalized silica nanoparticles (SiO₂-APTES) for high selectivity detection of lead ions. *Materials Chemistry and Physics*, 318, 129253. <https://doi.org/10.1016/j.matchemphys.2024.129253>

190. Pasternack, R.M., Amy, S.R. & Chabal, Y.J. (2008). Attachment of 3-

(Aminopropyl)triethoxysilane on Silicon Oxide Surfaces: Dependence on Solution Temperature. *Langmuir*, 24(22), 12963-12971. <https://doi.org/10.1021/la8024827>

191. Berktaş, I., Ghafar, A.N., Fontana, P., Caputcu, A., Menciloglu, Y. & Okan, B.S. Facile Synthesis of Graphene from Waste Tire/Silica Hybrid Additives and Optimization Study for the Fabrication of Thermally Enhanced Cement Grouts. *Molecules*, 25(4), 886. <https://doi.org/10.3390/molecules25040886>

192. Innocenzi, P., Falcaro, P., Grosso, D. & Babonneau, F. (2003). Order-disorder transitions and evolution of silica structure in self-assembled mesostructured silica films studied through FTIR spectroscopy. *Journal of Physical Chemistry B*, 107(20), 4711-4717. <https://doi.org/10.1021/jp026609z>

193. Lei, Z., Pang, X., Li, Na, Lin, L. & Li, Y. (2009). A novel two-step modifying process for preparation of chitosan-coated $\text{Fe}_3\text{O}_4/\text{SiO}_2$ microspheres. *Journal of Materials Processing Technology*, 209(7), 3218-3225. <https://doi.org/10.1016/j.jmatprotec.2008.07.044>

194. Dugas, V. & Chevalier, Y. (2003). Surface hydroxylation and silane grafting on fumed and thermal silica. *Journal of Colloid and Interface Science*, 264(2), 354-361. [https://doi.org/10.1016/S0021-9797\(03\)00552-6](https://doi.org/10.1016/S0021-9797(03)00552-6)

195. Sehlleier, Y.H., Abdali, A., Schnurre, S.M., Wiggers, H. & Schulz, C. (2014). Surface functionalization of microwave plasma-synthesized silica nanoparticles for enhancing the stability of dispersions. *Journal of Nanoparticle Research*, 16, 2557. <https://doi.org/10.1007/s11051-014-2557-1>

196. Qiao, B., Wang, T.-J., Gao, H. & Jin, Y. (2015). High density silanization of nano-silica particles using γ -aminopropyltriethoxysilane (APTES). *Applied Surface Science*,

351, 646-654. <https://doi.org/10.1016/j.apsusc.2015.05.174>

197. Almatarneh, M.H., Elayan, I.A., Al-Sulaibi, M., Khawaldeh, A.A., Saber, S.O.W., Al-Qaralleh, M. et al. (2019). Unimolecular Decomposition Reactions of Propylamine and Protonated Propylamine. *ACS Omega*, 4(2), 3306-3313. <https://doi.org/10.1021/acsomega.8b02792>

198. Dugas, V. & Chevalier, Y. (2011). Chemical Reactions in Dense Monolayers: In Situ Thermal Cleavage of Grafted Esters for Preparation of Solid Surfaces Functionalized with Carboxylic Acids. *Langmuir*, 27(23), 14188-14200. <https://doi.org/10.1021/la2029438>

199. Yantasee, W., Lin, Y., Fryxell, G.E., Alford, K.L., Busche, B.J., & Johnson, C.D. (2004). Selective Removal of Copper(II) from Aqueous Solutions Using Fine-Grained Activated Carbon Functionalized with Amine. *Industrial & Engineering Chemistry Research*, 43(11), 2759-2764. <https://doi.org/10.1021/ie030182g>

200. Simonin, J.-P. (2016). On the comparison of pseudo-first order and pseudo-second order rate laws in the modeling of adsorption kinetics. *Chemical Engineering Journal*, 300, 254-263. <https://doi.org/10.1016/j.cej.2016.04.079>

201. Feng, X.; Long, R.; Wang, L.; Liu, C.; Bai, Z.; Liu, X. A Review on Heavy Metal Ions Adsorption from Water by Layered Double Hydroxide and Its Composites. *Sep. Purif. Technol.*, 2022, 284, 120099. <https://doi.org/10.1016/j.seppur.2021.120099>

202. Hao, J.; Ji, L.; Li, C.; Hu, C.; Wu, K. Rapid, Efficient and Economic Removal of Organic Dyes and Heavy Metals from Wastewater by Zinc-Induced In-Situ Reduction and Precipitation of Graphene Oxide. *J. Taiwan Inst. Chem. Eng.*, 2018, 88, 137-145. <https://doi.org/10.1016/j.jtice.2018.03.045>

203. Wang, L.; Shi, C.; Pan, L.; Zhang, X.; Zou, J. J. Rational Design, Synthesis, Adsorption Principles and Applications of Metal Oxide Adsorbents: A Review. *Nanoscale*, 2020, 12 (8), 4790-4815. <https://doi.org/10.1039/C9NR09274A>
204. Gupta, K.; Joshi, P.; Gusain, R.; Khatri, O. P. Recent Advances in Adsorptive Removal of Heavy Metal and Metalloid Ions by Metal Oxide-Based Nanomaterials. *Coord. Chem. Rev.*, 2021, 445, 214100. <https://doi.org/10.1016/j.ccr.2021.214100>
205. Fayyazi, F.; Haghshenas, D. F.; Kowsari, E.; Ghazitabar, A. Synthesis of a Three-Dimensional Reduced Graphene Oxide Aerogel Decorated with (Fe₃O₄@ SiO₂-NH₂)-COC₂H₄COOH for Adsorption of Heavy Metal Cations. *J. Mol. Liq.*, 2023, 386, 122512. <https://doi.org/10.1016/j.molliq.2023.122512>
206. Shen, L.; Wang, J.; Li, Z.; Fan, L.; Chen, R.; Wu, X.; Zeng, W. A High-Efficiency Fe₂O₃@ Microalgae Composite for Heavy Metal Removal from Aqueous Solution. *J. Water Process Eng.*, 2020, 33, 101026. <https://doi.org/10.1016/j.jwpe.2019.101026>
207. Tao, Q.; Bi, J.; Huang, X.; Wei, R.; Wang, T.; Zhou, Y.; Hao, H. Fabrication, Application, Optimization and Working Mechanism of Fe₂O₃ and Its Composites for Contaminants Elimination from Wastewater. *Chemosphere*, 2021, 263, 127889. <https://doi.org/10.1016/j.chemosphere.2020.127889>
208. Chen, J.; Wang, N.; Liu, Y.; Zhu, J.; Feng, J.; Yan, W. Synergetic Effect in a Self-Doping Polyaniline/TiO₂ Composite for Selective Adsorption of Heavy Metal Ions. *Synth. Met.*, 2018, 245, 32-41. <https://doi.org/10.1016/j.synthmet.2018.08.006>
209. Siddeeg, S. M. A Novel Synthesis of TiO₂/GO Nanocomposite for the Uptake of Pb²⁺ and Cd²⁺ from Wastewater. *Mater. Res. Express*, 2020, 7 (2), 025038. <https://doi.org/10.1088/2053-1591/ab7407>

210. Behnajady, M. A.; Bimeghdar, S. Synthesis of Mesoporous NiO Nanoparticles and Their Application in the Adsorption of Cr (VI). *Chem. Eng. J.*, 2014, 239, 105-113. <https://doi.org/10.1016/j.cej.2013.10.102>
211. Bhardwaj, S.; Sarkar, T. Core–Shell Type Magnetic Ni/NiO Nanoparticles as Recyclable Adsorbent for Pb (II) and Cd (II) Ions: One-Pot Synthesis, Adsorption Performance, and Mechanism. *J. Taiwan Inst. Chem. Eng.*, 2020, 113, 223-230. <https://doi.org/10.1016/j.jtice.2020.08.011>
212. Hashem, B. A. Y.; Alswat, A. A.; Ali, S. L.; Al-Odaini, N. A.; Alshorifi, F. T. Facile Synthesis of NiO–CuO/Activated Carbon Nanocomposites for Use in the Removal of Lead and Cadmium Ions from Water. *ACS Omega*, 2022, 7 (50), 47183-47191. <https://doi.org/10.1021/acsomega.2c06352>
213. Rubab, R.; Ali, S.; Rehman, A. U.; Khan, S. A.; Khan, A. M. Templated Synthesis of NiO/SiO₂ Nanocomposite for Dye Removal Applications: Adsorption Kinetics and Thermodynamic Properties. *Colloids Surf. A*, 2021, 615, 126253. DOI: <https://doi.org/10.1016/j.colsurfa.2021.126253>
214. Dhiman, V.; Kondal, N. ZnO Nanoadsorbents: A Potent Material for Removal of Heavy Metal Ions from Wastewater. *Colloids Interface Sci. Commun.*, 2021, 41, 100380. <https://doi.org/10.1016/j.colcom.2021.100380>
215. Cuppett, J. D.; Duncan, S. E.; Dietrich, A. M. Evaluation of Copper Speciation and Water Quality Factors That Affect Aqueous Copper Tasting Response. *Chem. Senses*, 2006, 31 (7), 689-697. <https://doi.org/10.1093/chemse/bjl010>
216. Natarajan, S., Bajaj, H.C., Tayade, R.J. (2018). Recent advances based on the synergetic effect of adsorption for removal of dyes from waste water using

- photocatalytic process. *J. Environ. Sci.*, 65, 201-222.
<https://doi.org/10.1016/j.jes.2017.03.011>
217. Saruchi, Kumar, V., Dhami, J.K. et al. (2022). Synthesis and characterization of Aloe-vera-poly(acrylic acid)-Cu-Ni-bionanocomposite: its evaluation as removal of carcinogenic dye malachite green. *J Polym Res.*, 29, 49.
<https://doi.org/10.1007/s10965-022-02898-7>
218. Nidhi Verma, Tejpal S. Chundawat, Harish Chandra, Dipti Vaya (2023). An efficient time reductive photocatalytic degradation of carcinogenic dyes by TiO₂-GO nanocomposite. *Materials Research Bulletin*, 158, 112043.
<https://doi.org/10.1016/j.materresbull.2022.112043>
219. George Z. Kyzas, Jie Fu, Kostas A. Matis (2013). The Change from Past to Future for Adsorbent Materials in Treatment of Dyeing Wastewaters. *Materials*, 6(11), 5131-5158. <https://doi.org/10.3390/ma6115131>
- 220 Ahmad, A., Mohd-Setapar, S.H., Chuong, C.S., Khatoon, A., Wani, W.A., Kumar, R., Rafatullah, M. (2015). Recent advances in new generation dye removal technologies: Novel search for approaches to reprocess wastewater. *RSC Adv.*, 5, 30801–30818. <https://doi.org/10.1039/C4RA16959J>
221. Yagub, M.T., Sen, T.K., Afroze, S., Ang, H.M. (2014). Dye and its removal from aqueous solution by adsorption: A review. *Adv. Colloid Interface Sci.*, 209, 172–184.
<https://doi.org/10.1016/j.cis.2014.04.002>
222. Asmaa Elsherbeny Moharm, Gamal A. El Naeem, Hesham M. A. Soliman, Ahmed I. Abd-Elhamid, Ali A. El-Bardan, Taher S. Kassem, AbdElAziz A. Nayl, Stefan Bräse (2022). Fabrication and Characterization of Effective Biochar Biosorbent

Derived from Agricultural Waste to Remove Cationic Dyes from Wastewater. *Polymers*, 14(13), 2587. <https://doi.org/10.3390/polym14132587>

223. Jayashree Samantray, Amit Anand, Barsha Dash, Malay Kumar Ghosh, Ajaya Kumar Behera (2022). Silicate minerals - Potential source of potash - A review. *Minerals Engineering*, 179, 30, 107463. <https://doi.org/10.1016/j.mineng.2022.107463>

224. Hao Li, Xueping Chen, Danqing Shen, Fan Wu, Roser Pleixats, Jianming Pan (2021). Functionalized silica nanoparticles: classification, synthetic approaches and recent advances in adsorption applications. *Nanoscale*, 13, 15998-16016. <https://doi.org/10.1039/D1NR04048K>

225. Bhanita Goswami, Debajyoti Mahanta (2019). Polyaniline coated nickel oxide nanoparticles for the removal of phenolic compounds: Equilibrium, kinetics and thermodynamic studies. *Colloids and Surfaces A*, 582, 123843. <https://doi.org/10.1016/j.colsurfa.2019.123843>

226. El-Qanni, A., Nassar, N. N., Vitale, G. (2017). Experimental and Computational Modeling Studies on Silica-Embedded NiO/MgO Nanoparticles for Adsorptive Removal of Organic Pollutants from Wastewater. *RSC Adv.*, 7 (23), 14021-14038. <https://doi.org/10.1039/C7RA00615B>

227. Mustafa, S., Mahmood, F., Shafqat, U., Hussain, S., Shahid, M., Batool, F., Elnour, R.O., Hashem, M., Asseri, T.A.Y., Shahzad, T. (2023). The Biosynthesis of Nickel Oxide Nanoparticles: An Eco-Friendly Approach for Azo Dye Decolorization and Industrial Wastewater Treatment. *Sustainability*, 15, 14965. <https://doi.org/10.3390/su152014965>

228. Rimsha Rubab, Shahid Ali, Attiq Ur Rehman, Safyan Akram Khan, Asad Muhammad Khan (2021). Templated synthesis of NiO/SiO₂ nanocomposite for dye removal applications: Adsorption kinetics and thermodynamic properties. *Colloids and Surfaces A: Physicochemical and Engineering Aspects*, 615, 126253. <https://doi.org/10.1016/j.colsurfa.2021.126253>
229. Yu, J., & Tobilko, V. (2024). Removal of methylene blue from water by NiO-modified silica gel. *Technology audit and production reserves*, 6(3 (80)), 47-52. <https://doi.org/10.15587/2706-5448.2024.319822>
230. Brahim El Ghmari, Hanane Farah, Abdellah Ech-Chahad (2023). Biosynthesis, Characterization of Nickel (II) Oxide Nanoparticles NiO and their High- Efficient Photocatalytic Application. *Int. J. Nanosci. Nanotechnol.*, 19, 3, 135-147. <https://doi.org/10.22034/ijnn.2023.560608.2262>
231. Rebelo, Q. H. F., Ferreira, C. S., Santos, P. L., Bonacin, J. A., Passos, R. R., Pocrifka, L. A., Paula, M. M. S. (2018). Synthesis and characterization of a nanocomposite NiO/SiO₂ from a sustainable source of SiO₂. *Particulate Science and Technology*, 37(8), 911–915. <https://doi.org/10.1080/02726351.2018.1455781>
232. Carlos Sergio Ferreira, Carlos Sergio Ferreira, Pãmyla L. Dos Santos, Pãmyla L. Dos Santos, Juliano Bonacin, Juliano BonacinShow, Leandro Pocrifka, Leandro Pocrifka (2015). Rice Husk Reuse in the Preparation of SnO₂/SiO₂ Nanocomposite. *Materials Research*, 18(3), 639-643. <https://doi.org/10.1590/1516-1439.009015>
233. Anna Murashkevich, Anna Murashkevich A. S. Lavitskaya, T. I. Barannikova, I. M. Zharskii (2008). Infrared Absorption Spectra and Structure of TiO₂-SiO₂

Composites. *Journal of Applied Spectroscopy*, 75(5), 730-734.
<https://doi.org/10.1007/s10812-008-9097-3>

234. Gisi, De S., Lofrano, G., Grassi, M. and Notarnicola, M. (2016). Characteristics and adsorption capacities of low-cost sorbents for wastewater treatment: A review, *Sustainable Materials and Technologies*, 9, 10-40.
<https://doi.org/10.1016/j.susmat.2016.06.002>

235. Chowdhury, I.R., Chowdhury, S., Mazumder, M.A.J. and Al-Ahmed, A. (2022). Removal of lead ions (Pb^{2+}) from water and wastewater: a review on the low-cost adsorbents, *Applied Water Science*, 12:185. <https://doi.org/10.1007/s13201-022-01703-6>

236. Tony, M.A. (2021). Low-cost adsorbents for environmental pollution control: a concise systematic review from the prospective of principles, mechanisms and their applications, *Journal of Dispersion Science and Technology*, 43(11), 1612-1633.
<https://doi.org/10.1080/01932691.2021.1878037>

237. Aboudi Mana, S.C., Hanafiah, M.M. and Chowdhury, A.J.K. (2017). Environmental characteristics of clay and clay-based minerals, *Geology, Ecology, and Landscapes*, 1(1), 155-161. <https://doi.org/10.1080/24749508.2017.1361128>

238. Xie, F., Gao, C. and Averous, L. (2024). Alginate-based materials: Enhancing properties through multiphase formulation design and processing innovation, *Materials Science and Engineering R*, 159, 100799.
<https://doi.org/10.1016/j.mser.2024.100799>

239. Karapinar, N. (2016). Removal of heavy metal ions by ferrihydrite: an opportunity to the treatment of acid mine drainage, *Water, Air, & Soil Pollution*, 227:193. <https://doi.org/10.1007/s11270-016-2899-7>
240. Rout, K., Mohapatra, M. and Anand, S. (2012). 2-Line ferrihydrite: synthesis, characterization and its adsorption behaviour for removal of Pb(II), Cd(II), Cu(II) and Zn(II) from aqueous solutions, *Dalton Transactions*, 41, 3302-3312. <https://doi.org/10.1039/c2dt11651k>
241. Jasim, A.Q. and Ajjam, S.K. (2024). Removal of heavy metal ions from wastewater using ion exchange resin in a batch process with kinetic isotherm, *South African Journal of Chemical Engineering*, 49, 43-54. <https://doi.org/10.1016/j.sajce.2024.04.002>
242. Sabzehmeidani, M.M., Mahnaee, S., Ghaedi, M., Heidari, H., et al. (2021). Carbon based materials: a review of adsorbents for inorganic and organic compounds, *Materials Advances*, 2, 598-627. <https://doi.org/10.1039/d0ma00087f>
243. Eberle, S., Börnick, H. and Stolte, S. (2022). Granular natural zeolites: cost-effective adsorbents for the removal of ammonium from drinking water, *Water*, 14(6):939. <https://doi.org/10.3390/w14060939>
244. Sutirman, Z.A., Sanagi, M.M. and Aini, W.I.W. (2021). Alginate-based adsorbents for removal of metal ions and radionuclides from aqueous solutions: A review, *International Journal of Biological Macromolecules*, 174, 216-228. <https://doi.org/10.1016/j.ijbiomac.2021.01.150>
245. Elwakeel, K.Z., Ahmed, M.M., Akhdhar, A., Sulaiman, M.G.M., et.al. (2022). Recent advances in alginate-based adsorbents for heavy metal retention from water: a

- review, *Desalination and Water Treatment*, 272, 50-74.
<https://doi.org/10.5004/dwt.2022.28834>
246. Sosa Lucio, M.D., Oh, E.-J. et.al. (2023). Effects of processing conditions on the properties of porous diatomite granules prepared by sodium alginate gelation, *Applied Sciences*, 13(16):9474. <https://doi.org/10.3390/app13169474>
247. Kołodyńska, D., Gęca, M., Skwarek, E. and Goncharuk, O. (2018). Titania-coated silica alone and modified by sodium alginate as sorbents for heavy metal ions, *Nanoscale Research Letters*, 13:96. <https://doi.org/10.1186/s11671-018-2512-7>
248. Pylypenko, I.V. (2024). Removal of chromium (VI) from aqueous solutions by granular composites based on laponite and alginate ionotropically cross-linked by iron and zirconium ions, *Voprosy khimii i khimicheskoi tekhnologii*, 2, 75-82.
<https://doi.org/10.32434/0321-4095-2024-153-2-75-82>
249. Tzu, T.W., Tsuritani, T. and Sato, K. (2013). Sorption of Pb(II), Cd(II), and Ni(II) toxic metal ions by alginate-bentonite, *Journal of Environmental Protection*, 4, 51-55.
<https://doi.org/10.4236/jep.2013.41b010>
250. Hood, C. and Pensini, E. (2022). Alginate-bentonite clay composite porous sorbents for Cu(II) and Zn(II) removal from water, *Water, Air, & Soil Pollution*, 233:137. <https://doi.org/10.1007/s11270-022-05609-6>
251. Zhao, L., Basly, J.-Ph. and Baudu, M. (2024). Simultaneous adsorption of chromate and arsenate onto ferrihydrite/alginate composite beads: competition and mechanism, *Environmental Research*, 250, 118440.
<https://doi.org/10.1016/j.envres.2024.118440>
252. Bondarieva, A., Tobilko, V., Kholodko, Yu. and Kornilovych B. (2019). Obtaining

of iron-containing silicate composites for contaminated water purification from arsenic compounds, *Technology Audit and Production Reserves*, 3(3(47)), 14-19. doi: <https://doi.org/10.15587/2312-8372.2019.173710>

253. Fomenko, O., Makovetskyi, O., Bondarieva, A., Tobilko, V., & Yu, J. (2024). Obtaining granular adsorbents based on biopolymers and clay minerals. Bulletin of NTUU «Igor Sikorsky Kyiv Polytechnic Institute», Series «Chemical Engineering, Ecology and Resource Saving», (3), 93–103. <https://doi.org/10.20535/2617-9741.3.2024.312425> (in Ukraine)

254. Zlopasa, J., Norder, B., Koenders, E.A.B. and Picken, S.J. (2016). Rheological investigation of specific interactions in Na Alginate and Na MMT suspension, *Carbohydrate Polymers*, 151, 144-149. <https://doi.org/10.1016/j.carbpol.2016.05.055>

255. Benli, B., Boylu, F., Can, M.F. et.al. (2011). Rheological, electrokinetic, and morphological characterization of alginate-bentonite biocomposites, *Journal of Applied Polymer Science*, 122(1), 19-28. <https://doi.org/10.1002/app.33627>

256. Zhang, X., Chen, J., Shao, X. et al. (2023). Structural and physical properties of alginate pretreated by high-pressure homogenization, *Polymers*, 15:3225. <https://doi.org/10.3390/polym15153225>

257. Pieczara, G., Manecki, M., Pzepa, G., Borkiewicz, O., et al. (2020). Thermal stability and decomposition products of P-doped ferrihydrite, *Materials*, 13(18):4113. <https://doi.org/10.3390/ma13184113>

258. Yang, N., Wang, R., Rao, P., Yan, L., et.al. (2019). The fabrication of calcium alginate beads as a green sorbent for selective recovery of Cu(II) from metal mixtures, *Crystals*, 9(5):255. <https://doi.org/10.3390/cryst9050255>

259. Navid Ranjbar, Carsten Kuenzel (2017). Cenospheres: A review, *Fuel*, 207, 1–12, <https://doi.org/10.1016/j.fuel.2017.06.059>